Mechanisms of Spindle Disassembly and Microtubule-kinetochore Attachment in the yeast *Saccharomyces cerevisiae*

by

Adrianne Barber Pigula

A dissertation submitted in partial satisfaction of the requirements for the degree of

Doctor of Philosophy

in

Molecular and Cell Biology

in the

Graduate Division

of the

University of California, Berkeley

Committee in Charge:

Professor Georjana Barnes, co-chair

Professor David Drubin, co-chair

Professor Rebecca Heald

Professor W. Zacheus Cande

Associate Professor Sanjay Kumar

Fall 2012

ABSTRACT

Mechanisms of Spindle Disassembly and Microtubule-kinetochore Attachment in the yeast *Saccharomyces cerevisiae*

by

Adrianne Barber Pigula

Doctor of Philosophy in Molecular and Cell Biology

University of California, Berkeley

Professors Georjana Barnes and David Drubin, co-chairs

The timely regulation of spindle disassembly is essential for cells to coordinate mitotic exit with cytokinesis. In the budding yeast *Saccharomyces cerevisiae*, the microtubule-associated protein She1 functions in one of at least three parallel pathways that promote spindle disassembly. She1 phosphorylation by the Aurora kinase Ipl1 facilitates a role for She1 in late anaphase, when She1 contributes to the depolymerization of microtubules and shrinkage of spindle halves. By examining genetic interactions between known spindle disassembly genes, I identified components of the Hog (High Osmolarity Glycerol response) pathway, and found that three genes in this pathway, *SHO1*, *PBS2*, and *HOG1*, are necessary for proper localization of She1 to the anaphase spindle. Hog pathway mutants exhibited spindle disassembly defects, as well as mislocalization of the NoCut checkpoint proteins Boi1 and Boi2 from the bud neck. Moreover, Boi2, but not Boi1, plays a role in spindle disassembly that places it in a pathway with Sho1, Pbs2, and Hog1. A non-classical nuclear localization signal, the importin Nmd5, and exportin Crm1/Xpo1 – all necessary for Hog1 trafficking – are also necessary for proper She1 localization to the spindle and bud neck. Together, my data suggest a process by which cells monitor events at the spindle and bud neck, and describe a novel role for Hog pathway signaling in mitosis.

I also studied mechanisms by which spindle microtubules attach to kinetochores. I generated two new alleles of *NDC80*, a component of the essential Ndc80 complex, which tethers the outer kinetochore to spindle microtubules and participates in chromosome segregation. Deletions of an internal loop within the coiled-coil region of Ndc80 render cells temperature sensitive and unable to make stable microtubule-kinetochore attachments, resulting in metaphase arrest and DNA mis-segregation phenotypes. These alleles have been useful in helping us understand the required geometry of proteins in the outer kinetochore, and how protein-protein interactions promote the stable microtubule-kinetochore attachments necessary for high-fidelity chromosome segregation.

TABLE OF CONTENTS

LIST OF FIGURES

LIST OF TABLES

ABBREVIATIONS

MT – microtubule
Kt – kinetochore
SPB – spindle pole body
aMT – astral microtubule
ipMT – interpolar microtubule
kMT – kinetochore microtubule
CENIII – centromere of Chromosome III
MAP – microtubule associated protein
Hog pathway – high osmolarity glycerol response pathway
MAPK – mitogen activated protein kinase
MAPKK – mitogen activated protein kinase kinase
MAPKKK – mitogen activated protein kinase kinase kinase
MEN – mitotic exit network
FEAR – Cdc14 early release pathway
SGA – synthetic genetic array
APC – anaphase promoting complex

ACKNOWLEDGEMENTS

I'd like to thank David and Georjana for allowing me to be a part of their lab for the past six years. The opportunity to study biology in such an incredible environment has been a gift that I have never taken for granted, and I genuinely appreciate everything you have done for me. Thank you! I would also like to thank my thesis committee, Eva Nogales, and the MCB GAO for their support on many levels, and especially for listening to me and offering suggestions when I struggled in frustration with my project. My labmates have been exceptionally wonderful colleagues and friends, and I'm greatly fortunate to have benefited from their knowledge and expertise. Yidi Sun, Connie Peng, Anthony Cormier, Ann Marie Faust, and Nate Krefman have all offered me wonderful advice throughout the years, and made our various tubulin preps much more fun. Thank you! I'd particularly like to thank those who have come before me with regard to the projects I've worked on – Jonathan Wong and Jeff Woodruff, for beginning work with She1, Iain Cheeseman, Stefan Westermann, and Hong-Wei Wang for robustly developing the Dam1 and Ndc80 projects, and Yuko Nakajima and Randall Tyers for mentoring me so vigilantly when I encountered difficult technical hurdles regarding Ndc80 biochemistry. Claudio Ciferri and Greg Alushin, both from Eva Nogales' lab, collaborated with me on the Ndc80 project, sharing their patience and suggestions as freely as their expertise. Jesse Patterson from Jeremy Thorner's lab helped me to first discover the PY-NLS in She1, and answered all kinds of questions I had about MAPK signaling.

Previous mentors and academic advisors have played a huge role in encouraging me to this point, in particular Li Yu-Lee, Sunny Cooke, and Teresa Viancour. I'm not sure what any of them saw in me other than a rather ingenuous passion for biology, but they taught me how to engage with science and research, and how to design experiments and contextualize results. I could not have asked for better coaches along the way. I am extremely fortunate to benefit from the encouragement of family and friends, beginning with my folks, Sonny and Lynda. There simply is not a way to express my gratitude for having such a close and supportive family. Enduring friendships with the Flory family, Catherine Noel, Jackie Heilman, Roland Cirilo, Nathalie Faulk, Kirsten Kohlhauff, Abraham Rodriguez, and Cooper Quintin have helped anchor my academic goals, as well as keep them in perspective with the rest of life. Thank you so much for being a part of this journey.

Chapter 1: General Introduction

Across species, genomic stability critically depends on the faithful replication of DNA and distribution of genetic material to daughter cells. The budding yeast *Saccharomyces cerevisiae* is an excellent model organism for studying cell cycle progression and mitosis, as it is genetically tractable, amenable to biochemistry and cell biology techniques, and its mitotic machinery shares a large degree of conservation with the mitotic machinery in higher eukaryotes.

Progression through the cell cycle is highly regulated by the cyclin-dependent kinase Cdk1 in association with cyclins specific to cell cycle phase. When bound to the late G1/early S-phase specific cyclins, Clb5 and Clb6, Cdk1 promotes DNA synthesis and mitotic spindle assembly (reviewed in Sullivan and Morgan, 2007). As DNA is replicated, cohesins are deposited between sister chromatids to bind them together, and condensins help the DNA pack into condensed chromosomes. G1/S-phase cyclins are degraded in early mitosis, as M-phase cyclins accumulate and adjust the specificity of Cdk1 for mitotic substrates.

Budding yeast chromosomes possess a 125-bp "point" centromere that serves as a platform for assembly of the kinetochore, a hierarchically arranged complex of ~65 proteins that establishes an attachment site for spindle microtubules (reviewed in Westermann et al., 2007). In contrast to kinetochores in fission yeast and in more complex eukaryotes, budding yeast kinetochores are attached to the spindle by a single microtubule. However, budding yeast maintain the conserved requisite that sister chromatids make bipolar attachments to the spindle prior to anaphase onset. The essential Dam1 and Ndc80 complexes are facilitators of microtubule-kinetochore attachments in yeast. Mechanisms of microtubule capture and bi-orientation have been dissected using conditionally active centromeres that form *de novo* kinetochores and spindle attachments (Dewar et al., 2005; Tanaka et al., 2005; Tanaka et al., 2007). These studies have suggested that kinetochores are initially captured by the lateral sides of microtubules through interactions with the Ndc80 complex, and that this side-on attachment is converted into a stable end-on attachment through interaction with the Dam1 complex (Tanaka et al., 2005; Tanaka et al., 2007).

Bipolar orientation of chromosomes is detected by two interrelated mechanisms, the Spindle Assembly Checkpoint (SAC), and the detection of tension across sister kinetochores. The SAC is non-essential in budding yeast unless the spindle is compromised, and operates by sensing unattached kinetochores. Checkpoint proteins Mad1-3, Bub1, Bub3, and Mps1 detect microtubule occupancy at the kinetochore, and Mad2 binds to unattached kinetochores in a conformation that sequesters Cdc20, an activator of the Anaphase Promoting Complex (APC) (Hardwick and Murray, 1995; Wang and Burke, 1995; Fang et al., 1998). The APC is an E3 ubiquitin ligase whose primary target, Pds1 (securin), is an inhibitor of separase. Upon degradation of Pds1, separase cleaves cohesin, thereby relieving cohesion between sister chromatids in an irreversible step that initiates anaphase (Uhlmann et al., 2000).

Tension-sensing monitors the integrity of spindle-kinetochore attachments. Incorrect spindle attachments can satisfy the SAC, for example during syntelic attachment (when both kinetochores are attached to microtubules emanating from the same SPB), underscoring the need for a mechanism that detects the generation of tension across sister kinetochores. End-on, amphitelic attachments generate tension, produced by the oppositional forces of microtubule depolymerization and sister

chromatid cohesion (Pinsky and Biggins, 2005). Chromosomes with malformed syntelic spindle attachments do not generate tension, and importantly, are corrected by the essential kinase Ipl1 (Dewar et al., 2004; Pinsky et al., 2006; Cheeseman et al., 2002; Maure et al., 2007; Kang et al., 2001). Ipl1 is part of the chromosome passenger complex (CPC), and phosphorylates various kinetochore complexes to promote microtubule detachment in the absence of tension. Microtubule detachment is recognized by the SAC, and mitosis is delayed until proper microtubule-kinetochore interactions form (Pinksy et al., 2006). Although the precise mechanism by which tension is sensed remains elusive, the importance of this system is highlighted in *ipl1* temperature sensitive mutants that display high frequencies of chromosome mis-segregation without activating the SAC (Chan and Botstein, 1993). The Dam1 complex, which localizes to kinetochores and microtubules, and the Ndc80 complex, which is stably associated with the outer kinetochore, are important targets of Ipl1 that mediate microtubule attachment (Shang et al., 2003; He et al., 2001; DeLuca et al., 2006; Cheeseman et al., 2001; Hofmann et al, 1998; Janke et al., 2002).

As important as is the establishment of stable spindle-kinetochore attachments, is the coordination of mitotic exit, spindle disassembly, and cytokinesis. Mitotic cyclins are degraded by the APC at the onset of anaphase, attenuating phosphorylation of mitotic substrates by Cdk1 (reviewed in Sullivan and Morgan, 2007). Active separase also contributes to the Cdc14 early release (FEAR) pathway. Cdc14, a phosphatase that opposes Cdk1 phosphorylation, is sequestered in an inactive form in the nucleolus by interaction with Net1 (Cfi1), a component of the nucleolar silencing RENT complex. Phosphorylation of Net1 by Cdk1/Clb2 releases Cdc14, but until anaphase this phosphorylation is opposed by a second phosphatase, PP2A, and its regulatory subunit Cdc55. By restraining PP2A activity towards phospho-Net1, separase preserves Cdk1 phosphorylation of Net1, and transient release of Cdc14 from the nucleolus (Queralt et al., 2006; reviewed in Stegmeir and Amon, 2004, and D'Amours and Amon, 2004). Cdc14 is then able to dephosphorylate some Cdk1 targets, such as the CPC component and Ipl1 activator Sli15/INCENP, the Dam1 complex subunit Ask1, and the spindle stabilizing protein Fin1 (Woodbury and Morgan, 2007).

The FEAR network partially activates Cdc14 during early anaphase, but this process is not essential to mitotic exit. However, full activation of Cdc14 and mitotic exit is dependent on a pathway called the Mitotic Exit Network (MEN). The MEN requires the activity of several kinases upstream of Cdc14, including Dbf2/Mob1, and Cdc15 (Luca et al., 2001; reviewed in Stegmeir and Amon, 2004). Cdc15 is activated by FEAR-released Cdc14, and the essential spindle-pole body and bud neck localized GTPase, Tem1. The Tem1 guanine-nucleotide exchange factor (GEF), Lte1, and GTPase-activating proteins (GAPs) Bfa1 and Bub2, are similarly localized to the daughter spindle-pole body. The polo-kinase Cdc5, whose activity rises in anaphase, phosphorylates and inhibits Bfa1/Bub2 GAP activity, thereby holding Tem1 in a GTP-bound state that is capable of activating Cdc15 (reviewed in Stegmeir and Amon, 2004, and D'Amours and Amon, 2004).

Full activation of Cdc14 is necessary for dephosphorylating and activating a range of Cdk1 substrates important for anaphase and cytokinesis, as well as Sic1 and Swi5, transcription factors which drive expression of genes that guide the following G1 phase (reviewed in Sullivan and Morgan, 2007). Dephosphorylated Cdh1 also serves to

activate the APC toward substrates whose degradation is required for anaphase exit, such as spindle stabilizing microtubule proteins including Fin1, Ase1, and Cin8. The removal of these proteins from the midzone during anaphase B helps to destabilize interpolar spindle microtubules, and contributes to spindle disassembly (Woodbury and Morgan, 2007; reviewed in Stegmeir and Amon, 2004).

The CPC complex is also involved in spindle disassembly. After chromosome segregation, the CPC complex re-localizes to the spindle midzone, where it phosphorylates the microtubule stabilizing protein Bim1, and the dynein regulator She1 (Woodruff et al., 2010). Phosphorylation of Bim1 removes it from the spindle and midzone, at the same time the microtubule depolymerase Kip3 helps shrink interpolar microtubules. She1 phosphorylation by Ipl1 activates She1 toward spindle disassembly, possibly by mediating She1 localization to spindle or astral microtubules. In G1, She1 localizes to astral microtubules, where it inhibits dynein activity by restricting the association of dynein and its activators, p150glued and dynamitin (Woodruff et al., 2009). This inhibition is relieved at anaphase onset, when dynein activity is required to position the spindle across the bud neck and extend it along the mother-daughter bud axis. Increased dynein activity correlates with an absence of She1 on astral microtubules. However, it is unclear whether Ipl1 phosphorylation of She1 directly affects She1 localization to the spindle, astral microtubules, or bud neck, or whether it may indirectly contribute to She1 localization, for example, by promoting nuclear import or export.

In addition to She1, numerous mitotic proteins localize to the bud neck. The cytokinetic ring apparatus, composed of septins, myosin I, and actin machinery, is assembled at the bud neck in S-phase, and promotes abscission of cells at the completion of anaphase, after the spindle has disassembled. Work within the past five years has uncovered a checkpoint, the NoCut pathway, which ensures cytokinesis is delayed until chromosome segregation has occurred (Norden et al., 2006; Mendoza et al., 2009; Neurohr et al., 2011). The NoCut pathway coordinates signaling between the spindle and bud neck through the localization of two anillin-like proteins, Boi1 and Boi2. In addition to localizing at sites of polarized growth and to functioning in cell polarity and bud emergence, Boi1 and Boi2 localize to the bud neck during cytokinesis in an Ipl1-dependent manner (Norden et al., 2006). It has been proposed that active, chromatin- or midzone-associated Ipl1 excludes Boi1 and Boi2 from the nucleus, allowing them to localize to the cortex and inhibit septin funtion and cytokinesis. However, after chromatin has cleared the midzone in telophase, Ipl1 is no longer active towards Boi1 and Boi2, they are sequestered in the nucleus, and cytokinesis progresses. This model is corroborated by experiments on cells expressing a non-cleavable form of cohesin. Such cells abort cytokinesis presumably through activation of the NoCut pathway, and eventually re-enter the cell cycle as bi-budded cells. However, in *boi1Δ boi2Δ* cells, the NoCut pathway is compromised, and cells are unable to delay abscission until chromatin has been cleared from the midzone. Cytokinesis progresses prematurely, resulting in a DNA “cut” phenotype. Separase is also implicated in the NoCut pathway, but interestingly, it is its downstream role in Cdc14 release and not in cohesin cleavage that seems important for NoCut signaling. In the separase mutant *esp1-1*, chromosomes do not segregate properly, but cytokinesis is not delayed, again resulting in the “cut” phenotype. Mutants that affect Ipl1 activity also impact signaling through the

NoCut pathway. A phospho-defective form of Sli15, Sli15-6A, localizes to the midzone and mimics FEAR- and Cdc14- dependent deactivation of Ipl1. A *SLI15-6A* mutant, or even a catalytically-dead allele of *ESP1*, *Esp1*^{C1531A}, rescued the "cut" phenotype of *esp1-1* cells by restoring NoCut signaling, thereby coupling the timing of mitotic exit with cytokinesis (Norden et al., 2006). These and other results model the CPC as a sensor when it is at the midzone; in the presence of chromatin, Ipl1 remains active and enforces delay of cytokinesis. However, when chromatin has cleared the midzone, Ipl1 activity diminishes and cytokinesis is licensed (Norden et al., 2006; Mendoza et al., 2009).

Genome-wide high-throughput two-hybrid and synthetic genetic screens have been powerful tools to systematically identify interactions between genes, and to thus implicate a protein in a biological process in which it was previously not known to function (Tong et al., 2004; Wong et al, 2007; Costanzo et al, 2010). By evaluating these types of genetic interactions, I identified *SHO1* as a candidate gene functioning in the process of spindle disassembly. A transmembrane osmosensor, Sho1 is part of the Hog (High Osmolarity Glycerol response) pathway, a mitogen-activated protein kinase (MAPK) signaling cascade that ultimately activates Hog1 for nuclear entry (reviewed in Clotet and Posas, 2007, and Hohmann et al., 2007). In the nucleus, Hog1 influences the transcription of genes required for osmostress response, namely those involved in the intracellular production of glycerol as a counterbalancing osmolyte (Reiser et al., 2000; Westfall et al., 2008). Like Boi1 and Boi2, Sho1 localizes to the bud neck and sites of polarized growth, and appears to affect the localization of Boi1 and Boi2 to the bud neck during anaphase and cytokinesis. *sho1Δ* cells also exhibit spindle morphologies reminiscent of *she1Δ* spindles; spindle disassembly is delayed in these mutants until the cytokinetic ring contracts and breaks the spindle. A model currently under investigation is that Sho1 may affect She1 activity or localization through Boi2, and that these interactions are important for spindle positioning across the bud neck, and for spindle disassembly during anaphase. This would represent a novel function for Sho1, distinct from its role in osmostress signaling. Suggestion of a mitotic role for Sho1 also came from work with a MEN mutant, *cdc15-2*. The temperature-sensitivity of a *cdc15-2* can be suppressed by osmostressing the cells with media containing sorbitol (Reiser et al., 2006). This suppression is dependent on *SHO1*, *HOG1*, and the MAPKK *PBS2*, and operates through a mechanism that involves Cdc14 release by the FEAR pathway. However, the mechanism by which Sho1 promotes Cdc14 release under stress conditions, as well as Sho1's role in mitotic exit during non-stress conditions, has not been well characterized.

Chapter 2: An environmental sensing pathway contributes to spindle disassembly in budding yeast

Introduction

Microtubule dynamics play important roles in every stage of mitosis. In early M phase, microtubules help drive the separation of Microtubule Organizing centers (MTOCs) to establish a bipolar spindle. In yeast, the MTOC is referred to as the Spindle Pole Body (SPB). These interpolar microtubules (ipMTs) lengthen as the organizing centers (MTOCs/SPBs) separate and opposing forces are generated by microtubules attached through the kinetochore to each chromatid (kinetochore microtubules, kMTs). Together, the MTs form an array called the mitotic spindle. A third class of microtubules, astral microtubules (aMTs), attach the SPBs to the cell cortex and help position the spindle along the mother-bud axis in yeast or perpendicular to the division plane in mammalian cells. Over the course of mitosis, the dynamics of microtubules are modulated by several classes of proteins, including +TIP proteins (such as EB1/Bim1) which stabilize microtubule plus ends and promote growth, crosslinking proteins (such as Ase1 and Cin8) which stabilize lateral interactions between ipMTs of the midzone, and motor proteins (such as Kar3 and dynein) (reviewed in Westermann et al., 2007 and Khmelinskii and Schiebel, 2008).

She1 is one important regulator of microtubule dynamics in budding yeast and it appears to have several functions in the cell (Markus et al., 2012, Bergman et al., 2012, Woodruff et al., 2009, and Woodruff et al., 2010). Beginning in G1, She1 localizes to the SPB and restricts the activity of dynein by inhibiting its interaction with dynactin until anaphase, when dynein is required for spindle positioning prior to elongation into the bud (Woodruff et al., 2009). In M phase, She1 also localizes to the kinetochore and along spindle microtubules, and to the bud neck (Woodruff et al., 2009 and Woodruff et al., 2010). In anaphase of mitosis, She1 promotes spindle disassembly; *she1Δ* cells rely on contraction of the cytokinetic ring to induce spindle breakage, and spindle halves depolymerize at reduced rates in these *she1Δ* cells (Woodruff et al, 2010).

Following chromosome bi-orientation and satisfaction of the Spindle Assembly Checkpoint (SAC), several processes must coordinate anaphase and spindle disassembly. At a regulatory level, these include attenuating Cdk1 activity by cyclin B destruction, and increasing the availability and activity of Cdc14 phosphatase via the FEAR and MEN pathways, to oppose Cdk1 activity and shift the cell into anaphase (Taylor et al., 1997, Visintin et al., 1998, reviewed in Stegmeier and Amon, 2004 and Sullivan and Morgan, 2007). The mitotic kinase Ipl1, as part of the four subunit Chromosomal Passenger Complex (CPC) also re-localizes to the spindle midzone at anaphase onset (Buvelot et al., 2003, Nakajima et al., 2011), where it participates in the NoCut pathway, a checkpoint that ensures that segregating chromosomes have cleared the midzone prior to cytokinetic ring contraction (Norden et al., 2006, Medoza et al., 2009). The NoCut pathway monitors the presence of chromatin in the midzone via the activity of midzone-localized Ipl1.

In contrast to spindle assembly, a maturation process that occurs from G1 through metaphase and can span 30-40 min, spindle disassembly is rapid and irreversible, occurring in only a few minutes at the end of anaphase (Maddox et al., 2000). At least three pathways contribute to spindle disassembly (Woodruff et al., 2010). One pathway involves the APC^{Cdh1} dependent degradation of midzone proteins such as Cin8 and Ase1, which stabilize interpolar microtubules, leading to separation of

the spindle halves. In a second pathway, the microtubule depolymerase Kip3 destabilizes microtubules and promotes shrinkage of spindle halves. A third pathway is dependent on the activity of Ipl1 towards spindle proteins. Phosphorylation of the microtubule stabilizing protein Bim1 by Ipl1 leads to Bim1 removal from the spindle, and inhibits interpolar microtubule growth. Ipl1 phosphorylation of She1 on five residues is also important for its role in spindle disassembly. Mutating the five residues to phospho-defective alanines (*she1-5A*), or inhibiting Ipl1 function with a temperature-sensitive allele, leads to reduced She1 phosphorylation, and delays in spindle disassembly (Woodruff et al., 2010).

Results

The environmental stress-sensing Hog pathway has genetic and physical interactions with spindle disassembly pathways.

I examined genome-wide synthetic genetic array (SGA) interaction data (Costanza et al., 2010) in an effort to identify additional candidate genes participating in the three known spindle disassembly pathways represented by: *CDH1*, *KIP3*, and *SHE1*. This technique was successfully used in the past to identify novel components of these pathways (Woodruff et al., 2010). I reasoned that a candidate gene which demonstrated synthetic growth defects with genes in any two of the three known pathways would be a candidate to function in the third pathway. I therefore performed pairwise comparisons of gene deletion strains possessing negative genetic interaction scores with *cdh1Δ*, *kip3Δ*, and *she1Δ* (Figure 2.1A). Interestingly, a deletion mutant of the putative osmosensor *SHO1* showed negative genetic interactions with both *cdh1Δ* and *kip3Δ*, which led me to hypothesize that it might function in the *SHE1* branch of the spindle disassembly pathway.

Sho1 is a transmembrane protein component of the Hog (High Osmolarity Glycerol response) pathway that, together with Msb2, acts as the most upstream sensor of osmotic (sorbitol) stress (Maeda et al., 1995, Posas and Saito, 1997, Raitt et al., 2000, Reiser et al., 2000, Cullen et al., 2004, reviewed in Schwartz and Madhani, 2004 and Clotet and Posas, 2007). Cells exposed to sorbitol initiate a Sho1-dependent MAPK (Mitogen Activated Protein Kinase) signaling cascade that requires the scaffold Ste11, and the MAPKK Pbs2. Pbs2 phosphorylation activates the MAPK Hog1, which transiently translocates into the nucleus to stimulate expression of genes involved in glycerol production (Figure 2.1B).

Hog pathway activation has also been implicated in early cell cycle arrest due to Hog1's transcriptional down regulation of the G1 cyclins *CLN1* and *CLN2*, and phosphorylation of the DNA synthesis inhibitor Sic1, which preserves it from degradation and therefore slows S phase (Escote et al., 2004). Moreover, Hog1 activation also delays G2 by cyclin-CDK inhibition (Alexander et al., 2001). In contrast, Hog pathway activation has been shown to promote mitotic exit. Osmotically shocking cells with media containing sorbitol rescues the anaphase arrest of *cdc15-2* mutants in a *SHO1* dependent manner. This rescue has been linked to the release of Cdc14 phosphatase from the nucleolus (Reiser et al., 2006).

Consistent with the hypothesis resulting from the synthetic genetic array approach, I found that there were no synthetic growth defects between mutants in the Hog pathway and a *she1Δ* mutant (Figure 2.1C), which suggests that if Hog pathway mutants do function in spindle disassembly, then it is likely through the She1 pathway and not the Cdh1 or Kip3 pathways. I also examined physical and genetic interaction profiles of Hog pathway components (Figure 2.2) and noticed that in high-throughput genome wide screens (Costanzo et al., 2010, Tong et al., 2004), the *sho1Δ* mutant showed multiple genetic interactions with mitotic genes including those encoding microtubule associated proteins, APC subunits (in addition to Cdh1), kinetochore subunits, and chromatin remodeling complexes. While these genetic interactions appeared specific to Sho1, and not to the Hog pathway in general, other components of the Hog pathway exhibit physical interactions with proteins in cell polarity pathways, and bud neck-localized proteins which have been implicated in cytokinesis (Costanzo et al., 2010, Tong et al., 2004). Sho1 itself localizes to the cell cortex of emerging bud tips and growing buds, and to the bud neck during cytokinesis (Raitt et al., 2000). Interestingly, the NoCut pathway proteins Boi1 and Boi2 show similar localization patterns, as well as genetic interactions with dynein subunits (Norden et al., 2006, Costanzo et al., 2010, Tong et al., 2004). Additionally, Boi2 physically interacts with Sho1 and Msb1 (Tong et al., 2002, Drees et al., 2001).

Figure 2.1

A

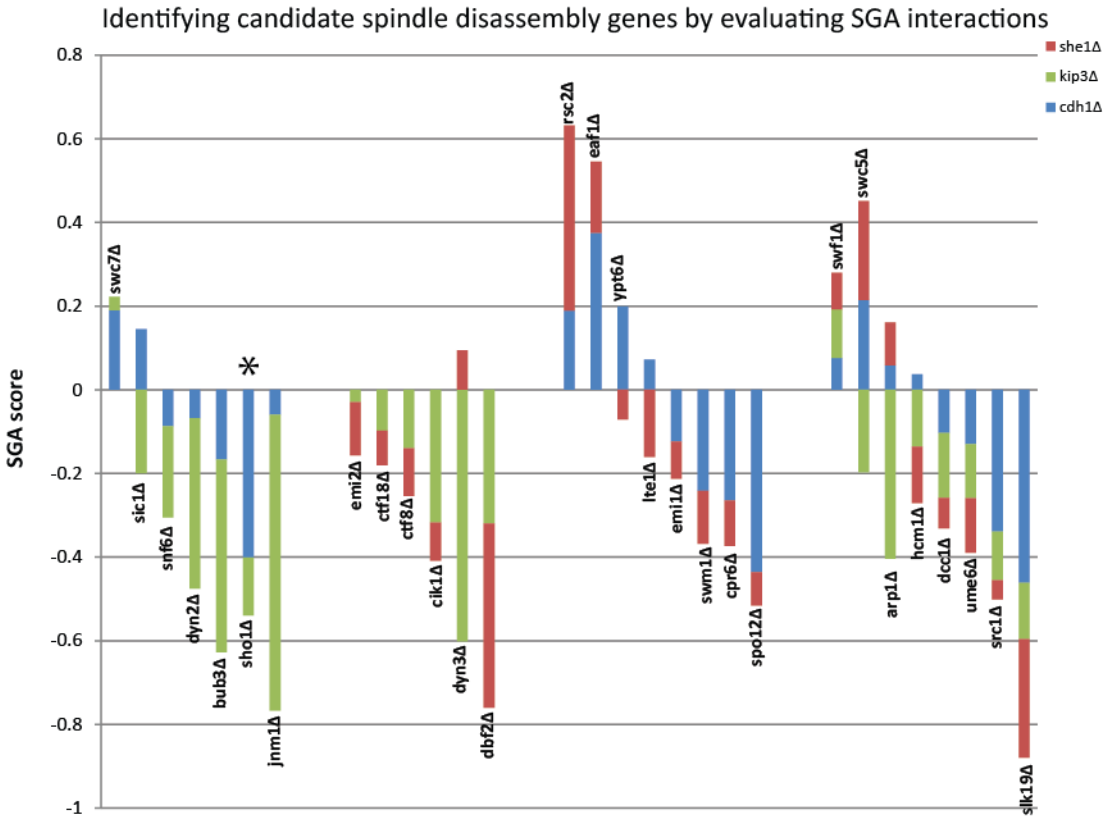

B

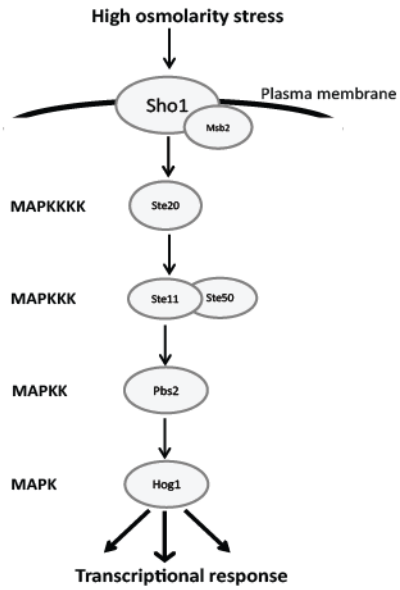

C

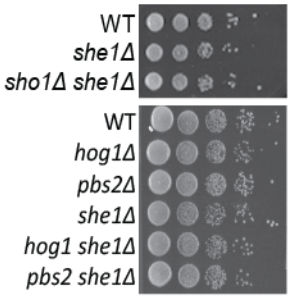

Figure 2.1 The transmembrane osmosensor Sho1 and the associated Hog MAPK pathway are candidates for regulating spindle disassembly. (A) Comparison of Synthetic Genetic Array (SGA) scores for genes that showed synthetic interactions with deletion mutants: *she1Δ*, *kip3Δ*, or *cdh1Δ*. For each gene represented by a bar on the graph, the SGA scores between that gene and *she1Δ* (in red), *kip3Δ* (green), and/or *cdh1Δ* (blue) are represented by the magnitude of the bar in the graph. Negative values represent negative genetic interactions (the double mutant cells grew worse than either single mutant cell), and positive values represent positive genetic interactions (the double mutant cells grew better than either single mutant cells). Hybrid blue and green bars indicate genes that are likely involved in the She1 pathway of spindle disassembly; hybrid green and red bars indicate genes that are likely involved in the Cdh1 pathway; hybrid red and blue bars indicate genes that are likely involved in the Kip3 pathway. *SHO1* is designated by an asterisk. SGA scores are from Costanzo et al., 2010. (B) Schematic of the Sho1 MAPK cascade (adapted from Reiser et al., 2000). (C) Serial dilutions of indicated strains were spotted onto YPD plates and grown at 25°C for three days.

Figure 2.2

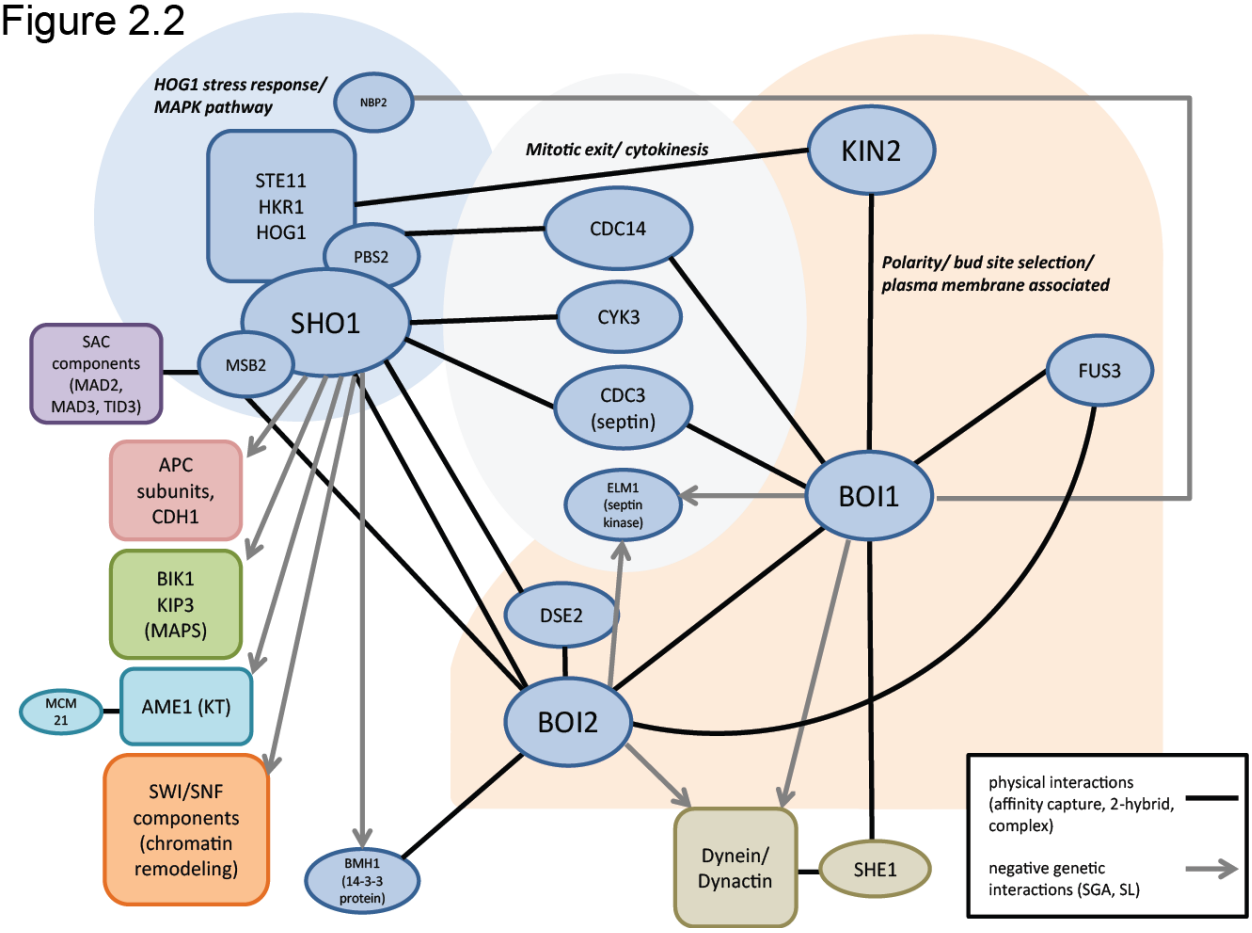

Figure 2.2 Interaction map between genes/proteins of interest. Schematic of genetic interactions (grey arrows) and physical interactions (black lines) between genes/proteins involved in the Hog pathway (upper left), kinetochore and spindle organization (lower left), cytokinetic ring organization and function (middle), and polarity pathways (right). Interactions were described using annotations curated by the SGD database (www.yeastgenome.org), personal annotations from literature, and data from within our lab (Woodruff, unpublished).

Hog pathway and *boi2Δ* mutant cells exhibit spindle disassembly defects

I investigated whether *sho1Δ*, *pbs2Δ*, and *hog1Δ* mutants showed any spindle disassembly defects. I used a Myo1-GFP fusion protein to identify the cytokinetic ring, and a GFP-Tub1 protein to identify the mitotic spindle. I used these two fluorescent proteins in conjunction in order to determine when the spindle separated into halves relative to the time when the cytokinetic ring began to constrict (Figure 2.3 A-E). As previously described, wild type spindles broke to form two half spindles before the cytokinetic ring began to constrict (Fig. 2.3A, left panel, and Woodruff et al., 2010). This can be seen in a kymograph showing GFP-Myo1 fluorescence over time (Fig. 2.3A, right panel), where the yellow arrowhead indicates when the spindle breaks. However, similar to *she1Δ* spindles, *sho1Δ*, *pbs2Δ*, and *hog1Δ* spindles broke into half spindles only after the cytokinetic ring began to constrict (Fig. 2.3 B-E). I quantified this phenotype by measuring the length of Myo1-GFP fluorescence, corresponding to the diameter of the cytokinetic ring, before the spindles had broken and the cytokinetic ring was at its maximum size (Fig. 2.3H, initial length, L_i). I also measured the length of Myo1-GFP fluorescence when the spindle broke into half spindles (length at break, L_b), and compared L_b/L_i ratios. The wild type L_b/L_i ratio was 0.97 +/-0.009 (Fig. 2.3H and Table 2.1), reflecting the observation that the cytokinetic ring had not begun to constrict when the spindle broke. However, L_b/L_i ratios for *she1Δ*, *sho1Δ*, *pbs2Δ*, and *hog1Δ* mutants were 0.68 (+/- 0.027), 0.67 (+/- 0.030), 0.64 (+/- 0.021), and 0.59 (+/- 0.021), respectively. This indicates that the cytokinetic ring had constricted 30-40% by the time the spindles broke in these cells.

Because of the many genetic and physical interactions between the Hog pathway, NoCut pathway, and She1, I wanted to determine if *boi1Δ* and *boi2Δ* mutants showed spindle disassembly phenotypes. Strikingly, *boi2Δ* spindles showed the same delay in spindle disassembly that Hog pathway and *she1Δ* mutants did; the L_b/L_i ratio for *boi2Δ* cells was 0.75 +/- 0.025 (Fig. 2.3G-H and Table 2.1). However, I determined that *boi1Δ* spindle disassembly occurred identically to wild type, as *boi1Δ* spindles disassembled before ring contraction, and the the L_b/L_i ratio for *boi1Δ* cells was 0.97 +/- 0.007 (Fig. 2.3 F and H, and Table 2.1).

Figure 2.3

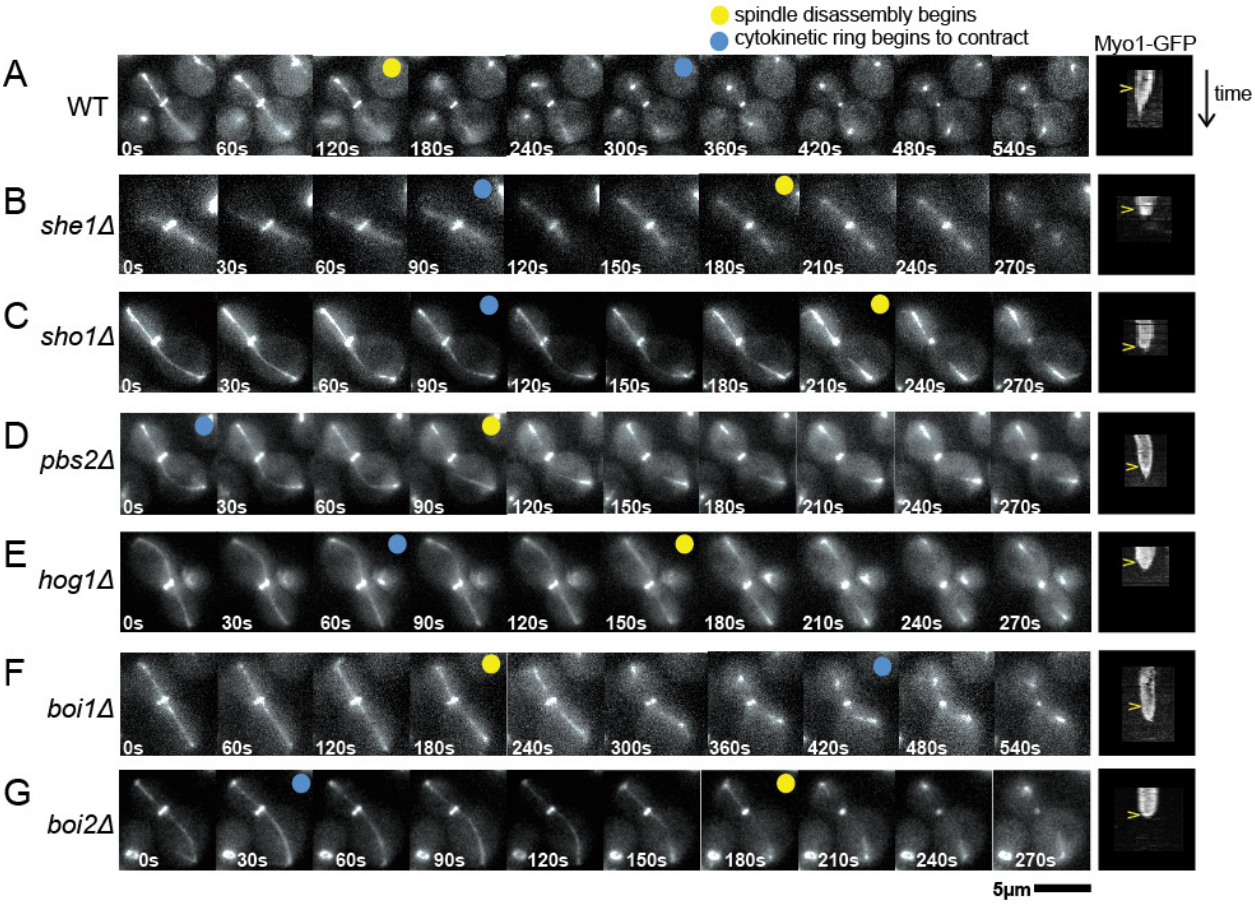
spindle disassembly begins
cytokinetic ring begins to contract
Myo1-GFP
time
A
WT
0s 60s 120s 180s 240s 300s 360s 420s 480s 540s
B
she1Δ
0s 30s 60s 90s 120s 150s 180s 210s 240s 270s
C
sho1Δ
0s 30s 60s 90s 120s 150s 180s 210s 240s 270s
D
pbs2Δ
0s 30s 60s 90s 120s 150s 180s 210s 240s 270s
E
hog1Δ
0s 30s 60s 90s 120s 150s 180s 210s 240s 270s
F
boi1Δ
0s 60s 120s 180s 240s 300s 360s 420s 480s 540s
G
boi2Δ
0s 30s 60s 90s 120s 150s 180s 210s 240s 270s
5μm

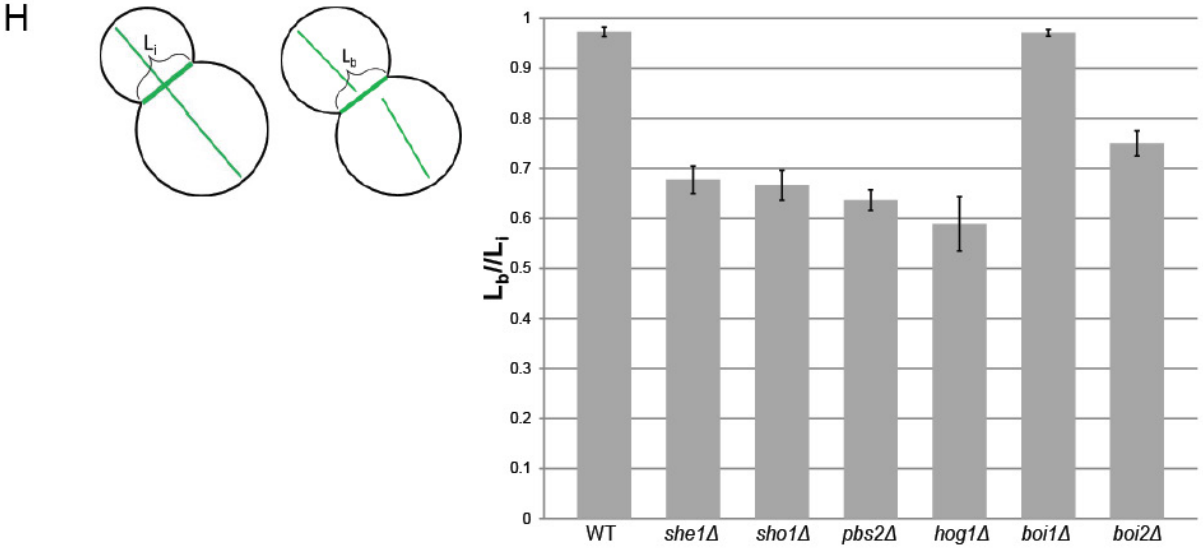
H
L_i
L_b
L_b/L_i
0
0.1
0.2
0.3
0.4
0.5
0.6
0.7
0.8
0.9
1
WT
she1Δ
sho1Δ
pbs2Δ
hog1Δ
boi1Δ
boi2Δ

Figure 2.3 Cytokinetic ring contraction precedes spindle disassembly in Hog pathway mutants and *boi2Δ* cells. (A-H) Left panels: time-lapse images of indicated strains possessing integrated *GFP-TUB1* and *MYO1-GFP* markers, to label the spindle and bud neck, respectively. Images were captured 30 sec apart at 23°C, but have been selected to show similar events for each strain. Right panels: kymograph showing the cytokinetic ring over time (read from top to bottom; pixels in the kymographs are 30 sec apart). Yellow arrowheads indicate when the spindle breaks. (I) Graphical representation of Table 2.1. Initial length of Myo1-GFP fluorescence was measured when the bud neck was the widest (L_i), and when the spindle broke (L_b). L_b/L_i ratios were plotted (error bars represent S.E.M.)

Table 2.1

	L_b/L_i (SEM)
WT	0.97 (0.009)
she1Δ	0.68 (0.027)
sho1Δ	0.67 (0.030)
pbs2Δ	0.64 (0.021)
hog1Δ	0.59 (0.054)
boi1Δ	0.97 (0.007)
boi2Δ	0.75 (0.025)

Table 2.1: Cytokinetic ring contraction precedes spindle disassembly in Hog pathway mutants and *boi2Δ* cells. *GFP-TUB1 MYO1-GFP* strains of the indicated genotypes were imaged as in Figure 2.3. Initial length of Myo1-GFP fluorescence was measured when the bud neck was the widest (L_i), and when the spindle broke (L_b). L_b/L_i ratios were determined. A model I analysis of variance test produced p-values of <0.001 when the wild type ratio was directly compared to mutants, except for the *boi1Δ* mutant, which had a p-value of 0.872.

I also studied the kinetics with which mitotic half spindles depolymerized in these Hog pathway and NoCut pathway mutants. Previous work used analysis of microtubule depolymerization rates and the frequency of microtubule rescue events to help define three spindle disassembly pathways present in wild type cells and essential for viability (Woodruff et al., 2010). I noticed that prior to spindle breakage, the spindles of cells with a *sho1Δ*, *pbs2Δ*, *hog1Δ*, or *boi2Δ* mutation often bowed and bent severely (Fig. 2.4 C-E, G). When the spindles broke, they often broke in the interior of the cell rather than in the wild type location of the site of cytokinesis. It is possible that a weak "stress point" was introduced where the spindle bowed, and bending at that location resulted in spindle breakage. This phenotype was similar to that seen for *she1Δ* spindles, but was distinct from spindle breakage for wild type and *boi1Δ* cells, wherein the spindles remained straight and broke near the site of cytokinesis (Fig. 2.4 A-B, F).

Half spindle depolymerization rates also reflected a similarity between a *she1Δ* mutant, and *sho1Δ*, *pbs2Δ*, *hog1Δ*, or *boi2Δ* mutant cells (Table 2.2). All of these mutants showed reduced rates of spindle disassembly on the same order as the *she1Δ* mutant, consistent with the conclusion that these genes function in the same pathway within the cell. As another example of the functional difference between *boi1Δ* and *boi2Δ* mutants, I did not see a change in *boi1Δ* half spindle shrinkage rates. These results constitute one of only a few differences noted between *boi1Δ* and *boi2Δ* mutant cells, and suggest distinct functions for Boi1 and Boi2. I could not evaluate spindle phenotypes of *boi1Δ boi2Δ* spindles because the double mutant is inviable in our strain background.

Figure 2.4

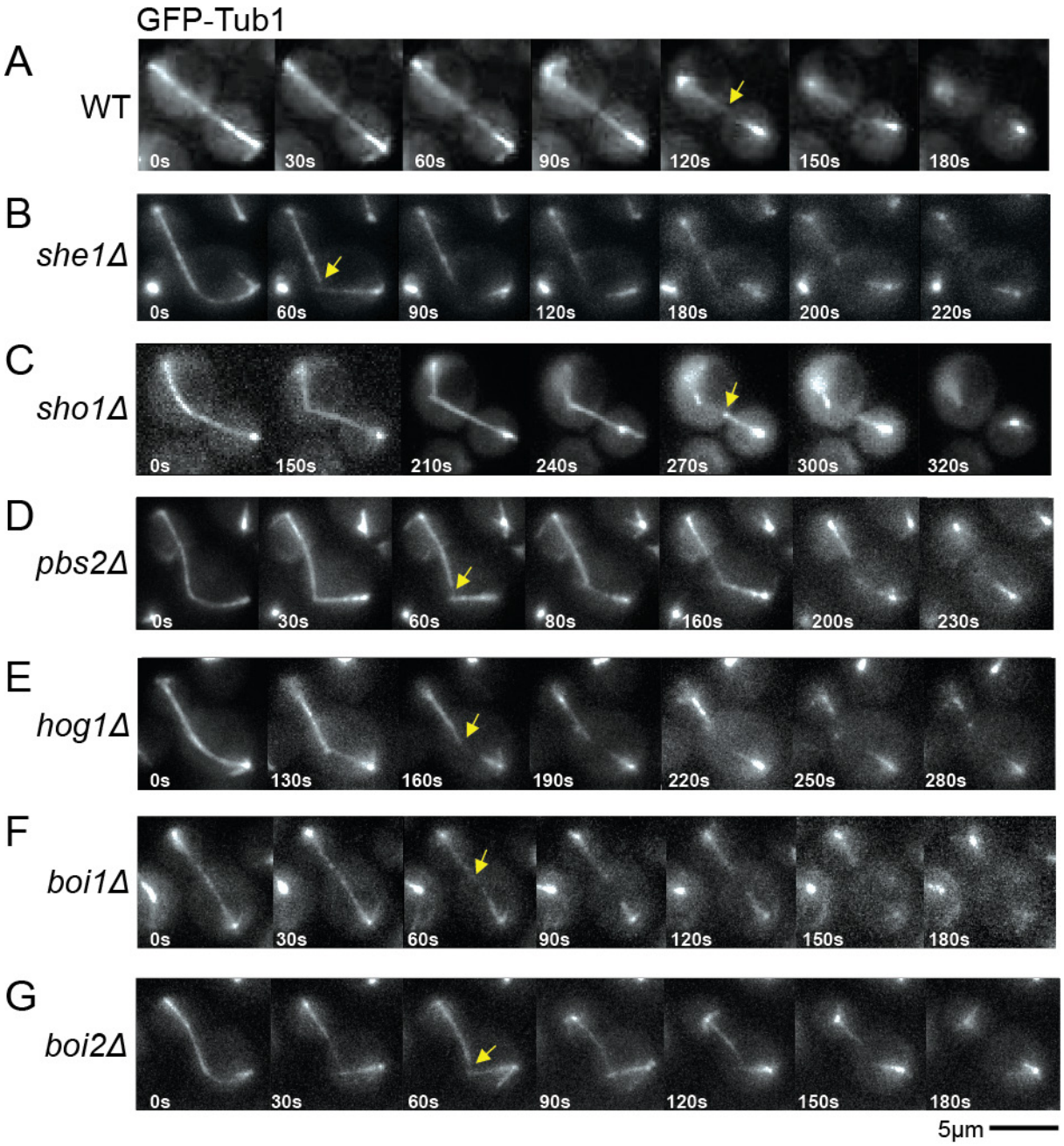

Figure 2.4 Spindle disassembly is delayed in Hog pathway mutants and *boi2Δ* cells. (A-G) Time-lapse images of strains expressing GFP-Tub1 to monitor spindle disassembly. Images were captured 10sec apart at 23°C, but have been selected to show similar events for each strain. Yellow arrows indicate when the spindle breaks.

Table 2.2

	half-spindle shrinkage rate (μm/s)	recovery frequency (F_{rec}/s)	n
WT	0.064 (+/- 0.003)	0.006	116
she1Δ	0.037 (+/- 0.003)	0.006	110
sho1Δ	0.034 (+/-0.002)	0.006	117
hog1Δ	0.033 (+/-0.004)	0.006	102
pbs2Δ	0.035 (+/-0.003)	0.014	233
boi1Δ	0.061 (+/-0.005)	0.005	50
boi2Δ	0.037 (+/- 0.002)	0.006	125

Table 2.2: Half-spindle depolymerization rates are decreased in Hog pathway mutants and in *boi2Δ* cells. GFP-Tub1 expressing strains were imaged every 10 sec, and lengths of half-spindles were measured at each time point after the spindles broke. Recovery events were scored each time a half-spindle switched from shrinking to growing. Shrinkage rates were calculated from the slope of the half-spindle lengths when plotted versus time (mean +/- S.E.M.). A model I analysis of variance test produced p-values of <0.001 when the wild type shrinkage rate was directly compared to the rates for mutants, except for the *boi1Δ* mutant, which had a p-value of 0.53.

Boi1 and Boi2 are mislocalized from the bud neck in Hog pathway mutants

I used a genomically integrated GFP tag fused to either Boi1 or Boi2 to observe the localization of these proteins in Hog pathway mutants. In *sho1Δ, pbs2Δ*, and *hog1Δ* cells, I saw a polarized distribution of Boi1 and Boi2. As previously reported, Boi1 and Boi2 localized to the membrane of daughter cells as buds emerged in S phase and continued growing during G2 (Norden et al., 2006 and data not shown). However, in large budded cells (late M phase), all of the detectable Boi1 and Boi2 re-localized to the bud neck in approximately 55% of wild type cells (Fig. 2.5). Additionally, a smaller but significant portion of large budded wild type cells did not display Boi1 or Boi2 at the bud neck nor elsewhere on the membrane; in approximately 40% of cells for Boi1-GFP, and 30% of cells for Boi2-GFP, the GFP fusion proteins could not be detected anywhere in the cell. However, in *sho1Δ, pbs2Δ*, and *hog1Δ* cells, I found that both Boi1 and Boi2 were mislocalized from the bud neck of large-budded cells. In *sho1Δ* cells, Boi1 was entirely displaced from the bud neck, and was randomly distributed between the mother cell and bud (Fig. 2.5A). Boi2 only partially localized to the bud neck in *sho1Δ* cells, although it appeared to be recruited to the membrane near the bud neck more so than Boi1. In *pbs2Δ* and *hog1Δ* cells, Boi1 and Boi2 were only able to localize to the bud neck in a wild type fashion less than 20% of the time. Most often, these cells displayed additional patches of Boi1 and Boi2 elsewhere in the cell. These patches appeared membrane associated and often occurred adjacent to the bud neck, although they were also found along the plasma membrane, away from the bud neck (Fig 2.5A). Neither Boi1 nor Boi2 was mislocalized from the bud neck in *she1Δ* cells. I scored each genotype for mislocalization of Boi1 and Boi2, and the results are shown in Fig. 2B.

Sho1 is a transmembrane protein which localizes to the bud neck (Raitt et al., 2000), and it is possible that deleting it causes a change in membrane integrity, or causes general disorganization of the bud neck that prevents proteins from localizing properly. Therefore the mislocalization of Boi1 and Boi2 could be an indirect consequence of upsetting the structural integrity of the bud neck. To evaluate whether this was the case, I checked the localization of the septin Cdc3, a component of the cytokinetic ring machinery (Madden and Snyder, 1998), in Hog pathway mutants. In *sho1Δ, pbs2Δ*, and *hog1Δ* mutant cells, Cdc3-GFP localized to the bud neck in a wild type manner (Fig. 2.6), even in cells that appeared to have multiple bud necks as a result of failed cell divisions. This suggests that the mislocalization of Boi1 and Boi2 in Hog pathway mutants is specific, and not a consequence of general disorganization of the bud neck.

Figure 2.5

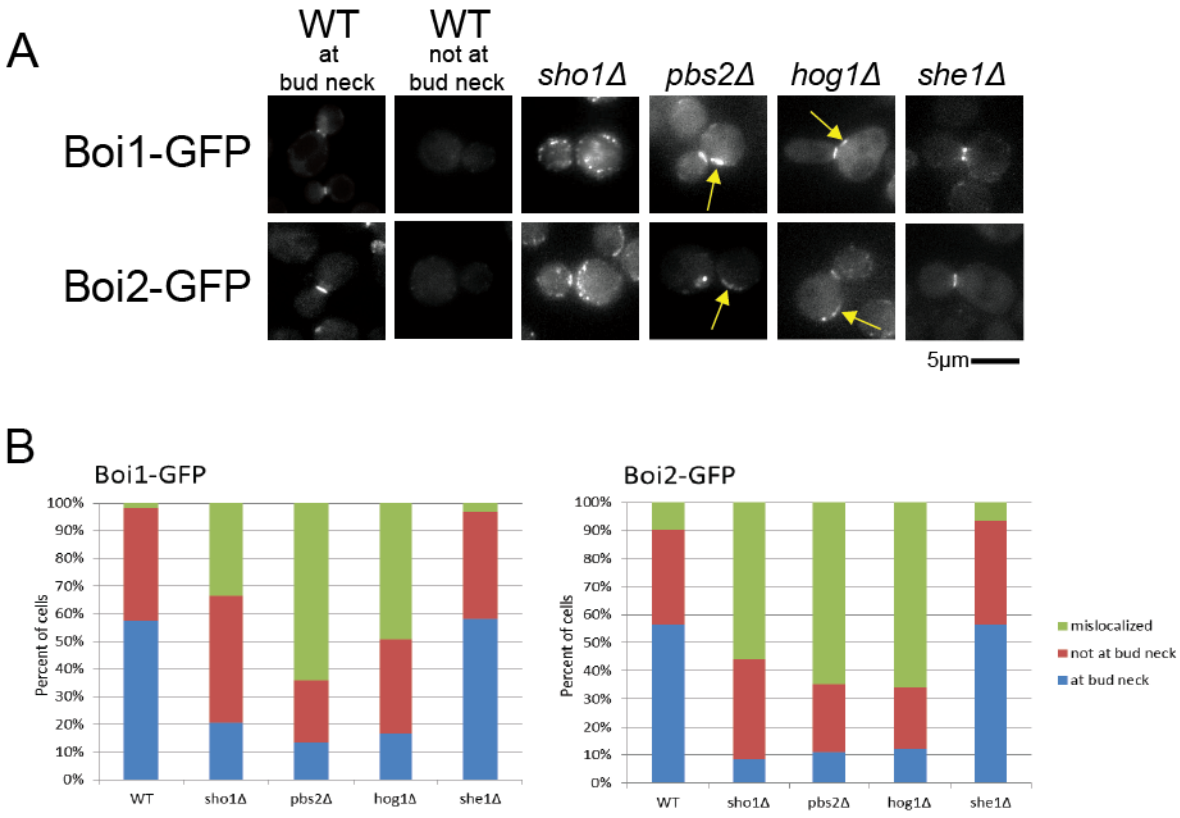

Figure 2.5 Boi1 and Boi2 are mislocalized in Hog pathway mutants. (A) Epifluorescent images of live large-budded cells with the indicated genotype and carrying endogenously tagged Boi1-GFP (top panels) or Boi2-GFP (bottom panels). Yellow arrows indicate patches of Boi1 or Boi2 that are mislocalized from the bud neck. (B) Quantitation of Boi1 and Boi2 mislocalization. Approximately 130 large-budded cells from 3 different days were scored for each strain. "At bud neck" indicates Boi1 or Boi2 localized properly to the bud neck; "not at bud neck" indicates no Boi1 or Boi2 was present at the bud neck, but was not detectably mislocalized (as in the "WT not at bud neck" panels shown in 2.5A); "mislocalized" indicates Boi1 or Boi2 either localized away from the bud neck, or to other regions of the cell in addition to the bud neck.

Figure 2.6

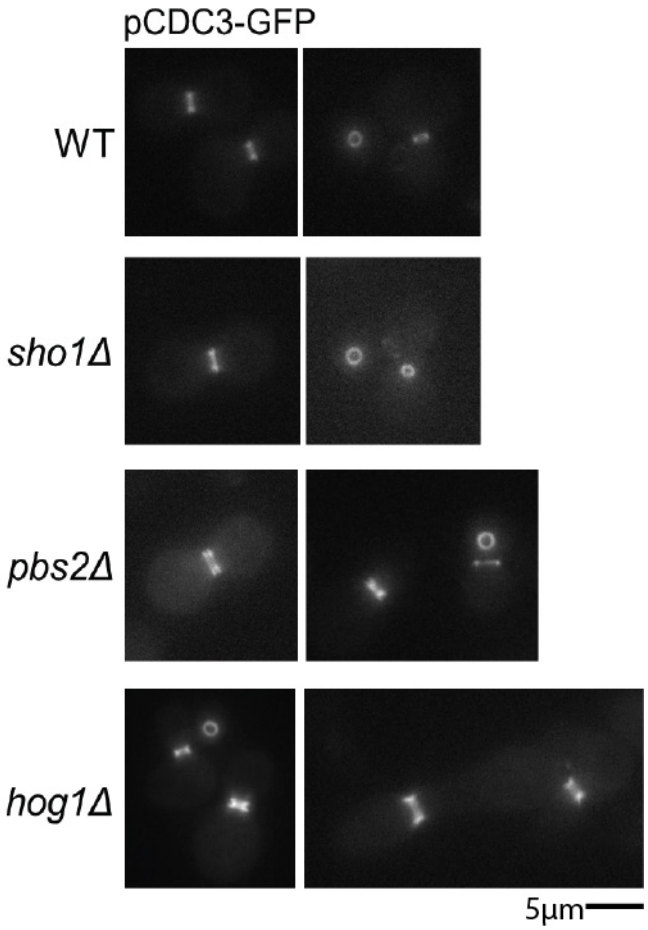

Figure 2.6 The septin Cdc3 is not mislocalized from the bud neck of Hog pathway mutants. Strains of the indicated genotype were transformed with plasmid-borne *CDC3-GFP* and were imaged with epifluorescence microscopy. Left and right panels were imaged under the same conditions, but show the bud neck from different angles (side-on or end-on).

The mislocalization of Boi1 and Boi2 in *sho1Δ, pbs2Δ*, and *hog1Δ* cells is somewhat different than what has been previously reported (Norden et al., 2006). In the previous study, the authors reported the same polarized localization of Boi1-GFP and Boi2-GFP that I found in S phase and G2 cells. They also reported seeing re-localization of Boi1 and Boi2 to the bud neck of large-budded cells, as I did. However, they additionally detected Boi1 and Boi2 in the nucleus of G1 cells that had been arrested with α-factor, and in the nucleus of *ipl1-321* cells at the non-permissive temperature. Boi1 and Boi2 are *in vivo* targets of Cdk1 (McCusker et al., 2007), and while they possess several Ipl1 phosphorylation consensus sites, mutating these sites does not alter Boi1 and Boi2 localization (Norden et al., 2006). In their NoCut pathway model, Norden et al. proposed that Ipl1 activity is required for the shuttling of Boi1 and Boi2 between the nucleus and bud neck, where they serve as checkpoint proteins and inhibit abscission. This model suggests that Boi1 and Boi2 are able to relate the activity of Ipl1 at the spindle midzone, thought to derive from Ipl1's association with unsegregated chromatin (Mendoza et al., 2009), to the bud neck in order to delay cytokinesis until chromatin is segregated. However, I never observed an enrichment of Boi1-GFP or Boi2-GFP in the nucleus, either in asynchronously growing cells, or in cells arrested in G1 with α-factor (data not shown). Additionally, I did not see enrichment of genomically tagged, endogenously expressed Boi2-3GFP in the nucleus (data not shown). It is unclear why I did not see these proteins in the nucleus. Boi1-GFP and Boi2-GFP photobleach quite quickly, making it difficult to take extended time-lapse movies of cells expressing these fusion proteins. In short movies, and even in Boi2-3GFP movies, however, I still did not see fluorescence in the nucleus. It could be that nuclear localization of Boi1 and Boi2 is transient, and I simply missed capturing images at critical time points. Alternatively, it could be that due to expression levels in our strain background, there was not enough Boi1-GFP or Boi2-GFP in the nucleus to detect. It is interesting that a significant percentage of Boi1 and Boi2 did not localize to the bud neck or plasma membrane, even in wild type large-budded cells (at least 20% of cells of all genotypes studied exhibited this phenotype). It might be that the Boi1 and Boi2 in these cells does localize to the nucleus, but the GFP signal is too weak to detect with our cameras. Relatedly, the previously published description of nuclear Boi2-GFP (Norden et al., 2006) was based on imaging cells that expressed Boi2-GFP from a multicopy plasmid. It is possible that this plasmid-borne Boi2-GFP was overexpressed relative to the endogenous Boi2-GFP strains that I imaged, and was either more easily detected in the nucleus, or does not go to the nucleus except when it is overexpressed. Regardless of the nuclear localization phenotypes, the mislocalization phenotypes I see in *sho1Δ, pbs2Δ*, and *hog1Δ* have not been previously documented, and suggest a role for the Hog pathway in recruiting Boi1 and Boi2 to the bud neck. One possibility is that Boi1 and Boi2 physically interact with Sho1 through SH3 domains (Tonikian et al., 2009).

She1 is mislocalized in Hog pathway and *boi2Δ* mutant cells

Because the delay in spindle disassembly for Hog pathway mutants and *boi2Δ* cells was evocative of a *she1Δ* spindle phenotype, I thought it was important to evaluate

She1 protein localization in *sho1Δ, pbs2Δ*, *hog1Δ*, and *boi2Δ* mutants. In wild type cells, She1-3GFP localizes to the SPBs and decorates short, metaphase spindles very brightly. As the spindle begins to elongate in anaphase, however, She1 is cleared from the midzone, and becomes enriched at the spindle poles (Fig. 2.7A). She1 also localizes to the bud neck throughout mitosis until the end of anaphase, but because it is obscured by She1 fluorescence at the spindle, it is difficult to determine whether bud neck intensity changes over the course of mitosis, and precisely when it disappears from the bud neck.

When I examined She1 in *sho1Δ* cells, I found that it still localized to SPBs, the spindle, and the bud neck. Strikingly, it did not undergo the same midzone clearance that She1 undergoes in wild type cells. Instead, She1-3GFP brightly decorated the entire spindle throughout anaphase. Strikingly, in these *sho1Δ* cells, She1 remained associated with the plus ends of depolymerizing microtubules once the spindle broke into spindle halves, a localization pattern never observed in wild type cells (Fig. 2.7B).

In *pbs2Δ*, *hog1Δ*, and *boi2Δ* mutant cells, similar to *sho1Δ* cells, She1 inappropriately localized along the length of the spindle as it elongated (Fig. 2.7C-D, F). However, She1-3GFP did not appear to decorate the entire spindle as densely in *pbs2Δ*, *hog1Δ*, and *boi2Δ* mutants, compared to *sho1Δ* cells. Rather, there were bright patches of She1 along the spindle in *pbs2Δ*, *hog1Δ*, and *boi2Δ* cells that were not excluded from the midzone until the spindle fully elongated (Fig. 2.7C, 12' and15' images, and Fig. 2.7F, 22' and 23' images). Sometimes, however, these patches were not excluded from the midzone at all (Fig. 2.7D, 27' and 36' images). Within populations of each of the *pbs2Δ*, *hog1Δ*, and *boi2Δ* mutants, I saw cells with both localization patterns – some that did finally exclude She1 from the spindle midzone, and some that did not. This was in contrast to *boi1Δ* mutant cells, where She1 localization appeared wild type, further highlighting a difference between *boi1Δ* and *boi2Δ* mutations.

Figure 2.7

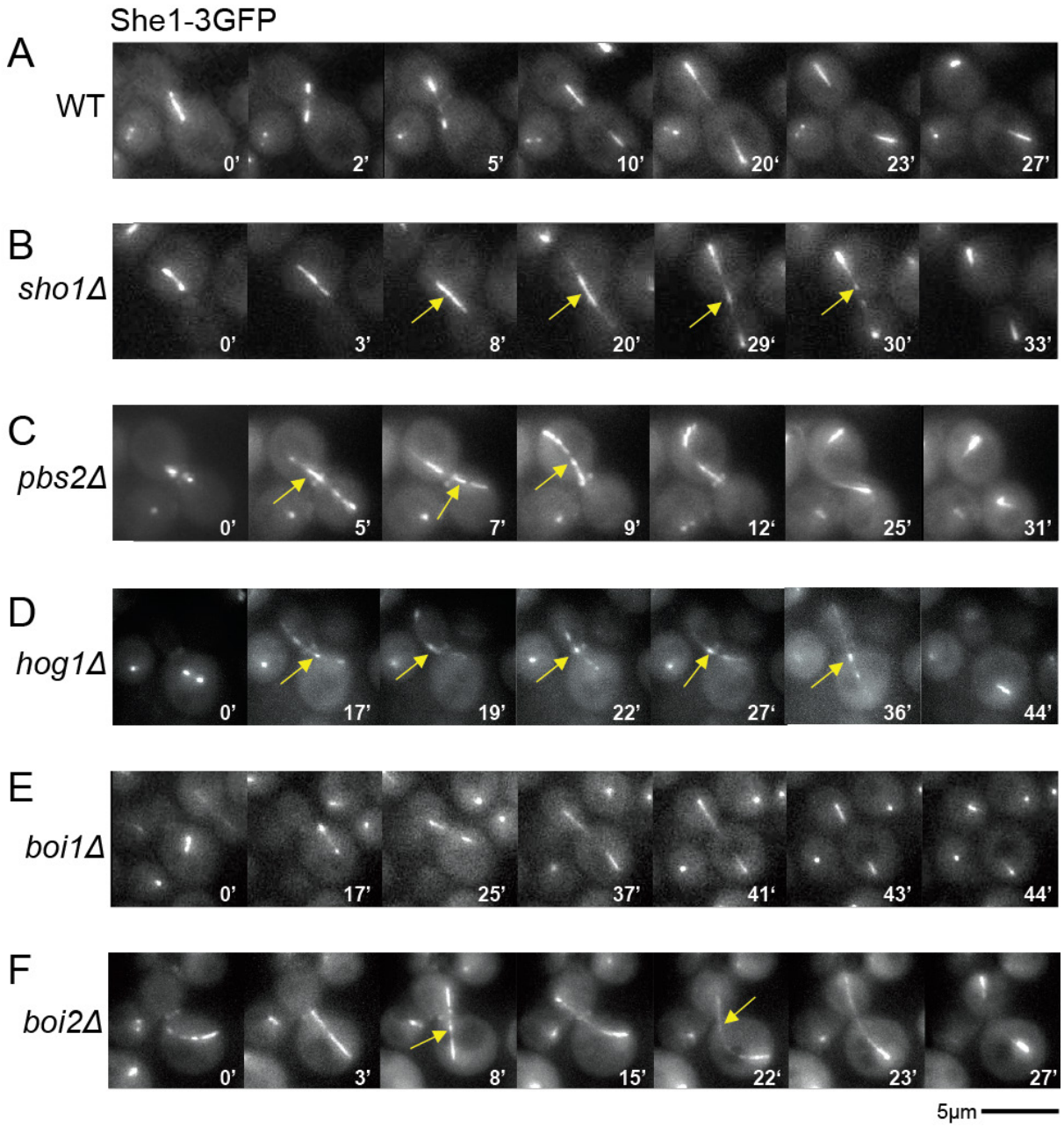

Figure 2.7 She1 is mislocalized along the spindle in Hog pathway mutants and *boi2Δ* cells. (A-F) Time-lapse images of endogenously tagged She1-3GFP strains of the indicated genotype. She1 is present at the bud neck in all strains. Whereas in wild type cells, She1 is cleared from the spindle midzone as the spindle elongates, Hog pathway mutants and *boi2Δ* cells retain She1 at the spindle midzone (yellow arrows).

She1 is displaced from the bud neck of Hog pathway mutants upon sorbitol treatment

The Hog pathway is an environmental stress sensing and response pathway that equips cells with a mechanism to offset increases in turgor pressure by producing intracellular glycerol as an osmolyte (reviewed in Schwartz and Madhani, 2004, and Clotet and Posas, 2007). Sho1 is exclusively membrane localized, and despite possessing a nuclear localization signal, Pbs2 is cytoplasmically localized. Only Hog1, upon phosphorylation and activation by Pbs2, localizes to the nucleus, where it activates transcription of glycerol biosynthesis genes (Brewster et al., 1993, Ferrigno et al., 1998).

Because Hog pathway mutants affected She1 localization to the mitotic spindle, I was interested in determining whether exposing Hog pathway mutants to osmo-stress could also elicit changes in She1 localization. I followed She1-3GFP in *sho1Δ, pbs2Δ*, and *hog1Δ* mutant cells, before and after treatment with 1M sorbitol, an osmo-stressor known to activate the Hog pathway. I looked at large-budded cells in anaphase, with She1 present both on the spindle and at the bud neck (Fig. 2.8). Upon sorbitol treatment, all cells underwent slight shrinkage within 1-2 minutes. Wild type cells retained She1 at the bud neck and spindle after sorbitol treatment (Fig. 2.8A). There was a slight increase in She1-3GFP fluorescence after sorbitol treatment, but the fluorescence was diffuse, making it difficult to determine whether it was due to She1 re-localization, or an artifact of sorbitol treatment. I also examined *boi2Δ* mutant cells under the same conditions (Fig. 2.8B), and found that like wild type cells, She1 was not displaced from the spindle or bud neck of *boi2Δ* cells after sorbitol treatment.

I analyzed *sho1Δ, pbs2Δ*, and *hog1Δ* mutant cells in the same manner. Strikingly, I found that within 2 minutes of sorbitol treatment, these cells displaced She1 from their bud neck (Fig. 2.8 C-E). As in wild type cells, I also found an increase in diffuse She1 fluorescence after treating these mutant cells with sorbitol. In some cells of each mutant genotype, it appeared as though She1 was accumulating in the nucleus, by comparison to the location of the spindle. This is especially apparent in Fig. 2.8G, a *hog1Δ* cell with two spindles. She1 disappeared from the bud neck within 2 minutes of sorbitol treatment, and appeared to concentrate within the large, malformed nucleus over the next several minutes.

Figure 2.8

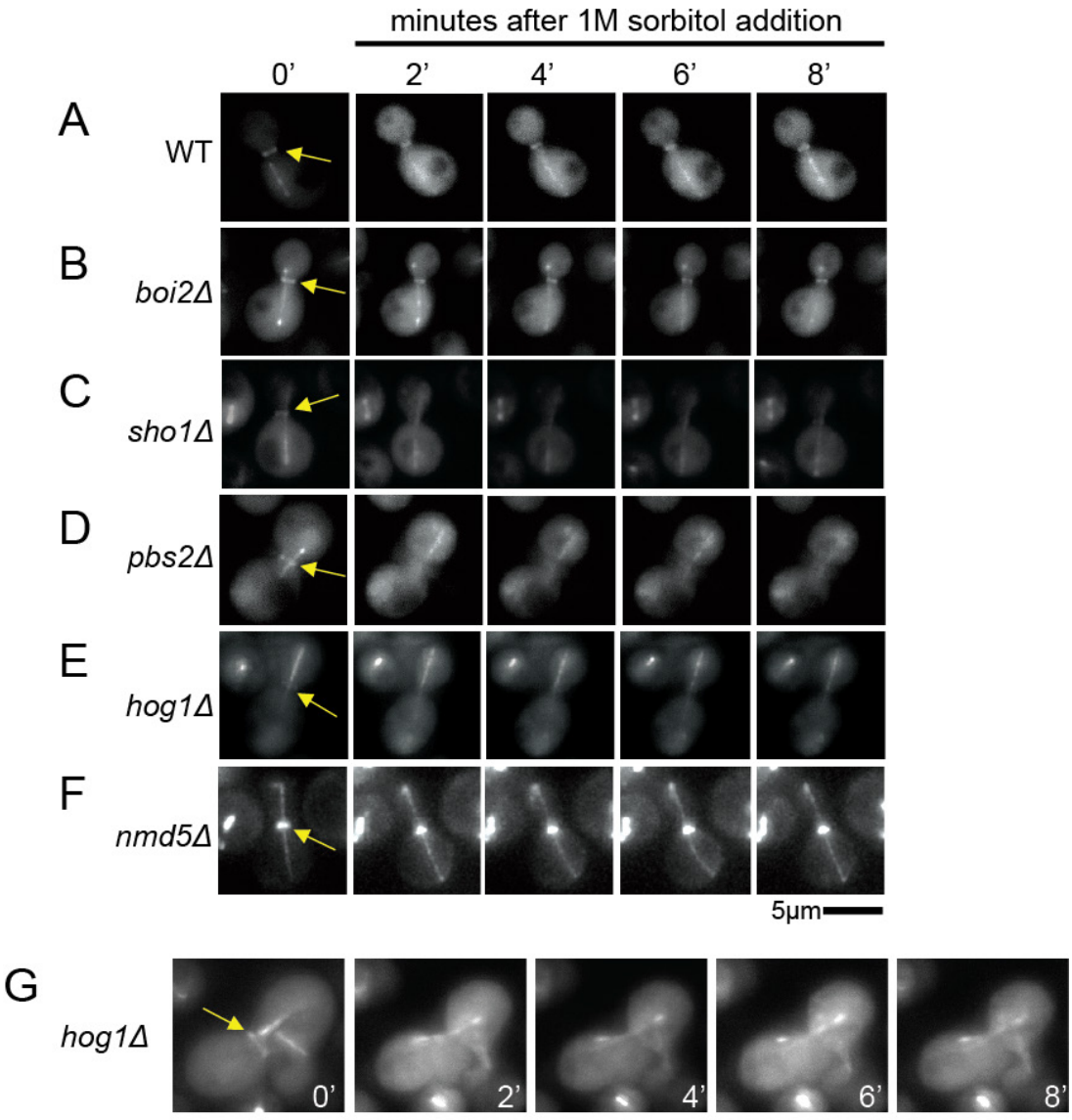

Figure 2.8 She1 is displaced from the bud neck in Hog pathway mutants upon sorbitol treatment. (A-F) She1-3GFP strains of the indicated genotypes were imaged in real time before (at 0’) and directly after replacement of imaging media with imaging media contain 1M sorbitol. Yellow arrows indicate She1 at the bud neck prior to sorbitol treatment. (G) A *hog1Δ* cell treated exactly the same as (E) is shown because it is one of a small percentage of *hog1Δ* cells (~5%) with two spindles. Within two minutes of sorbitol treatment, She1 is displaced from the bud neck.

She1 is phosphorylated in response to sorbitol treatment

To date, no one has described conditions or alleles of She1 that cause the protein to differentially localize to subcellular structures. Even phospho-defective She1, whose Ipl1 phosphorylation sites have been mutated to alanines (She1-5A), still localizes to the bud neck and mitotic spindle. The dramatic mislocalization of She1 from the bud neck of Hog pathway mutants upon sorbitol treatment led me to ask whether She1's change in localization was accompanied by changes in phosphorylation. To address this question, I performed western blots against She1-myc over a time-course after sorbitol treatment (Figs. 2.9 and 2.10). I used a She1-myc tagged strain, and ran TCA-precipitated protein samples on acrylamide gels supplemented with Phos-tag™ acrylamide, a reagent that retards the migration of phosphorylated species. This method has been used in the past to examine She1 phosphorylation (Woodruff et al., 2010).

Strikingly, even wild type cells demonstrated a modest increase in She1-phosphorylation after sorbitol treatment (Fig. 2.9A). This can be observed at 2 minutes after sorbitol addition, when the lower She1 band (corresponding to un-phosphorylated She1) is reduced in intensity, and the intensity of the ladder of phospho-She1 bands is increased. These phosphorylation events appeared to be transient, because after the 2 minute time-point, bands for phosphorylated She1 decreased in intensity, and the band for unphosphorylated She1 increased. I quantitated band intensities of phosphorylated and unphosphorylated She1, normalized them against a Pgk1 loading control, and plotted the results in Fig. 2.10.

Surprisingly, the She1-5A mutant also appeared slightly phosphorylated. However, it did not show the same levels of phosphorylation, or transient increase in phosphorylation, that wild type She1 showed. Instead, She1-5A appeared to be slightly phosphorylated at the 0 minute time-point (pre-sorbitol treatment) and continued to be only slightly phosphorylated until the 2 minute time-point after sorbitol addition, after which time phosphorylation began to decrease (Fig. 2.9A and 2.10C). In the *boi2Δ* mutant cells, She1 phosphorylation also followed this trend (Fig. 2.9A and 2.10C). However, the *boi1Δ* mutant did not show this result, and I found that She1 was phosphorylated in a wild type fashion (Fig. 2.9A and 2.10D).

Hog pathway mutants, like wild type cells, demonstrated a transient increase in She1 phosphorylation after treatment with sorbitol. However, *sho1Δ*, *pbs2Δ*, and *hog1Δ* cells showed more dramatic increases in phosphorylation after sorbitol addition (Fig. 2.9A). Levels of phosphorylated She1 increased ~0.8-1.4x in Hog1 pathway mutants at the 2 minute time-point, compared to wild type cells which increased only ~0.2x (Fig. 2.10B). These mutants also took a longer time to return to their baseline (pre-sorbitol) levels of phosphorylation. Whereas wild type cells took less than 5 minutes to return to their baseline levels of She1 phosphorylation, *pbs2Δ* cells took between 10 and 15 minutes. Levels of She1 phosphorylation never returned to baseline levels in *sho1Δ* and *hog1Δ* cells over the 60 minute time-course.

Figure 2.9

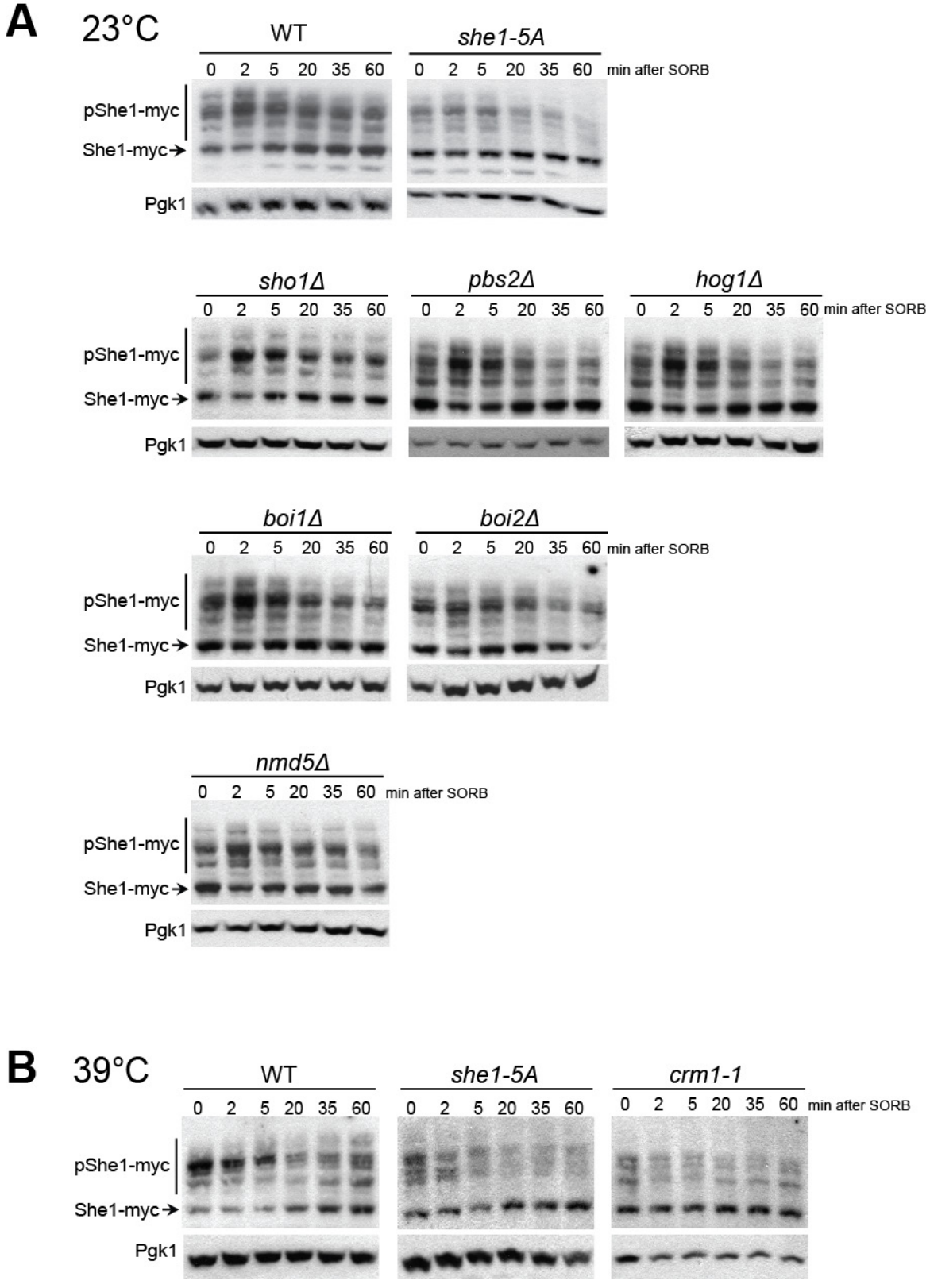
A
23°C
WT
she1-5A
0 2 5 20 35 60
min after SORB
pShe1-myc
She1-myc
Pgk1
sho1Δ
pbs2Δ
hog1Δ
boi1Δ
boi2Δ
nmd5Δ
B
39°C
crm1-1

Figure 2.9 She1 is phosphorylated in response to sorbitol treatment. (A) She1-myc containing strains of the indicated genotype were grown to mid-log phase in YPD at 23°C. 3M sorbitol in YPD was added to a final sorbitol concentration of 1M, cultures were rapidly mixed, and an equal amount of cells was harvested for each time point of the 60 min time-course. Cells were immediately TCA precipitated, and an equal volume of cells was loaded across lanes (0.5 O.D./lane). Upper panels of the western blots were probed with anti-Myc antibody, and bottom panels with anti-Pgk1. (B) As in (A), with the exception that cells had been grown at 39°C for two hours prior to sorbitol addition, and the time-course was performed at 39°C for the *crm1-1* ts allele.

Figure 2.10

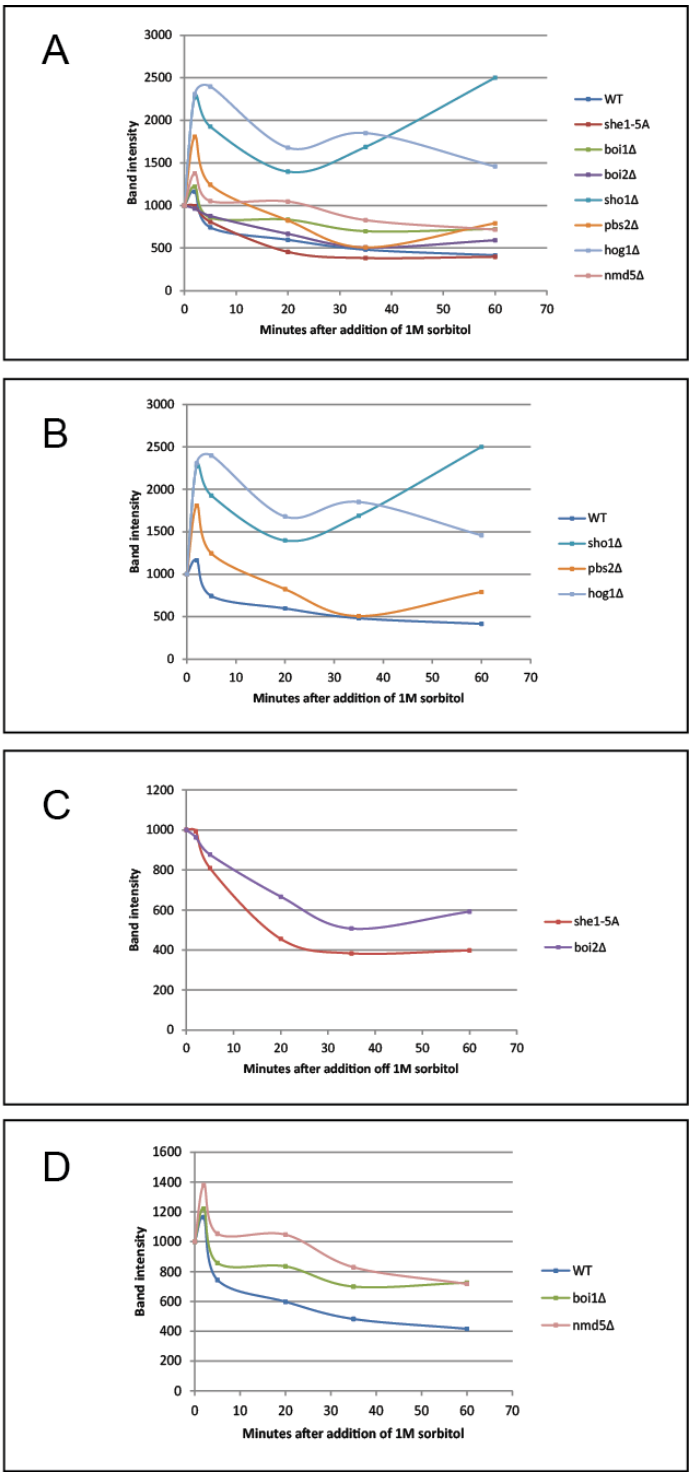

Figure 2.10 Quantitation of She1 phosphorylation. (A-D) Phosphorylated She1 bands (indicated by p-She1-myc in Figure 2.9) were quantitated. Densities of bands in non-saturated exposures were determined using ImageJ, and normalized against Pgk1 loading controls.

Together with the data showing re-localization of She1 from the bud neck to the nucleus in Hog pathway mutants subjected to sorbitol stress (Fig. 2.8), the She1 phosphorylation data begin to present a picture of how the Hog pathway influences She1. In wild type cells, She1 is not detectably removed from the bud neck upon activation of the Hog pathway, and there is a modest increase in She1 phosphorylation. It is not clear whether the She1 that was phosphorylated in wild type cells was already in the nucleus, or if sorbitol treatment caused an undetectable amount of She1 at the bud neck to translocate to the nucleus, where it was phosphorylated. Alternatively, She1 could be phosphorylated by a kinase other than Ipl1, either in the nucleus or in the cytoplasm. In *sho1Δ*, *pbs2Δ*, and *hog1Δ* mutant cells, sorbitol treatment results in all of the detectable She1 being removed from the bud neck, and is associated with a dramatic increase in She1 phosphorylation. In *boi2Δ* mutant cells, She1 is neither removed from the bud neck, nor transiently phosphorylated in response to sorbitol treatment.

A non-classical NLS sequence directs She1 to the nucleus

The rapid changes in localization and phosphorylation of She1 I observed in Hog pathway mutants led me to hypothesize that She1 could be actively transported into the nucleus in response to osmotic stress. *S. cerevisiae* undergoes a closed mitosis, where the nuclear envelope remains intact as the cell divides, and active transport across the Nuclear Pore Complexes is required for proteins larger than ~40-60kDa (reviewed in Nigg, 1997, and Chook and Süel, 2011). At 38kDa, She1 may or may not require active transport into the nucleus based on size alone, although She1-3GFP very likely does.

Classical nuclear localization sequences (NLS's) are monopartite or bipartite, typically basic sequences in cargo proteins that are recognized by an importin α subunit of a heterodimeric NLS receptor. An Importin β subunit binds and translocates the NLS receptor and cargo into the nucleus in a Ran-dependent manner (reviewed in Nigg, 1997, Xu et al., 2010, and Chook and Süel, 2011). More recently, non-classical NLS's have been discovered to contribute to the nuclear trafficking of proteins and some mRNAs. A large family of MAP kinases, including Hog1, the mating fusion MAPK Fus3, Kss1, Hrp1, and even Cdc28 (Cdk1), possess an alternative, non-classical NLS, defined by the consensus sequence [R/H/K]-$X_{(2-5)}$-P-Y, where X is any amino acid (Ferrigno et al., 1998, Albertini et al., 1998, Jensen et al., 2000, Lange et al., 2008, reviewed in Xu et al., 2010). This NLS is often called a "PY motif" for short. She1 possesses a PY motif at Pro^{144} Tyr^{145} (Fig. 3.11A) that is conserved among closely related yeast species (Fig. 3.11B).

I investigated whether the PY motif in She1 is important for She1 function or localization by mutating Pro^{144} Tyr^{145} to alanines, a strategy used to study the nuclear import of MAPKs (Ferrigno et al., 1998). I called this allele *she1-PY-AA*. Interestingly, *she1-PY-AA* mutant cells grew more slowly than wild type cells at 25°C, are temperature sensitive at 30°C and 37°C, and are sensitive to benomyl, a microtubule poison that exacerbates growth phenotypes of cells with mutations that affect spindle stability (Fig. 3.11C). The growth phenotype of the *she1-PY-AA* cells shows them to be sicker than either *she1-5A* or *she1-5D* cells, expressing the phospho-defective and

phospho-mimetic versions of She1, where Ipl1 sites have been mutated to alanine or aspartate, respectively.

Figure 2.11

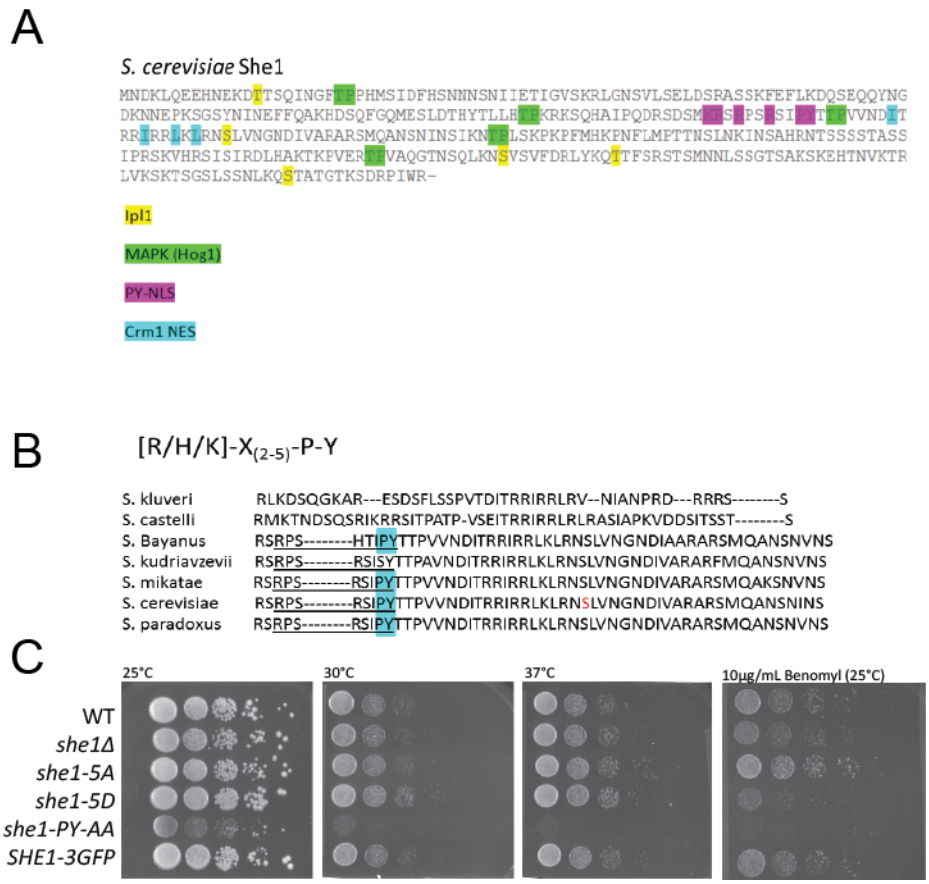

Figure 2.11 She1 contains a non-classical NLS sequence. (A) Amino acid sequence of *S. cerevisiae* She1. Highlighted in yellow are the five residues that fit the Ipl1 phosphorylation consensus motif, and were mutated to alanines to create the She1-5A allele (Woodruff et al., 2010) or aspartates to create the She1-5D allele (this study). In green are consensus sites for Hog1 phosphorylation which remain untested *in vivo*. In magenta are residues that satisfy the PY-NLS motif, and in blue are residues that satisfy the Crm1 NES motif. (B) Comparison of She1 PY-NLS motifs in species closely related to *S. cerevisiae*. PY residues are highlighted in blue. (C) Serial dilutions of strains of the indicated genotype were spotted onto YPD plates and grown at the indicated temperature for 1-3 days.

At least two importins have been found to bind to proteins containing PY-motifs and to import them into the nucleus. Kap104, the Kapβ2 in yeast, regulates asymmetric protein synthesis in daughter cells during the cell cycle by controlling the nuclear localization of Hrp1 and Nab2, mRNA binding proteins (Lange et al., 2008). Another importin, the importin β homolog Nmd5, is best characterized for importing transcription factors, such as TFIIS and Crz1 (involved in calcineurin signaling), into the nucleus (Polizotto et al., 2001). Hog1 is also dependent on Nmd5 for nuclear import, and furthermore, is dependent on the exportin Crm1 (Xpo1) for nuclear export (Ferrigno et al., 1998). Interestingly, She1 displays a yeast-2-hybrid interaction with Crm1, and Crm1 localizes to the kinetochore of SAC-arrested and SPBs of cycling cells, two locations in the cell where She1 is present (Neuber et al., 1998). Crm1 has also been implicated in removing the SAC protein Mad1 from the kinetochore (Scott et al., 2009).

I determined the localization of She1 in cells with the *she1-PY-AA* allele, as well as *nmd5Δ*, *kap104Δ*, and *crm1-1* (a temperature-sensitive allele of *CRM1*) mutant cells. I crossed She1-3GFP, as well as a *she1-5A-3GFP*, into each of these strains,. My observations are presented in Figure 2.12. She1-5A-3GFP strongly localized to the bud neck and spindle (Fig. 2.12A), although there was a significant amount of background fluorescence that prohibited me from clearly determining She1 localization over the course of mitosis. She1-PY-AA-3GFP localized to neither the bud neck nor the spindle, and most often appeared as diffuse fluorescence in the cytoplasm. In some cells, She1-PY-AA-3GFP foci appeared as dots in the mother cell and bud (Fig. 2.12A, asterisks). Further experiments with an SPB marker such as Spc42-mRFP, or staining for SPB proteins, will allow me to determine if these dots are SPBs. In contrast to *kap104Δ* cells, which displayed wild type patterns of She1 localization, She1 in *nmd5Δ* cells only weakly localized to the spindle, and localized very strongly to the bud neck, even until the very end of cytokinesis. Conversely, in *crm1-1* cells at the non-permissive temperature, She1 strongly localized to the spindle in a pattern that was reminiscent of Hog pathway mutants and *boi2Δ* cells (Fig. 2.12B).

I was not able to study the *she1-PY-AA* allele in a GFP-Tub1 or Myo1-GFP GFP Tub1 background because although diploids from these crosses grew well (indicating *she1-PY-AA* is not a dominant negative allele), upon sporulation I could not recover progeny with the *she1-PY-AA* allele and spindle disassembly markers. Additionally, I was hesitant to study the spindle disassembly phenotypes of *nmd5Δ* and *crm1-1* mutants because these genes affect the import and export of a wide variety of proteins, and would therefore likely show pleiotropic mitotic defects.

However, I did study the effects of sorbitol treatment on *nmd5Δ* and *crm1-1* mutant cells. When I treated *nmd5Δ* cells with 1M sorbitol, She1-3GFP did not disappear from the bud neck as it had in Hog pathway mutants, and remained very strongly localized to the bud neck (Fig. 2.8F). She1 phosphorylation after sorbitol treatment of *nmd5Δ* cells appeared wild type; there was a small increase in She1 phosphorylation 2 minutes after sorbitol treatment, followed by a rapid decrease in phosphorylation (Fig. 2.9A and 2.10D).

She1 phosphorylation at 39°C, the non-permissive temperature for *crm1-1*, showed a slightly different pattern than it did at 23°C (Fig. 2.9B). While the phosphorylation of She1 in wild type cells was induced after sorbitol treatment, She1-5A was only weakly phosphorylated at 39°C, and sorbitol treatment did not induce

phosphorylation. Interestingly, in the *crm1-1* mutant, She1 was not substantially phosphorylated either before or after sorbitol treatment. This implies that, in the case of the *crm1-1* mutant at the non-permissive temperature and without sorbitol treatment, She1 strongly localizes to the spindle, yet is not phosphorylated.

Figure 2.12

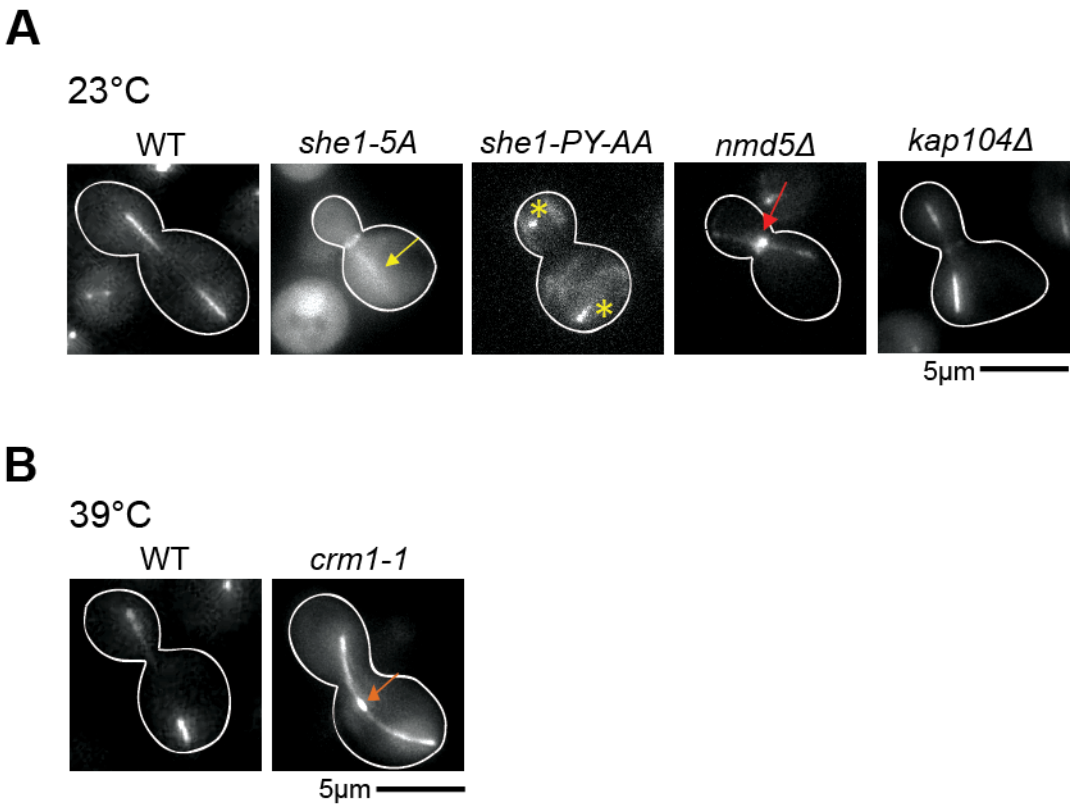

Figure 2.12 Proper She1 localization depends on its PY-motif, Nmd5, and Crm1. (A) Still images of cells of the indicated genotype expressing She1-3GFP. *she1-5A* and *she1-PY-AA* alleles were fused to *3GFP* exactly as they were for WT, *nmd5Δ*, and *kap104Δ* strains. Strains were imaged at 23°C. Yellow arrow: She1-5A weakly localizes to the spindle. Yellow asterisks: She1-PY-AA potentially localizes to the spindle pole bodies. Red arrow: She1 is enriched at the bud neck of *nmd5Δ* mutant cells. (B) Still images of WT and *crm1-1* cells expressing She1-3GFP at 39°C, the non-permissive temperature for *crm1-1*. Orange arrow: She1 inappropriately localizes to the midzone of *crm1-1* mutant cells.

Discussion

For several years, we have known that She1 localizes to the mitotic spindle, bud neck, spindle pole bodies, and astral MTs (Wong et al., 2007, Woodruff et al., 2009, Woodruff et al., 2010). Previous work described She1's role in inhibiting dynein activity until it is required for spindle positioning in anaphase (Woodruff et al., 2009), and showed that phosphorylation of She1 by Ipl1 is required to promote spindle disassembly (Woodruff et al., 2010). In this study, I expanded our knowledge of the She1 spindle disassembly pathway by investigating the contribution of the Hog pathway and NoCut checkpoint proteins Boi1 and Boi2 to the regulation of She1 localization and spindle phenotypes. Based on the results of my experiments, I have constructed a model for how the Hog pathway influences spindle disassembly through She1 (Fig. 2.13).

The Hog pathway contributes to Spindle Disassembly through She1 function

I have shown that the Hog pathway mutants *sho1Δ*, *pbs2Δ*, and *hog1Δ* have spindle disassembly phenotypes similar to *she1Δ* mutants; namely, they do not disassemble spindles until after cytokinetic ring contraction, and once spindles have broken into half-spindles, microtubules depolymerize ~1.7x slower than in wild type cells. She1 localization is also perturbed in Hog pathway mutants. Though She1 still localizes to the bud neck in *sho1Δ*, *pbs2Δ*, and *hog1Δ* cells, it strongly decorates the spindle at inappropriate times during anaphase, as if it cannot be excluded or removed from the spindle midzone. This finding highlights the somewhat paradoxical nature of She1: although She1 binds and destabilizes microtubules *in vitro* (Markus et al, 2012, and Jeff Woodruff, unpublished data) and is required for timely spindle disassembly *in vivo* in wild type cells, it does not localize to the site most critical to the destabilization of spindle microtubules during anaphase: the midzone. Moreover, She1 localization in the Hog pathway mutants and *boi2Δ* cells shows that enriching She1 at the midzone, or in the case of the *sho1Δ* mutant even at the depolymerizing ends of spindle microtubules, will not promote spindle disassembly.

These results indicate that there is a complexity to She1 function and regulation that we do not yet understand. In wild type cells and in every deletion mutant I studied except the *nmd5Δ* mutant, She1 was eventually removed from the bud neck during anaphase. The cell may use She1 localization as a way of signaling between the spindle and bud neck, similar to manner in which the NoCut pathway times chromosome segregation with cytokinesis. The NoCut checkpoint protein Boi2 may in fact play a part in She1 signaling. At the bud neck, the Hog pathway may promote interactions between She1 and other proteins that are necessary for She1 signaling. These interactions or post-translational modifications may be disrupted in Hog pathway mutants, such that She1 loses a feature necessary for its role in spindle disassembly. Hence, although more She1 localizes to the spindle in Hog pathway mutants and *boi2Δ* cells, it is not competent to promote spindle disassembly.

Understanding She1 Phosphorylation

She1 is phosphorylated by Ipl1, and this phosphorylation is important for She1's role in spindle disassembly (Woodruff et al., 2010). However, even a She1-5A mutant lacking Ipl1 sites, appeared to be slightly phosphorylated at 23°C in my western blot

analysis. She1 does have 5 MAPK consensus sites (Fig. 2.11A) that are potential targets for Hog1 phosphorylation. In the future, it is important to determine whether She1-5A loses its slight phosphorylation in a *hog1Δ* background, or if making a version of She1 that cannot be phosphorylated by Ipl1 and Hog1 entirely abolishes phosphorylation.

She1 is phosphorylated in response to sorbitol stress in wild type cells, and strongly phosphorylated in response to sorbitol stress in Hog pathway mutants. This phosphorylation in Hog pathway mutants is accompanied by displacement of She1 from the bud neck, and She1 accumulation presumably in the nucleus where it can be phosphorylated by Ipl1. However, sorbitol treatment of Hog pathway mutants did not rescue the mitotic exit defect of a *cdc15-2* mutant in a previous study (Rieser et al., 2006), and because of this, it is unlikely that sorbitol stressing Hog pathway mutants would rescue their spindle disassembly phenotypes. Therefore, even in a situation where She1 is strongly phosphorylated, spindle disassembly would be delayed.

An important and as yet unexplored feature of She1 phosphorylation is its dephosphorylation. When cells are osmostressed, the Hog pathway promotes release of Cdc14 from the nucleolus, and an appealing hypothesis is therefore that Cdc14 dephosphorylation of She1, at the end of anaphase, is important for spindle disassembly. In the future, it is important to evaluate She1 phosphorylation in a *cdc14* mutant to see if, similar to sorbitol stressed Hog pathway mutants, She1 is strongly phosphorylated. Evaluating spindle disassembly phenotypes in the *she1-5D* mutant is also important. Although there is debate about whether phospho-mimetic mutations are truly analogous to the phosphorylated state, observing a delay in spindle disassembly with the *she1-5D* mutant would support the conclusion that She1 phospho-regulation is achieved through both kinase and phosphatase activities.

A separation of function for Boi1 and Boi2

Most prior studies have regarded the functions of Boi1 and Boi2 to be redundant based on their localization patterns, similarity in regulation, and structural homology: both proteins contain Ipl1 and Cdk1 phosphorylation sites, N-terminal SH3 domains, and C-terminal Pleckstrin Homology (PH) domains. However, the synthetic lethality of the *boi1Δ boi2Δ* double mutant suggests that they cannot be completely functionally redundant. Here I have shown that while Boi1 and Boi2 are mislocalized from the bud neck in Hog pathway mutants, She1 is mislocalized in *boi2Δ*, but not in *boi1Δ*, cells. Furthermore, only the *boi2Δ* mutant has a spindle disassembly phenotype which mimics that of a *she1Δ* mutant – delayed spindle breakage until the cytokinetic ring contracts, and delayed microtubule depolymerization rates for the half-spindles.

It is still unclear what the Boi1 and Boi2 mislocalization patterns mean. They differed slightly between *sho1Δ* cells and *pbs2Δ* or *hog1Δ* cells. In the *sho1Δ* mutant, I noticed that most of Boi1 and Boi2 was not at the bud neck, but associated with plasma membrane around the cell, whereas in *pbs2Δ* and *hog1Δ* mutants, at least some of the Boi1 and Boi2 localized to the bud neck. This possibly reflects a role for Sho1 in recruitment of Boi1 and Boi2 to the membrane, and could be further tested by direct measures of Sho1 interaction with Boi1/Boi2.

In a previous model of the NoCut pathway, Norden et al. (2006) proposed that when at the bud neck, Boi1 and Boi2 delay cytokinesis by inhibiting the activity of

septins, and when Boi1 and Boi2 are removed from the bud neck, cytokinesis proceeds. However, despite moderate (in the case of *pbs2Δ* and *hog1Δ* mutants) to severe (in the case of the *sho1Δ* mutant) displacement of Boi1 and Boi2 from the bud neck, I did not observe any of these cells undergoing premature cytokinesis. I did notice that a small percentage (~5%) of *pbs2Δ* and *hog1Δ* cells appeared multi-budded and had two spindles (for an example, see Fig. 2.8G), and perhaps this reflects a role for the NoCut pathway in previous cell divisions of this population. Coupled with the data showing a spindle disassembly delay for the *boi2Δ* mutant, the localization data for Boi1 and Boi2 argue that these proteins are not simply involved in the inhibition of septin function, but are also involved in monitoring other aspects of mitotic exit as well. Very interesting findings by the Kellogg lab support the idea that Boi1 is regulated by Cdk1 phosphorylation, and is a component of the pathway whereby Cdk1 monitors the overall growth and polarity of the cell (McCusker et al., 2007, Anastasia et al., 2012). We are not yet sure what impact, if any, Ipl1 phosphorylation has on Boi1 and Boi2, although Ipl1 activity is essential to the NoCut pathway (Norden et al., 2006, Mendoza et al., 2009). It would be very interesting to find that Boi2 is regulated more by Ipl1 than Cdk1 phosphorylation, and that it is a component of the pathway whereby Ipl1 monitors spindle integrity and chromosome segregation. My findings that place Boi2, but not Boi1, in a pathway with She1 and spindle disassembly corroborate a model wherein Boi1 and Boi2 are monitoring slightly different aspects of cell division (cell growth for Boi1, and nuclear division for Boi2), and signaling from both Boi1 and Boi2 is integrated at the bud neck to promote timely cytokinesis.

PY-motif NLS's, Nmd5, and Crm1 are required for Hog1 and She1 nuclear localization

I found that the importin Nmd5 and the exportin Crm1 play a role in the nuclear localization of She1. In *nmd5Δ* cells, but not *kap104Δ* cells, She1 strongly localized to the bud neck, although it still weakly localized to the spindle. The *nmd5Δ kap104Δ* double mutant did not abolish She1 localization to the spindle any more than did the *nmd5Δ* single mutant (data not shown). It is not clear why some She1 still makes it into the nucleus of *nmd5Δ* cells, but this suggests that another importin is also involved in She1 trafficking. Alternatively, perhaps the She1-3GFP is able to diffuse through NPCs, but active transport by Nmd5 is required for robust She1 import into the nucleus. The exportin Crm1 is involved in the export of She1 from the nucleus, as She1 strongly localizes to the spindle in a *crm1-1* mutant at the non-permissive temperature. Interestingly, some She1 in *nmd5Δ* cells, but very little She1 in *crm1-1* cells, is phosphorylated. One interpretation of these observations is that She1 requires trafficking or cycling between the nucleus and cytoplasm in order to become fully phosphorylated, perhaps through priming phosphorylation events.

Nmd5 and Crm1 are also required for Hog1 import and export from the nucleus (Ferrigno et al., 1998). Whether there is significance in She1 sharing this import and export machinery is unclear. It seems unlikely that there could be competition between Hog1 and She1 for access to Nmd5, as Nmd5 is reportedly expressed at approximately twice the level of Hog1 (13,500 copies of Nmd5 per cell versus 6,780 copies of Hog1), and two orders of magnitude higher than She1 (at 264 copies per cell) (Ghaemmaghami

et al., 2003). Nevertheless, there is more She1 on the spindle of Hog pathway mutants, including the *hog1Δ* mutant, and only in the absence of this pathway is She1 displaced from the bud neck after sorbitol stress. Therefore, it seems that She1 translocation into the nucleus and accumulation on the spindle is more efficient in the absence of Hog1. However, this could also be due to interruptions in She1 interactions or post-translational modifications in Hog pathway mutants.

Mutating She1's PY-motif, the cognate NLS for Nmd5, results in reduced viability and mislocalization of She1 from both the bud neck and nucleus. She1-PY-AA-GFP (data not shown) and She1-PY-AA-3GFP fluorescence appear diffuse in the cytoplasm. Presently, whether the She1-PY-AA mutation is functional, or simply leads to the generation of aggregates in the cytoplasm that may sequester She1 interacting proteins, making the growth phenotype indirect as a consequence, is not clear. Future characterization of this allele is necessary.

Interestingly, Boi2, but not Boi1, also has a PY-motif. The residues involved in the PY-motif of Boi2 are $P^{548}Y^{549}$. Intriguingly, Boi2 S^{546}, which falls within the consensus sequence of the NLS, is a consensus site for Ipl1 phosphorylation, inviting the hypothesis that Boi2's nuclear localization may be regulated by a PY-NLS, and furthermore, that Ipl1 phosphorylation may regulate the availability of this NLS for binding by importins.

Hog pathway activity during mitosis

I began this project by investigating the contribution of Sho1 to spindle disassembly and I decided to characterize spindle disassembly phenotypes in the absence of osmostress, since this was the condition used in the screen which first identified genetic interactions between *sho1Δ*, and *cdh1Δ* and *kip3Δ* (Costanzo et al., 2010). I also thought that it was important to understand whether *sho1Δ*, and later, other Hog pathway mutants had functions apart from their signaling activity when cells are stressed. My results show that the Hog pathway does in fact have a role in spindle disassembly even in unstressed conditions, but raise the question of how the Hog pathway, which depends on hierarchical activation of kinases Pbs2 and Hog1 via a signaling cascade, accomplishes its effects in the absence of a signal. I do not have a definitive answer for this, but have thought about whether it might be possible for Sho1 to detect a signal other than high extracellular osmolarity. The mechanism by which Sho1 responds to osmostress is still unclear, other than that it depends in part on an accessory transmembrane protein, Msb2 (Cullen et al., 2004). One possibility is that at the bud neck, changes in the structure or curvature of the plasma membrane might induce a conformational change in Sho1 and/or Msb2 that results in transient activation of the Hog pathway during mitotic exit. Alternatively, Msb2 is a putative substrate of Cdk1 (Ubersax et al., 2003), and both Sho1 and Msb2 interact with the Cdc42 pathway (Raitt et al., 2000), which influences septin organization and the actomyosin cytokinetic ring, so there may be mitotic inputs into the Hog pathway in the form of phospho-regulation or mitotic-specific protein-protein interactions that induce activation.

It is thought that Hog1 has a low level of basal activity, and shuttles in and out of the nucleus even in unstressed conditions (Ferrigno et al., 1998). Osmostress increases this activity by inducing phosphorylation of Hog1 by Pbs2, leading to the accumulation of Hog1 in the nucleus and downstream effects such as transcriptional regulation

(Ferrigno et al., 1998, Reiser et al., 2000). In the future, it will be important to carefully evaluate Hog1 phosphorylation and localization over the cell cycle, and to determine if there is an increase or peak of Hog1 activity at any point in mitosis.

Other members of my lab and I have noticed that She1 localization is dependent in part on cell density. In all of my experiments, I was careful to image only cells that were in the early part of log phase. Even at an OD_{600} of 0.7-0.8 (1.0-1.2x10^7 cells/mL, considered mid-log phase), She1-3GFP does not localize to the spindle well, but appears as diffuse staining throughout the cell (although it does localize to the bud neck). Similarly, Boi1-GFP and Boi2-GFP tend to appear hazy and diffuse within the cytoplasm if cells are too dense. This phenomenon is not only important to take into consideration when studying the localization of these proteins, but is interesting in that it implies that the functions of these proteins are coupled to cell density and potentially to cell growth and polarity pathways.

Figure 2.13

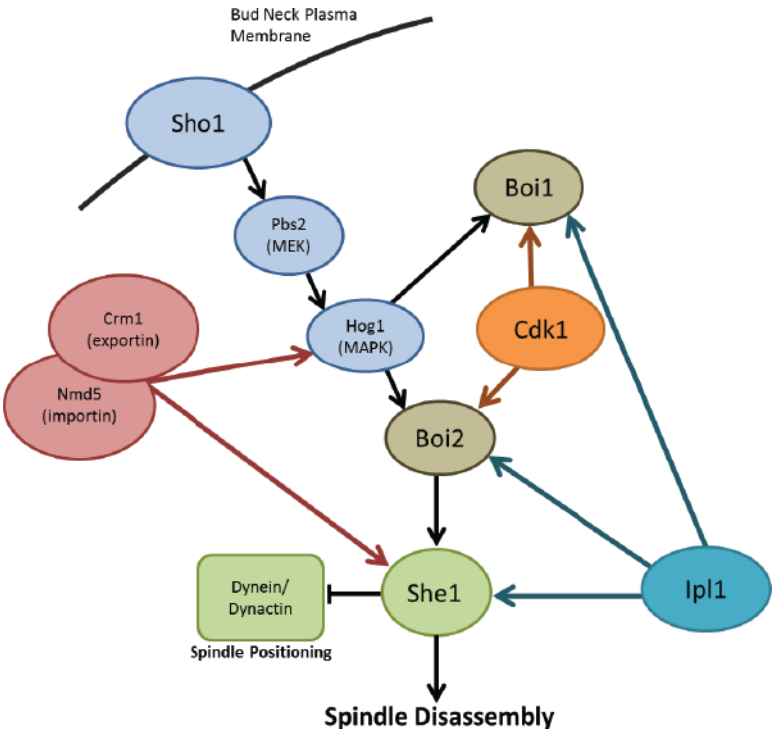

Figure 2.13 Model for Hog pathway activity towards She1 and NoCut proteins Boi1 and Boi2. The Hog pathway, composed of Sho1, Pbs2 and Hog1 (blue), affects the bud neck localization of NoCut proteins Boi1 and Boi2 (light brown), which are substrates of the mitotic kinases Cdk1 and Ipl1 (orange and teal). Hog pathway proteins and Boi2, but not Boi1, affect the spindle localization of She1 (green), an inhibitor of dynein function, and a positive regulator of spindle disassembly. Importin Nmd5 and exportin Crm1 (in red) affect the nucleo-cytoplasmic trafficking of both Hog1 and She1.

Methods

Yeast strains and media

Yeast strains used in this study are listed in Table 2.3. The *she1Δ*, *boi1Δ*, and *boi2Δ*, *nmd5Δ,* and *kap104Δ* strains originated in my lab and were generated by PCR product-mediated gene deletion (Longtine et al., 1998). The *sho1Δ* strain was from the Research Genetics collection, and was backcrossed to DDY904 prior to use in experiments. The *pbs2Δ* and *hog1Δ* strains were generously shared by the Thorner lab, and backcrossed prior to use. *she1-5D* (T14D, S165D, S269D, T280A, S325D) and *she1-PY-AA* (P144A, Y145A) were generated by Quickchange^{TM} site-directed mutagenesis of a plasmid containing wild type *SHE1* and ~250bp of the *SHE1* promoter. Plasmids were linearized in the promoter region and transformed into haploid *she1Δ::LEU2* cells. She1-3GFP strains were generated by cloning the last 500bp of *she1* mutant genes into pYS47, a *3GFP::HIS* plasmid. The plasmid was linearized outside of the *she1* coding sequence, and transformed into the appropriate mutant (*she1-5A*, *she1-5D*, or *she1-PY-AA*). Yeast were maintained on YPD (yeast peptone media with 2% glucose) using standard techniques.

Identifying candidate genes for spindle disassembly from genome-wide SGA studies

I evaluated mutants that were synthetic sick with *kip3Δ*, *cdh1Δ*, or *she1Δ* deletions by examining the supplemental data of Costanzo et al., 2010. I originally started with the dataset with a lenient cutoff applied (p-value < 0.05), and refined my list of candidate genes according to the dataset with an intermediate cutoff applied ($|\varepsilon| > 0.8$, p-value < 0.05). I organized the list of candidate genes according to those which shared genetic interactions with at least two of the three spindle disassembly genes (*kip3Δ*, *cdh1Δ*, and *she1Δ*), and chose to study candidates which, based on literature searches and additional large-scale analyses (mainly Tong et al., 2004, and Tonikian et al., 2009), displayed genetic and/or physical interactions with mitotic or spindle disassembly genes.

Fluorescence microscopy

Starter cultures of cells to be imaged were grown overnight in minimal media supplemented with 100mM casaminoic acids (imaging media). On the morning the day of imaging, cells were diluted to OD_{600} of 0.2 in imaging media containing 10mM N-acetyl-cysteine (to attenuate photobleaching). Cells were imaged at OD_{600} of 0.3-0.4; capturing cells in early log phase was essential to properly detect She1-3GFP on the spindle, and Boi1-GFP and Boi2-GFP at the bud neck.

Live cell microscopy at room temperature (23°C) was performed using a microscope (IX-71; Olympus), a 100x NA 1.4 objective, and a camera (Orca-ER; Hamamatsu Photonics). For time-lapse microscopy of shrinking half-spindles and cytokinetic ring contraction, images were collected at 10s and 30s intervals, respectively, with 300ms exposures. For time-lapse microscopy of She1-3GFP, images were collected at 1min intervals, with 300ms exposures. Each image represents a maximum intensity projection from a z stack containing five planes 0.4μm apart. For still images of Boi1-GFP and Boi2-GFP, z stacks of 7 images spaced 0.4μm apart were

collected to encompass the entire plasma membrane, and were acquired using 700ms exposures. Microscopy at 39°C was performed using an Olympus IX-81microscope equipped with a temperature-controlled enclosure (Precision Control Weather Station), 100x NA 1.4 objective and an Orca-ER camera (Hamamatsu Photonics). Wild type and *crm1-1* cells had been shifted to 39°C for two hours prior to imaging. All image processing was performed using MetaMorph and ImageJ.

Detection of phosphorylated She1 by western blot

Cells were grown in YPD to an OD_{600} 0.5 prior to sorbitol addition. 3M sorbitol in YPD was added to a final sorbitol concentration of 1M and cultures were rapidly mixed. For the *crm1-1* experiment, cells were grown at 39°C for two hours prior to sorbitol treatment. 2 OD_{600}'s of cells were harvested at each time point; cells were spun down and rapidly washed with 20% TCA to quench protease activity and maintain phosphorylation. Bead-beat TCA extracts were loaded onto 8% SDS-PAGE gels supplemented with 24μM Phos-Tag™ acrylamide (FMS Laboratory, Hiroshima University) and 24μM $MnCl_2$. Gels were run at a constant amperage of 20mA, transferred to nitrocellulose membranes, and probed with either 1:1000 mouse anti-Myc (9E10, purified by the Drubin/Barnes lab) or 1:1000 mouse anti-Pgk1 (Molecular Probes). Anti-mouse HRP conjugated secondary antibodies (GE Healthcare) were used at 1:10,000 dilutions. A 1:1 mixture of SuperSignal West Pico and SuperSignal West Femto substrates (Thermo Scientific) was used for ECL detection of bands.

Table 2.3 Yeast strains used in this study

Strain name	mating type	genotype	source
DDY902	*MATa*	*his3Δ200 ade2-1 ura3-52 leu2-3,112* (wild type)	Drubin/Barnes Lab
DDY904	*MATα*	*his3Δ200 lys2-801 ura3-52 leu2-3,112* (wild type)	Drubin/Barnes Lab
JBY 39	*MATa*	*GFP-TUB1::URA3*	Woodruff et al., 2009
JBY 58	*MATa*	*GFP-TUB1::URA3 she1Δ::LEU2*	Woodruff et al., 2009
JBY 233	*MATa*	*MYO1-GFP::HIS3 GFP-TUB1::URA3*	Woodruff et al., 2010
JBY 204	*MATa*	*MYO1-GFP::HIS3 GFP-TUB1::URA3 she1Δ::LEU2*	Woodruff et al., 2010
JBY 1	*MATα*	*she1Δ::LEU2*	Woodruff et al., 2009
APY 63	*MATα*	*sho1Δ::KanMX*	Res. Gen. collection
APY 168	*MATα*	*sho1Δ::KanMX she1Δ::LEU2*	this study
APY 149	*MATa*	*pbs2Δ::LEU2*	Jeremy Thorner Lab
APY 146	*MATa*	*hog1Δ::KanMX*	Jeremy Thorner Lab
APY 210	*MATα*	*pbs2Δ::LEU2 she1Δ::LEU2*	this study
APY 216	*MATα*	*hog1Δ::KanMX she1Δ::LEU2*	this study
APY 85	*MATα*	*sho1Δ::KanMX MYO1-GFP::HIS3 GFP-TUB1::URA3*	this study
APY 198	*MATα*	*pbs2Δ::LEU2 MYO1-GFP::HIS3 GFP-TUB1::URA3*	this study
APY 194	*MATα*	*hog1Δ::KanMX MYO1-GFP::HIS3 GFP-TUB1::URA3*	this study
APY 92	*MATα*	*boi1Δ::LEU2 MYO1-GFP::HIS3 GFP-TUB1::URA3*	this study
APY 90	*MATα*	*boi2Δ::HIS3 MYO1-GFP::HIS3 GFP-TUB1::URA3*	this study
APY 83	*MATα*	*sho1Δ::KanMX GFP-TUB1::URA3*	this study
APY 200	*MATα*	*pbs2Δ::LEU2 GFP-TUB1::URA3*	this study
APY196	*MATα*	*hog1Δ::KanMX GFP-TUB1::URA3*	this study
APY 94	*MATα*	*boi1Δ::LEU2 GFP-TUB1::URA3*	this study
APY 150	*MATα*	*boi2Δ::HIS3 GFP-TUB1::URA3*	this study
JBY 5	*MATa*	*BOI1-GFP::TRP1*	Jeff Woodruff
ACY 82	*MATa*	*BOI2-GFP::KanMX*	Anthony Cormier
APY 121	*MATα*	*sho1Δ::KanMX BOI1-GFP::TRP1*	this study
APY 183	*MATa*	*pbs2Δ::LEU2 BOI1-GFP::TRP1*	this study
APY 179	*MATα*	*hog1Δ::KanMX BOI1-GFP::TRP1*	this study
JBY 8	*MATα*	*she1Δ::LEU2 BOI1-GFP::TRP1*	Jeff Woodruff
APY 127	*MATα*	*sho1Δ::KanMX BOI2-GFP::KanMX*	this study
APY 181	*MATα*	*pbs2Δ::LEU2 BOI2-GFP::KanMX*	this study
APY 177	*MATα*	*hog1Δ::KanMX BOI2-GFP::KanMX*	this study
APY188	*MATα*	*she1Δ::LEU2 BOI2-GFP::KanMX*	this study
JBY 244	*MATa*	*SHE1-3GFP::HIS3*	Woodruff et al., 2009
APY 111	*MATa*	*sho1Δ::KanMX SHE1-3GFP::HIS3*	this study
APY 203	*MATa*	*pbs2Δ::LEU2 SHE1-3GFP::HIS3*	this study
APY 193	*MATa*	*hog1Δ::KanMX SHE1-3GFP::HIS3*	this study
APY 99	*MATa*	*boi1Δ::LEU2 SHE1-3GFP::HIS3*	this study
APY 187	*MATa*	*boi2Δ::HIS3 SHE1-3GFP::HIS3*	this study
APY 230	*MATa*	*nmd5Δ SHE1-3GFP::HIS3*	this study
APY 231	*MATa*	*kap104Δ SHE1-3GFP::HIS3*	this study
APY 232	*MATa*	*crm1-1 SHE1-3GFP::HIS3*	this study
APY 228	*MATa*	*she1-5D::HIS3::URA3::she1Δ::LEU2*	this study
APY 229	*MATa*	*she1-PY-AA::HIS3::URA3::she1Δ::LEU2*	this study
APY 233	*MATa*	*she1-5D-3GFP::HIS3::URA3::she1Δ::LEU2*	this study
APY 237	*MATa*	*she1-PY-AA-3GFP::HIS3::URA3::she1Δ::LEU2*	this study
JBY 305	*MATa*	*SHE1-13MYC::HIS3*	Woodruff et al., 2009
JBY 324	*MATa*	*she1-5A-13MYC::HIS3::URA3::she1Δ::LEU2*	Woodruff et al., 2009
APY 164	*MATa*	*sho1Δ::KanMX SHE1-13MYC::HIS3*	this study

APY 238	*MATa*	*pbs2Δ::LEU2 SHE1-13MYC::HIS3*	this study
APY 240	*MATa*	*hog1Δ::KanMX SHE1-13MYC::HIS3*	this study
APY 185	*MATa*	*boi1Δ::LEU2 SHE1-13MYC::HIS3*	this study
APY 167	*MATa*	*boi2Δ::HIS3 SHE1-13MYC::HIS3*	this study
APY 242	*MATa*	*nmd5Δ SHE1-13MYC::HIS3*	this study
APY 244	*MATa*	*kap104Δ SHE1-13MYC::HIS3*	this study
APY 246	*MATa*	*crm1-1 SHE1-13MYC::HIS3*	this study
APY 153	*MATα*	*pCDC3-GFP::URA3* in DDY 904	this study
APY 155	*MATα*	*pCDC3-GFP::URA3* in *sho1Δ::KanMX* (APY 63)	this study
APY 224	*MATa*	*pCDC3-GFP::URA3* in *hog1Δ::KanMX* (APY 146)	this study
APY 226	*MATa*	*pCDC3-GFP::URA3* in *pbs2Δ::LEU2* (APY 149)	this study

Table 2.4 Plasmids used in this study

plasmid name	resistance	description	source
pMVB100	Ampicillin	pCDC3-GFP::URA (ARS CEN plasmid)	Versele et al., 2004
pYS47	Ampicillin	p3GFP::HIS3 (integrating plasmid)	Wong et al., 2007
pAP30	Ampicillin	she1-5D::HIS3::URA3 (integrating plasmid)	this study
pAP31	Ampicillin	she1-PY-AA::HIS3::URA3 (integrating plasmid)	this study
pAP32	Ampicillin	she1-5A-3GFP::HIS3 (integrating plasmid)	this study
pAP33	Ampicillin	she1-5D-3GFP::HIS3 (integrating plasmid)	this study
pAP34	Ampicillin	she1-PY-AA-3GFP::HIS3 (integrating plasmid)	this study

Chapter 3: An insertion in the coiled-coil of the Ndc80 protein is required for proper NDC80 complex function

Introduction

Several decades of work have allowed us to generate a fairly complete "parts list" of ~65-70 proteins that comprise the budding yeast kinetochore, and much of current research is dedicated to understanding how these proteins interact on structural and regulatory levels to promote high fidelity chromosome segregation (reviewed in Westermann, et al., 2007). In *S. cerevisiae*, each kinetochore is occupied by a single microtubule (MT), and the essential outer kinetochore complexes, Dam1 and Ndc80, mediate microtubule-kinetochore attachment (reviewed in Westermann, et al., 2007). Careful work with conditional centromeres, whose function can be induced to study *de novo* kinetochore formation and MT capture, has demonstrated that the Ndc80 complex is important for initial lateral interaction between a MT and kinetochore, known as "side-on" capture, and the Dam1 complex is required for transitioning of these side-on attachments to stable, "end-on" attachments (Tanaka et al., 2005, Tanaka et al., 2007).

In addition to cooperating to promote stable MT-kinetochore attachments, various lines of evidence suggest that the Dam1 and Ndc80 complexes interact on a protein-protein level. *In vitro* translated Ndc80p binds to Dam1p, and *in vivo*, TAP-tag purification of either Dam1 or Ndc80 complex subunits pulls down the reciprocal complex (Shang et al., 2003). Both Ndc80 and microtubules are required for the delivery of the Dam1 complex to the kinetochore (Janke et al., 2001), and phospho-specific yeast two-hybrid interactions have been established between subunits of the heterotetrameric Ndc80 complex, and heterodecameric Dam1 complex (Wong et al., 2007). Additionally, both complexes are substrates of the Ipl1 kinase, which promotes detachment of MTs from kinetochores when these connections are not stable and able to bear tension across sister centromeres. Ipl1 phosphorylation seems to be much more important to the regulation of the Dam1 complex than the Ndc80 complex; phospho-defective *dam1* or *ask1* alleles show a wide range of growth defects and spindle and chromosome segregation defects (Cheeseman et al., 2002). However, mutating Ipl1 sites in Ndc80p, or deleting its phosphorylated N-terminus, has little consequence in vivo (Kemmler et al., 2009, and Hector Aldaz, unpublished data). *In vitro*, using phospho-mutant Dam1 complex, or phosphorylating Dam1 or Ndc80 with Ipl1, slightly reduces MT affinity, as does removing the N-terminus of Ndc80 (Westermann et al., 2005, Wei et al., 2007, Alushin et al., 2010).

I began my thesis work by trying to understand how the Dam1 and Ndc80 complexes collaborate to promote the formation of stable MT-kinetochore attachments. At the time, studies had been conducted to examine the binding of the individual complexes to MTs *in vitro*, using biochemical and fluorescence imaging-based tools, as well as electron micrography (Westermann et al., 2005, Westermann et al., 2006, Wang et al., 2007). Seminal work in my lab and the lab of Eva Nogales had shown that the Dam1 complex oligomerizes to form a ring around MTs *in vitro*, and this ring is able to diffuse along MTs, track depolymerizing MT ends, and even harness the force of peeling protofilaments to drive translocation of a polystyrene bead coupled to the complex (Westermann et al., 2006, Wang et al., 2007). However, we did not know in what geometry the Dam1 and Ndc80 complexes bound MTs when both were applied to MTs *in vitro*, and we did not know if the diffusion and MT end-tracking properties of the Dam1 complex could be extended to the Ndc80 complex via binding to Dam1.

I sought to purify recombinantly expressed Ndc80 complex for use in *in vitro* assays with the Dam1 complex, the latter being remarkably easy to purify owing to a polycistronic vector which expresses all 10 subunits (Miranda et al., 2005). In parallel, I also wished to study the complexes *in vivo*, to understand which subunits are important for interaction between the complexes, and how this interaction is regulated. Although I encountered technical difficulties purifying sufficient amounts of Ndc80 complex to use in *in vitro* experiments, I did generate two novel alleles of *NDC80* that allowed me to make insights into its function *in vivo*.

Results

An insertion in the coiled-coil domain of Ndc80 is important for cell fitness

The Ndc80 complex is a tetramer composed of Ndc80p, Nuf2p, Spc24p, and Spc25p. All four subunits have coiled-coil as well as globular head domains; Ndc80p and Nuf2p dimerize to form the microtubule-binding region of the complex through their heads and a calmodulin binding domain in Ndc80p, while their coiled-coil tails tetramerize with the Spc24/Spc25 dimer. The heads of the Spc24/Spc25 dimer are embedded in the outer kinetochore through interactions with the Knl1 and Spc105 complexes (Fig. 3.1A). Prior work using a chemical to crosslink proximal residues within the Ndc80 complex, followed by mass spec analysis, helped to identify contacts between the subunits of the complex (Maiolica et al., 2007). It also revealed the presence of a ~50 amino acid insertion in the coiled-coil domain of Ndc80p; the residues in this insertion do not conform to the alpha-helical repeat pattern, and instead form a putative "loop" within the coiled coil. The Ndc80 complex is conserved from fungi to humans, and sequence analysis revealed that amino acid insertion is also conserved, although it varies in length and location within the coiled-coil domain (Fig. 3.1B). At a sequence level, the loop appears relatively unstructured and does not align with any other proteins in BLAST searches, although some secondary structure prediction proteins assign it a short β-strand domain.

To investigate the function of this region of Ndc80p, I constructed a 14-amino acid and a 25-amino acid internal deletion of Ndc80p, aimed at eliminating the loop without interfering with surrounding sequences that are necessary for alpha-helical secondary structure. I integrated these mutations, which I refer to as Ndc80ΔG480-S493 and Ndc80ΔG480-G504 or "loopless Ndc80," into the yeast genome at the endogenous *NDC80* locus, such that they were the sole source of Ndc80p to the cell. Strikingly, both *ndc80ΔG480-S493* and *ndc80ΔG480-G504* were temperature sensitive alleles of *NDC80* which grew even less well than *ndc80-1*, a frequently used temperature sensitive allele with several point mutations and a C-terminal truncation. The alleles I generated also grew poorly, although not as poorly as the *ndc80-1* allele, on benomyl (Fig. 3.1C).

Figure 3.1

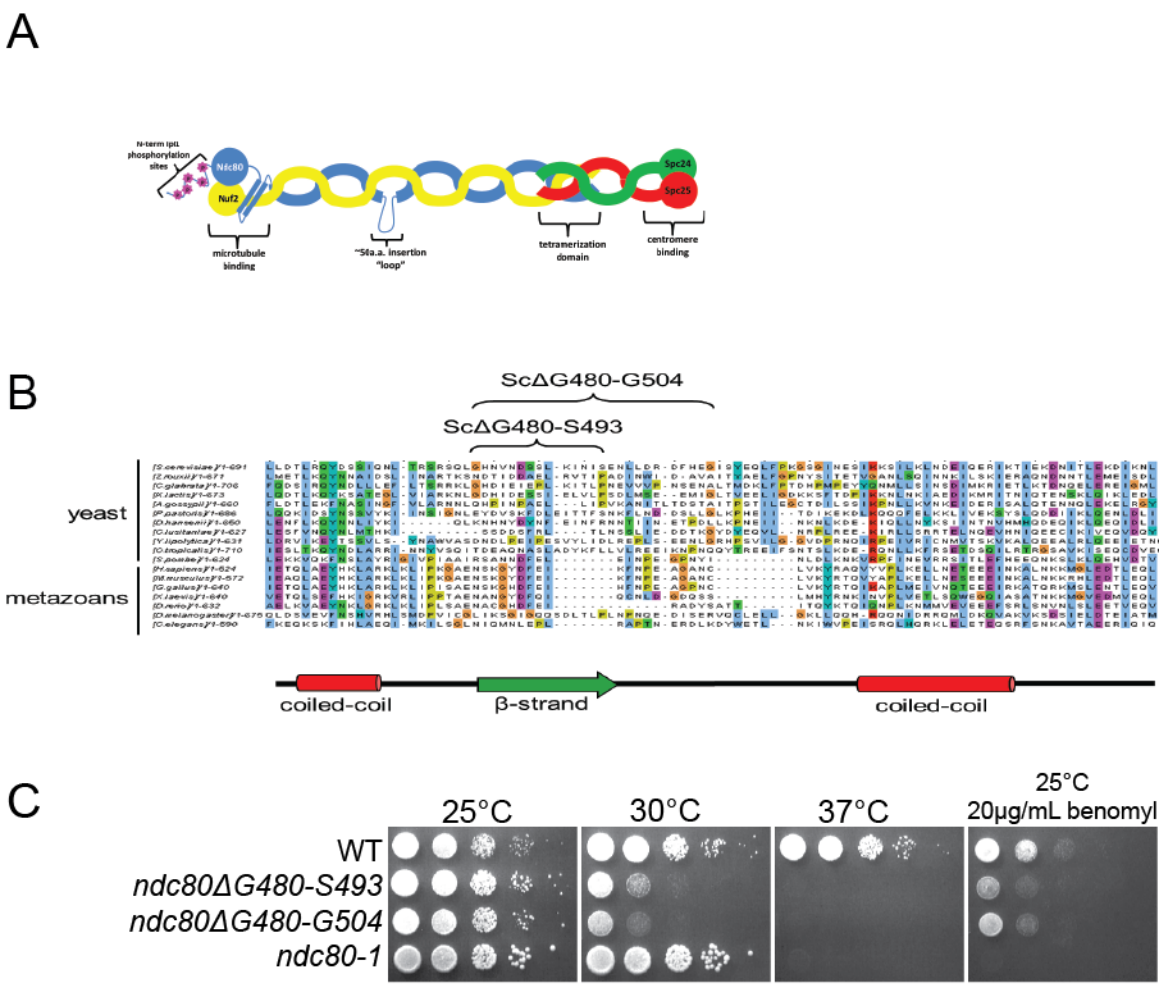

Figure 3.1 Ndc80 contains an insertion in its coiled-coil domain. (A) Cartoon of the Ndc80 complex showing its four subunits. The Ndc80/Nuf2 dimer binds microtubules, while the Spc24/Spc25 dimer is embedded in the kinetochore. An insertion of ~50 amino acids creates a "loop" in the coiled-coil domain of Ndc80p. (B) Cross-species conservation of the region of Ndc80 which contains the loop. (C) Deletions of the loop are temperature and benomyl sensitive in *S. cerevisiae*. Serial dilutions of cells with the indicated genotype were spotted onto YPD plates and incubated at indicated temperatures for 1-3 days.

***ndc80* alleles exhibit Spindle Assembly Checkpoint dependent delays in mitosis**

I further characterized the loopless *ndc80* alleles I generated by examining their mitotic phenotypes. The Spindle Assembly Checkpoint (SAC) is a highly conserved biochemical mechanism eukaryotes developed to monitor microtubule occupancy of kinetochores. In the absence of MT-kinetochore attachment, checkpoint proteins Mad1-3, Bub1 and Bub3 (in yeast) cycle on and off the kinetochore, and sequester Cdc20, an activator of the anaphase promoting complex (APC), in an inactive form. Silencing of the SAC occurs when kinetochores bind MTs, resulting in the release Cdc20 from Mad2. Active APC^{Cdc20} is then able to degrade securin, which activates separase towards its substrate cohesin. The degradation of cohesin allows the separation of sister chromatids, and marks the metaphase-to-anaphase transition.

In budding yeast, SAC checkpoint proteins are non-essential except in circumstances where MT-kinetochore attachment is compromised, and cells must delay anaphase until proper end-on MT-kinetochore attachments are formed. *ndc80-1* and *nuf2* alleles are able to satisfy the SAC and arrest at the metaphase-to-anaphase transition; however, cells with inactivated *spc24* or *spc25* cannot (Wigge et al., 1998, Wigge and Kilmartin, 2001). I evaluated levels of Pds1 (securin) in *ndc80* mutants, as a readout of SAC function. I arrested wild type and loopless *ndc80* cells with hydroxyurea to synchronize them in S-phase, then released cells into mitosis to evaluate Pds1 levels over a time-course (Fig. 3.2A). At the non-permissive temperature, *ndc80-1* cells arrest in metaphase with sustained levels of Pds1. Similarly, I found that both *ndc80ΔG480-S493* and *ndc80ΔG480-G504* mutant cells were unable to degrade Pds1 at time points when wild type cells were (Fig. 3.2A, compare 45min timepoints to 60min timepoints). This indicates that the SAC is still active in loopless *ndc80* mutants.

Mitotic mutants with compromised SACs are insensitive to deletion of checkpoint genes such as *MAD2*; however, those with functional SACs are sensitive. I combined *ndc80* alleles with a *mad2Δ*, to see if growth phenotypes were exacerbated by bypassing the SAC. I found that they were (Fig. 3.2B). *ndc80ΔG480-S493, mad2Δ* mutants and *ndc80ΔG480-G504, mad2Δ* mutants grew more poorly than *ndc80ΔG480-S493* or *ndc80ΔG480-G504* at non-permissive temperatures, indicating that SAC activity does provide the loopless *ndc80* mutants with a margin of fitness, and is intact even though Ndc80 function is perturbed.

Figure 3.2

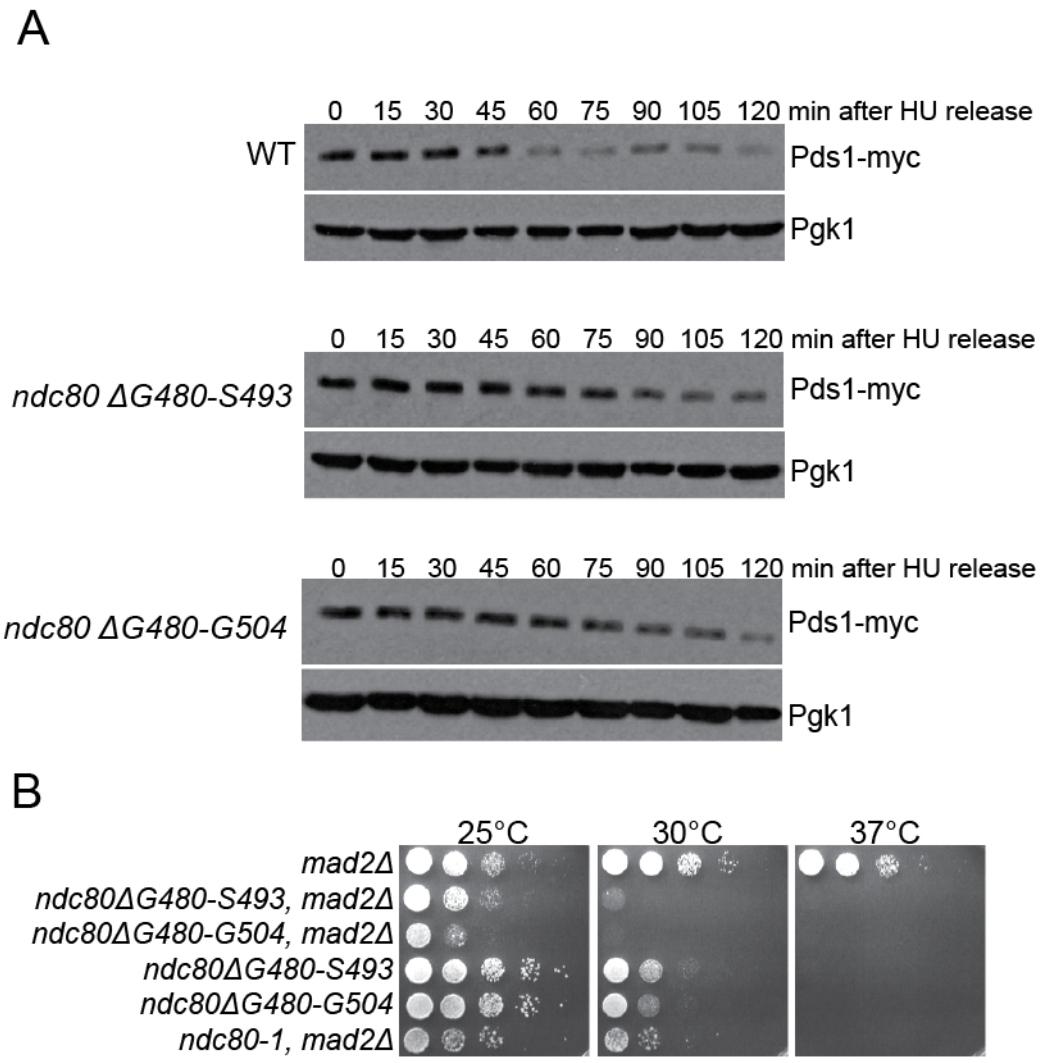

Figure 3.2 Loopless *ndc80* mutants exhibit Spindle Assembly Checkpoint dependent delays in mitosis. (A) Western blots of Pds1 (securin) in wild type, *ndc80ΔG480-S493*, and *ndc80ΔG480-G504* cells. Cells were arrested in S-phase with hydroxyurea (HU) for 2h, then shifted to 34°C for two hours before HU washout and harvesting at indicated time points. Pgk1 is shown as a loading control. (B) Deletion of the Spindle Assembly Checkpoint protein mad2Δ exacerbates the growth phenotype of *ndc80ΔG480-S493* and *ndc80ΔG480-G504* cells. Serial dilutions of cells with the indicated genotype were spotted onto YPD plates and incubated for 1-3 days at indicated temperatures.

Loopless *ndc80* alleles arrest in mitosis with short spindles and mis-segregated DNA

To examine the spindle phenotypes of the *ndc80* alleles I generated, I fixed and stained the mutants with anti-tubulin antibodies after shifting asynchronously growing cells to the non-permissive temperature of 37°C for 2 hours (Fig. 3.3). Whereas wild type populations of cells continued to cycle and undergo normal anaphase (Fig. 3.3, top panels), *ndc80ΔG480-S493* and *ndc80ΔG480-G504* cells frequently arrested in metaphase with short, very bright spindles. While the spindle MTs of these cells never elongated, I did observe that cytoplasmic MTs often extended into large buds, as if the spindle were attempting to position for elongation into the daughter cell. However, the DNA in *ndc80ΔG480-S493* and *ndc80ΔG480-G504* mutant cells very often did not segregate at all, and appeared as a large DAPI stained body associated with the short spindle (Fig. 3.3, lower right panel). This is very similar to what is seen in *ndc80-1* mutants; while the bud does grow to a large size, the spindle rarely elongates, and cells do not segregate DNA (Wigge et al., 1998). In both *ndc80ΔG480-S493* and *ndc80ΔG480-G504* mutant cells, I often saw large, multi-budded cells with multiple spindle and very disorganized DNA (Fig. 3.3, right middle panel), indicating that even while growing at the permissive temperature, prior to being shifted to 37°C, these cells probably underwent failed cytokinesis. Additionally, I often saw small foci of DAPI (DNA) staining in both *ndc80* mutants I generated (Fig. 3.3, white arrows in left panels). These foci sometimes did and sometimes did not associate with MTs, and never appeared in wild type cells. I concluded that these foci probably represented chromosomes with weak or non-existent MT attachments, or were chromosomes that had lost their spindle attachments and were in the process of being retrieved by MTs.

Figure 3.3

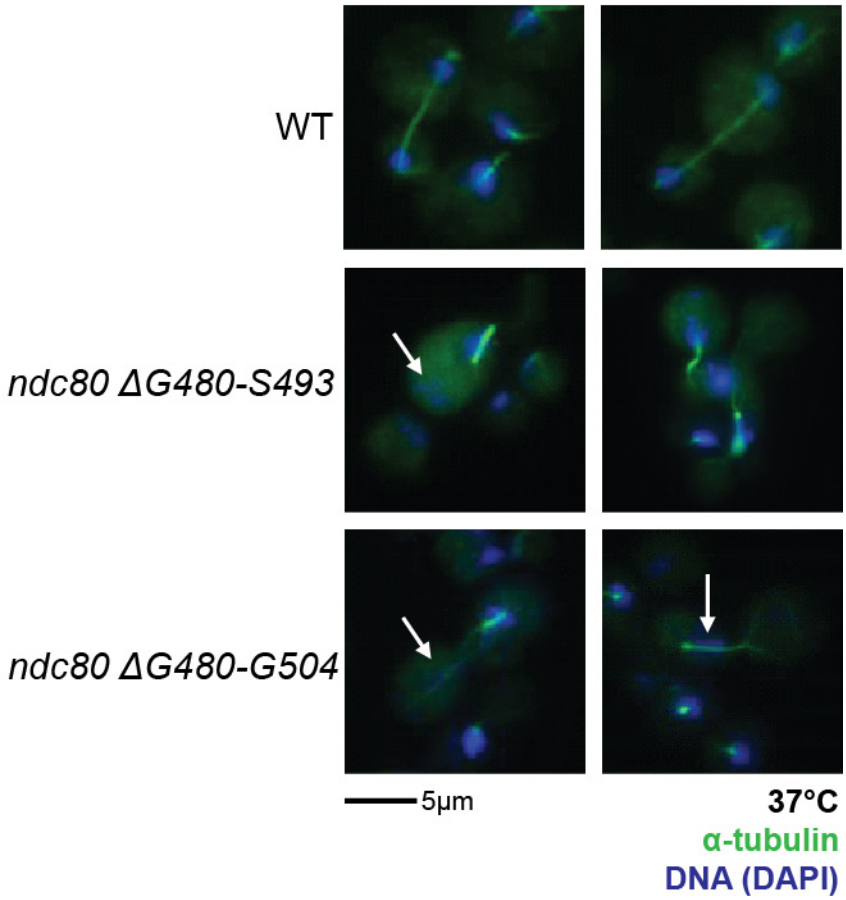

Figure 3.3 Loopless *ndc80* mutants display aberrant spindle morphologies and DNA mis-segregation phenotypes. Wild type, *ndc80ΔG480-S493*, and *ndc80ΔG480-G504* cells were shifted to 37°C for 2h prior to fixation and staining with anti-tubulin antibody (green) and DAPI (blue). Arrows indicate DNA that is mis-segregated or not associated with the spindle.

ndc80ΔG480-S493 mutant cells are defective in *CENIII* segregation

In characterizing the loopless ndc80 mutants up to this point, I could not discern any distinct differences between the *ndc80ΔG480-S493* and *ndc80ΔG480-G504* alleles. During this period, I was also dedicating a substantial amount of time to the purification of recombinant wild type and mutant Ndc80 complexes. To concentrate my efforts, I chose to use one allele, the *ndc80ΔG480-S493*, in pilot studies to further characterize the effects of deleting the loop in Ndc80.

To study the chromosome mis-segregation phenotype of *ndc80ΔG480-S493* mutant cells, I looked at the distribution of *CENIII*, the centromere of Chromosome III (Straight et al., 1996, Cheeseman et al., 2001a). I used a strain that had a an array of *Lac* operators (*LacO*) inserted at the *LEU2* locus very near *CENIII*, and could be induced to express the Lac Inhibitor fused to GFP (*pCu-LacI-GFP*). LacI-GFP bound to the *LacO* array, and fixed cells were stained with anti-GFP antibodies to determine the distribution of *CENIII*. I fixed wild type and *ndc80ΔG480-S493* mutant cells at various time points after releasing S-phase arrested at the non-permissive temperature of 37°C, and scored resulting phenotypes (Fig. 3.4). At the 0min time point, upon release from hydroxyurea, 90% of wild type cells had arrested in S-phase with small buds and their centromeres (LacI-GFP dots) could not be visibly separated (Fig. 3.4B-C). As cells began cycling, short metaphase spindles formed and eventually elongated, segregating the centromeres so that two LacI-GFP dots were visible in anaphase. By 60min, 60% of wild type cells were in metaphase or anaphase. However, *ndc80ΔG480-S493* mutant cells did not arrest well in S-phase, likely because even at the permissive temperature, cells are delayed in mitosis and do not make it to the beginning of the next cell cycle. This is evident at the 0min time point in *ndc80ΔG480-S493* cells, when nearly 70% of cells are in mitosis. Upon release from hydroxyurea and shifting to 37°C, even more cells accumulated in metaphase. I noticed that as *ndc80ΔG480-S493* cells spent time at 37°C, fewer cells were able to cycle into anaphase, and more cells arrested either in metaphase, or in a pre-anaphase state that was unique to the mutant (Fig. 3.4C, yellow and teal bars). While the mitotic spindle still appeared short and bright in mutant cells, cytoplasmic MTs appeared to elongate and try to position the spindle for elongation into the bud (Fig. 3.4C, teal bars corresponding to Class IV). The centromeres of these cells did not segregate into two dots, but always appeared on one side of the spindle.

The *CENIII* mis-segregation of the *ndc80ΔG480-S493* mutant correlates well with the cytology and increased Pds1 levels shown by these cells. It is likely that they arrest in metaphase with an active SAC because Ndc80 function is compromised, and they cannot make stable MT-kinetochore attachments.

Figure 3.4

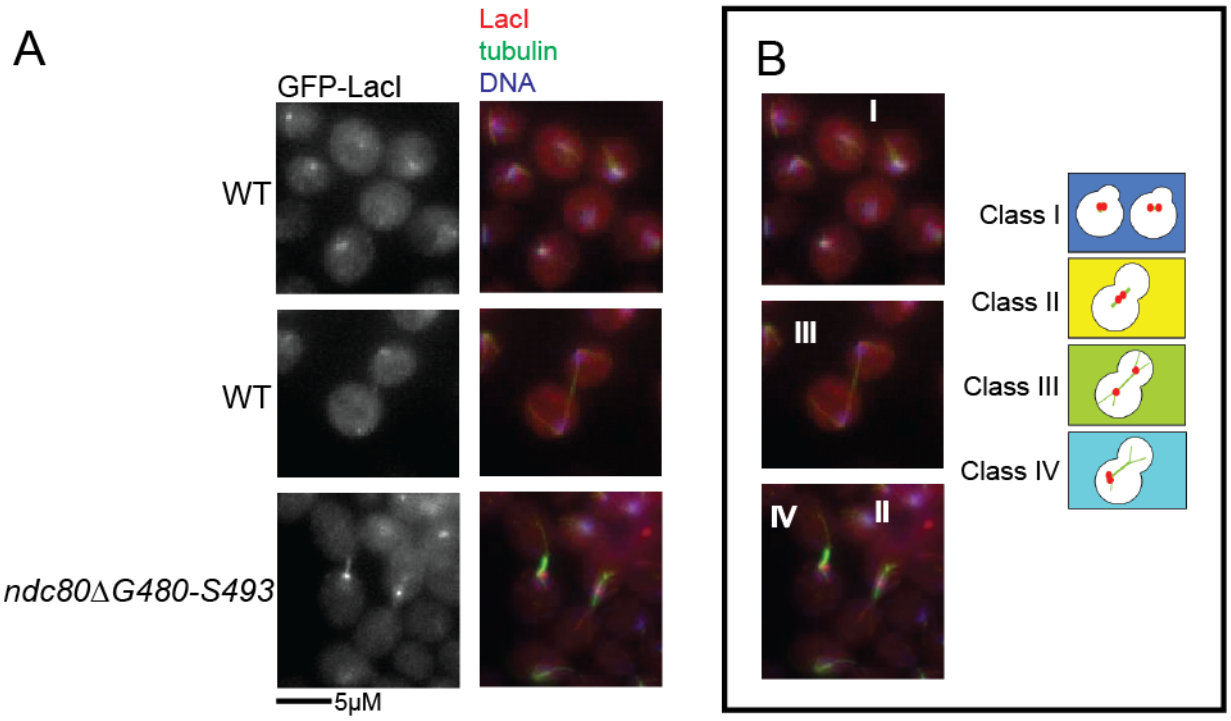
A
LacI
tubulin
DNA
GFP-LacI
WT
WT
ndc80ΔG480-S493
5μM
B
I
III
IV
II
Class I
Class II
Class III
Class IV

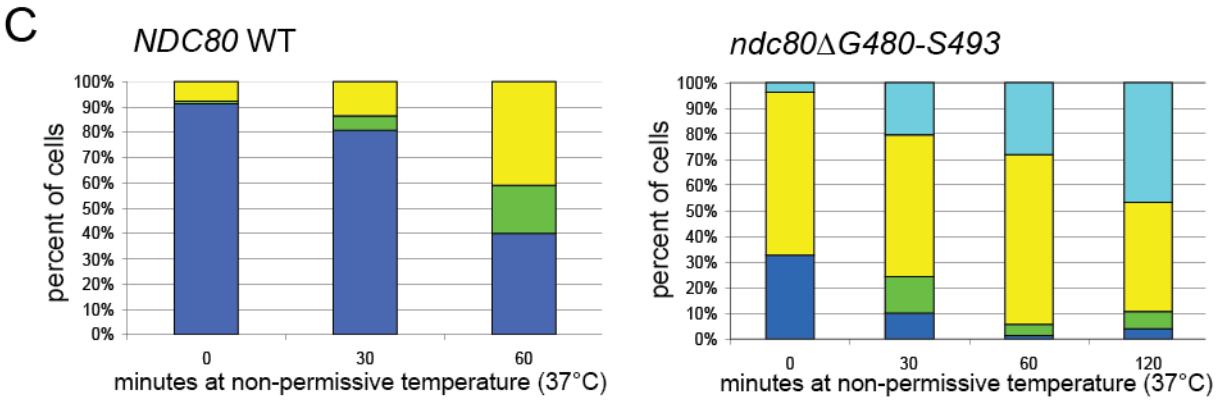
C
NDC80 WT
ndc80ΔG480-S493
percent of cells
100%
90%
80%
70%
60%
50%
40%
30%
20%
10%
0%
0
30
60
120
minutes at non-permissive temperature (37°C)

Figure 3.4 Chromosomes are mis-segregated in loopless *ndc80* mutants. (A) Fluorescent images of fixed cells stained for GFP-LacI (in red) tubulin (in green) and DNA (in blue). GFP-LacI was bound to a *LacO* array at the *LEU2* locus, and marks the centromere of Chromosome III. Left panels show GFP-LacI staining only and right panels are a merge of all three channels. (B) Phenotype categories scored in wild type and *ndc80ΔG480-S493* cells. Class I corresponded to cells which had not yet formed spindles and whose centromeres were not detectably separated. Class II corresponded to cells with a short metaphase spindle but had not yet segregated DNA, so the centromeres were not detectably separated, and localized to the middle of the spindle. Class III corresponded to anaphase cells with elongated spindles and separated centromeres. Class IV corresponded to cells with short spindles, or cells whose spindles had slightly elongated, and both centromeres localized to one end of the spindle. (C) Quantitation of centromere segregation phenotypes in WT and *ndc80ΔG480-S493* cells. Cells were arrested with hydroxyurea for 2h (blocking them in S-phase), then released at 37°C and fixed at indicated time points. At least 150 cells were counted for each time point.

Purifying recombinant Ndc80 complex for *in vitro* and structural studies

A previous electron microscopy study had shown that purified Ndc80 complex has a kink within its coiled-coil region (Wang et al., 2008). The coiled-coil region spans 560A, and the kink occurs ~160A away from the Ndc80/Nuf2 globular heads. It was proposed that the kink induces limited flexibility in the complex, which may be important as the complex adjusts its geometry to accommodate contacts with microtubules. The location of the kink correlates well to the location of the conserved "loop" in Ndc80p, and because the loopless alleles of *NDC80* had such strong phenotypes *in vivo*, I was interested in purifying loopless Ndc80 complex for *in vitro* and structural studies.

I encountered several technical hurdles in trying to express and purify either wild type or mutant Ndc80 complex. After working with a baculovirus expression system for some time, I switched to using a bacterial expression system developed in the lab of Stefan Westermann (Lampert et al., 2010). A schematic of the purification strategy is shown in Fig. 3.5 (for the full protocol, please see methods). Ultimately, although I was able to purify small amounts of both Ndc80-WT and Ndc80ΔG480-S493 complex, I was unable to eliminate contaminating proteins from my samples, and I was concerned that these complexes were not fully functional.

Figure 3.5

-Independently express 2 dimers in BL21 cells: Spc24-his$_6$/Spc25 (5-10L bacteria), and Ndc80-his$_6$/Nuf2 (22L bacteria)

-Prepare lysates, ammonium sulfate precipitation, resuspend pellet from 50% ammonium sulfate cut in 10mM imidazole His-trap buffer, apply to His-trap column

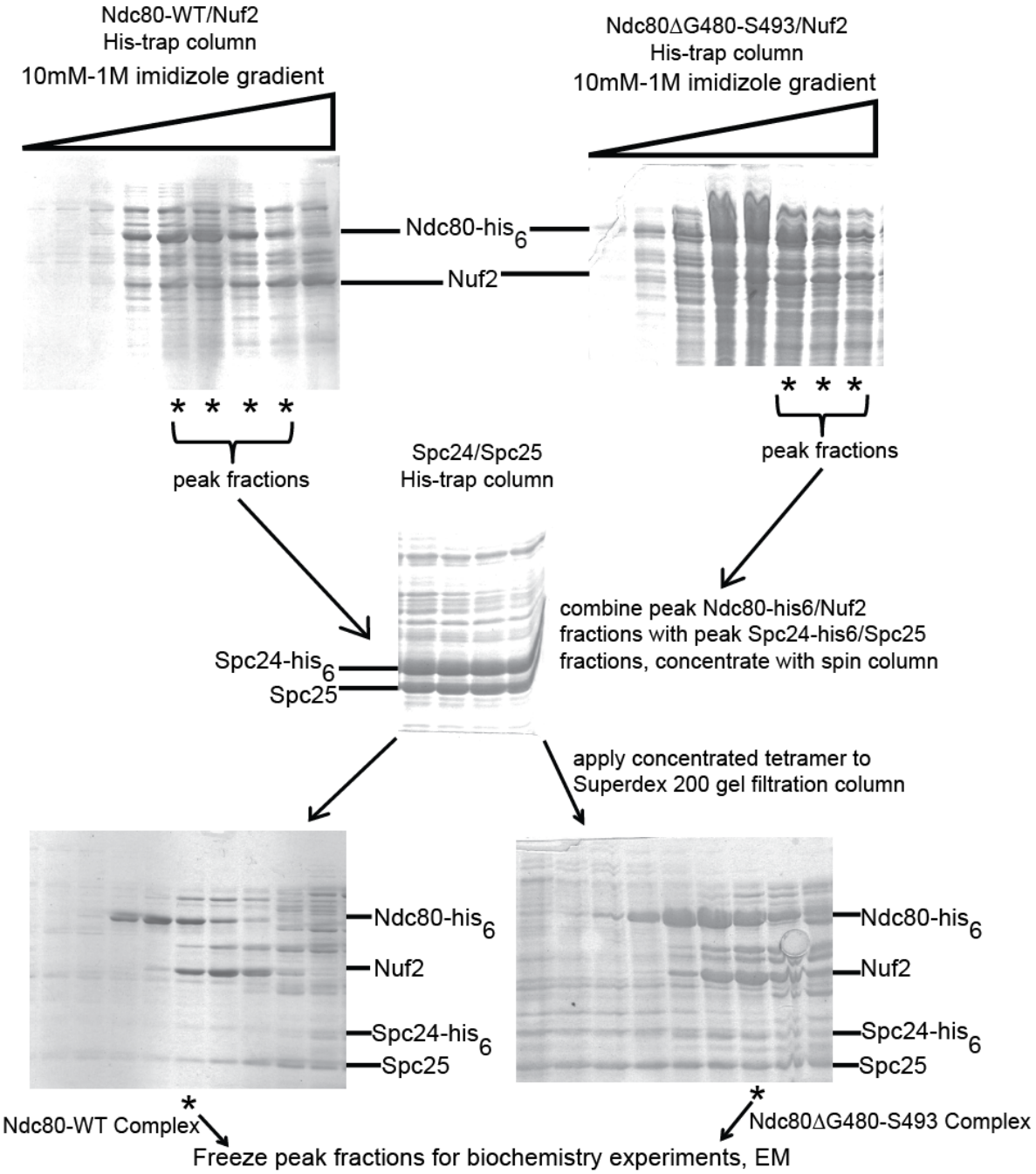

Figure 3.5 Purification of the Ndc80 complex from bacteria. The Ndc80 complex was expressed as two dimers, Ndc80-his_6/Nuf2 and Spc24-his_6-Spc25, which were combined *in vitro* to form the full complex (Lampert et al., 2010). For full description of the purification, see methods. Briefly, cell pellets expressing the Spc24/Spc25 dimer, Ndc80/Nuf2 (WT), or Ndc80/Nuf2 (Ndc80ΔG480-S493) were lysed by sonication in buffer containing protease inhibitors, then clarified by two rounds of centrifugation. The pellet resulting from a 50% ammonium sulfate cut was resuspended in buffer containing protease inhibitors and 10mM imidazole, then separated on a His-Trap column. The peak fractions were pooled, and the Spc24/Spc25 dimer was combined with either the Ndc80/Nuf2 (WT) dimer or the Ndc80/Nuf2 (Ndc80ΔG480-S493) dimer, concentrated, and loaded onto a Superdex 200 10/300 column. Peak fractions of Ndc80 complex eluted at similar volumes for the wild type and mutant complexes. They were immediately aliquoted, flash frozen, and stored at -80°C. SDS-PAGE gels were stained with Coomassie. Gels on the left show Ndc80-WT preparation and gels on the right show Ndc80ΔG480-S493 preparation.

Characterization of the Ndc80 complex *in vitro*

I wanted to confirm that the Ndc80 complex I had purified was functional using pre-existing assays for Ndc80 activity. I evaluated the binding of Ndc80-WT and Ndc80ΔG480-S493 complexes to microtubules, and in collaboration with the Nogales lab, looked at its structure by electron microscopy (EM).

Both the Ndc80-WT and Ndc80ΔG480-S493 complexes were soluble, and both bound taxol-stabilized MTs to some degree (Fig. 3.6A). However, I had reservations about the integrity of even the Ndc80-WT complex, because Coomassie stained SDS-PAGE gels from MT pelleting assays did not agree with western blots where I probed for Spc24-his_6. In the western blots, I saw that most of the Spc24 was in the pellet fractions (with MTs) after high-speed spins. However, by Coomassie, Spc24 and Spc25 could not be well detected because of their small size, and it did not look as though a proportional amount of Ndc80 or Nuf2 pelleted with MTs. This was also true for the Ndc80ΔG480-S493 complex. Although the Ndc80p in these complexes was also tagged with his_6, unfortunately I was never able to detect this subunit with our his_6 antibody.

Based on these results, I was concerned that the Ndc80 complexes I had purified were not behaving as tetramers, but dissociating into dimers or monomers in MT binding reactions. The Ndc80/Nuf2 is responsible for binding of the complex to MTs, so seeing that only the Spc24 subunit (or possibly the Spc24/Spc25 dimer) was enriched in pellet fractions led me to think that Spc24 (or the dimer) was dissociating from the complex and precipitating out of solution.

With the help of Greg Alushin from the Nogales lab, I also examined Ndc80-WT and Ndc80ΔG480-S493 complexes by EM. We applied the complexes to grids and negatively stained them with uranyl acetate (Fig. 3.6B). We did observe some Ndc80-WT complexes which appeared similar to what was seen in previous studies (Wang et al., 2008), and showed the kink in the coiled-coil region of the complex (Fig. 3.6B, left panels). However, it was difficult to identify single Ndc80ΔG480-S493 complexes because they often aggregated (Fig. 3.6B, right panels). Additionally, the globular heads of the complex appeared enlarged, and sometimes dissociated from the coiled-coil regions. Because of these inconsistencies, it was difficult to assign a structure to the Ndc80ΔG480-S493 mutant complex, and we could not conclude that this complex lacked the kink present in the WT complex.

Figure 3.6

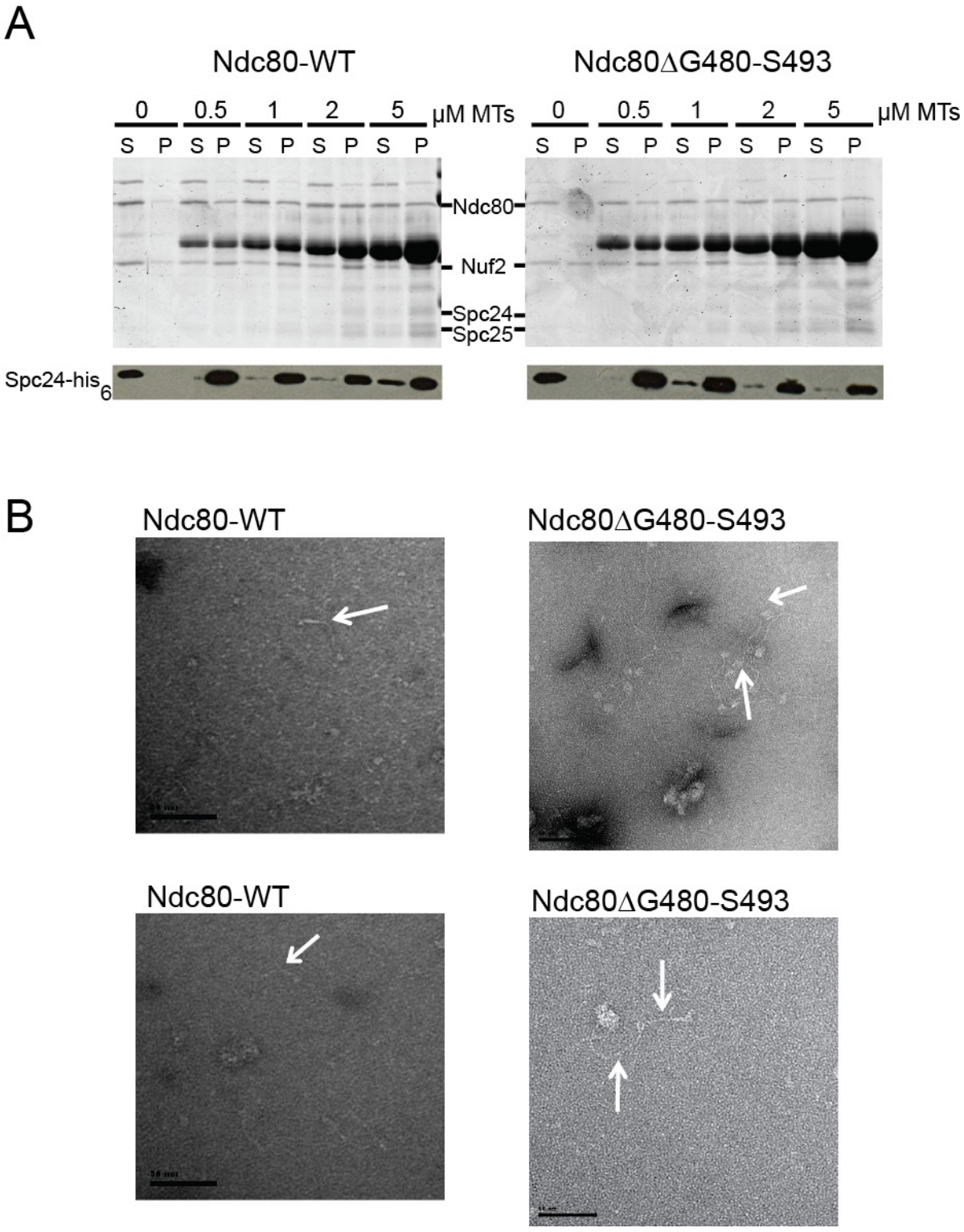
A
Ndc80-WT
Ndc80ΔG480-S493
0 0.5 1 2 5 μM MTs
S P S P S P S P S P
Ndc80
Nuf2
Spc24
Spc25
Spc24-his6
B
Ndc80-WT
Ndc80ΔG480-S493
Ndc80-WT
Ndc80ΔG480-S493

Figure 3.6 Wild type and mutant Ndc80 complexes bind microtubules. (A) Microtubule co-sedimentation assays with wild type Ndc80 complex (left) or Ndc80ΔG480-S493 complex (right). Top panels are Coomassie stained SDS-PAGE gels, and bottom panels are western blots probed with anti-his antibody to detect Spc24-his_6. S=supernatant and P=pellet from high-speed centrifugations. MTs=microtubules. 1μM complex was used in each experiment. (B) Electron micrographs of purified wild type Ndc80 complex (left) or Ndc80ΔG480-S493 complex (right). Black bars in all images are 50nm.

Discussion

In vivo studies of loopless *ndc80* mutants

I generated two new alleles of *NDC80* with deletions in their internal loop region, *ndc80ΔG480-S493* and *ndc80ΔG480-G504*. Both are loss-of-function temperature sensitive alleles, and at non-permissive temperatures, cells carrying either allele arrest in metaphase with short spindles and unsegregated DNA. This arrest is SAC dependent, similar to other alleles of *NDC80*. Cells with the *ndc80ΔG480-S493* or *ndc80ΔG480-G504* allele likely have a defect in their ability to make stable MT-kinetochore attachments, as they often have small foci of chromatin that is unclustered from the main mass of chromatin, and closely associated with the spindle. It may be this DNA, or weak attachments between clustered chromosomes and spindle MTs, that triggers the SAC.

In vitro studies of loopless Ndc80 complex

I sought to purify wild type and Ndc80ΔG480-S493 complexes for *in vitro* studies with MTs, and eventually the Dam1 complex. Unfortunately, I was not able to obtain enough of these complexes to do experiments, and the complexes I did purify were unstable in subsequent experiments. The Ndc80ΔG480-S493 complex in particular did not behave well; although its gel filtration elution profile was the same as the wild type complex, by EM it formed tangles and aggregates that prohibited us from characterizing its structure. It is not clear if this aggregation happened as I purified the complex, or as we were diluting it and preparing grids. However, neither the wild type nor Ndc80ΔG480-S493 complex behaved well in MT co-sedimentation assays, leading me to believe that there were problems with tetramerization of the complex.

In 2010 and 2011, three very nice papers were published on the Dam1 and Ndc80 complexes. The first, from Stefan Westermann's lab, showed that the Dam1 complex increases the affinity of the Ndc80 complex for MTs in a phospho-dependent manner, and can recruit the Ndc80 complex to the tips of growing and shrinking MTs (Lampert et al., 2010). In the second two, the Tanka and Toda labs showed that the loop of Ndc80 is important for viability, kinetochore-MT attachments, and recruitment of outer kinetochore proteins in budding and fission yeast (Maure et al., 2011, and Hsu and Toda, 2011). In budding yeast, the loop is important for kinetochore biorientation, via recruitment of the Dam1 complex to outer kinetochores to form end-on MT-kinetochore attachments. Maure et al. also used a fused version of the Ndc80 complex (Ndc80-Spc25 and Nuf2-Spc24 were fused) to show that a mutant in the loop region, Ndc80Δ490-510, could still bind MTs, and more robustly in the presence of the Dam1 complex. In fission yeast, Hsu and Toda showed that the Ndc80 loop binds Dis1/TOG, a microtubule-associated protein, to promote MT-kinetochore attachment and chromosome biorientation. Although neither of these papers reported structural evidence that loopless Ndc80 complex is missing its kink, the rest of their work supported the results I had obtained with my loopless *ndc80* alleles *in vivo*, and I stopped working on this project.

Methods

Yeast strains and media

Yeast strains used in this study are listed in Table 3.1. To construct the *ndc80ΔG480-S493* and *ndc80ΔG480-G504* alleles, plasmid-borne *NDC80* with a Nat^r or Hyg^r marker and 5' and 3' non-coding regions was PCR amplified with phosphorylated primers that began on either side of the region to be deleted. The linear product was ligated, and template DNA was digested with DpnI. The resulting clones were screened by sequencing to confirm deletion of the loop region. The *ndc80* mutant gene was amplified by PCR, and linear products were transformed into *NDC80/ndc80Δ::KanMX* heterozygous diploids, for recombination at the *NDC80* locus. Sporulated diploids gave 2:2 segregation patterns for viability; viable spores were sequenced to ensure the mutations had integrated correctly. Yeast were maintained on YPD (yeast peptone media with 2% glucose) using standard techniques.

Pds1 detection

Cultures were grown to mid-log phase and synchronized by the addition of 0.2M hydroxyurea for 2h at 25°C and 2h at 34°C prior to wash-out with warm YPD. Cells were harvested by OD_{600}, boiled in SDS-loading buffer, and an equal OD_{600} was loaded onto 10% acrylamide gels. Gels were transferred to nitrocellulose membranes and probed with 1:1000 mouse anti-myc (9E10, purified by the Drubin/Barnes lab) to detect Pds1-18myc, or 1:1000 mouse anti-Pgk1 (Molecular Probes). Anti-mouse HRP conjugated secondary antibodies (GE Healthcare) were used at 1:10,000 dilutions. SuperSignal West Pico substrate (Thermo Scientific) was used for ECL detection.

Immunofluorescence and Imaging

For tubulin and LacI-GFP staining, cultures in YPD were fixed with 4% formaldehyde for 1h at room temperature, and processed as described in Cheeseman et al., 2001a. For the LacI-GFP experiments, cells were induced with 250μM $CuSO_4$. Mouse anti-GFP antibody (Roche) was used at a dilution of 1:1000, and YOL134 (rat anti-yeast tubulin) was used at a dilution of 1:200. Rhodamine-conjugated anti-mouse and FITC-conjugated anti-rat secondary antibodies (Jackson ImmunoResearch Laboratories) were used at 1:400 dilutions. Slides were mounted in anti-fade mounting medium containing DAPI, and imaged with a fluorescent microscope (IX-71; Olympus), a 100x NA 1.4 objective, and a camera (Orca-ER; Hamamatsu Photonics)

Ndc80 complex purification

For bacterial expression of the complex, freshly transformed BL21 cells were inoculated into 11L of LB in a 12L fermentor (New Brunswick Scientific). 11L of cells were used for one Spc24-his_6/Spc25 purification, and 22L of cells were used for one Ndc80-his_6-WT/Nuf2 or Ndc80 his_6-ΔG480-S493/Nuf2 purification. Cells were grown to OD_{600} 0.8 at 37°C, then induced with 0.2mM IPTG for 12-14h at 17-18°C. Harvested cells were washed 1x with cold water, pelleted, and snap-frozen in 50mL falcon tubes. Pellets were resuspended in 250mL lysis buffer/11L starting culture. Lysis buffer contained: 10mM Hepes pH 7, 150mM NaCl, 10mM imidazole, 10% glycerol, 2x protease inhibitor tablets (complete, EDTA free, from Roche), 2mM PMSF. Resuspened

cells were sonicated 4x 20sec on ice (each falcon tube contained 30-40mL cells). Triton-X was added to a final concentration of 0.5%, and tubes were rocked at 4°C for 10min to complete lysis. Lysates were centrifuged for 10min, 6k rpm, in a Sorvall (xxx rotor), and supernatants were further clarified by centrifuging for 80min, 40k rpm, in a Beckman Ti45 rotor at 4°C.

Supernatants were pooled and ammonium sulfate precipitated by slowly adding finely ground ammonium sulfate to 50% saturation, with stirring, at 4°C. They were then centrifuged for 1h, 40k rpm, in a Beckman Ti45 rotor at 4°C. Supernatants were discarded, pellets were resuspended in fresh lysis buffer, and applied to a 5mL His-Trap column (GE Healthcare). After binding, the column was washed with 10 volumes low imidizole buffer (lysis buffer), and eluted with a 10 column volume gradient of 10mM-1M imidazole (in lysis buffer). Peak samples were pooled and dialyzed against 10mM Hepes pH 7, 150mM NaCl, 10% glycerol (gel filtration buffer) for 3hr 4°C using 3.5kDa MWCO Snakeskin dialysis tubing. The Spc24-his$_6$/Spc25 was typically purified first, and at this point it was flash frozen in aliquots and stored at -80°C.

The Ndc80-his$_6$-WT/Nuf2 or Ndc80-his$_6$-ΔG480-S493/Nuf2 dimer was purified in the same fashion, except it was not dialyzed for 3h. Peak His-Trap column fractions were combined with thawed, clarified Spc24-his$_6$/Spc25, and concentrated using a 10kDa MWCO centricon. Generally, ~11mL of Ndc80 complex was concentrated to ~0.6mL for loading onto a Superdex 10/300 Gel Filtration column (GE Healthcare). Gel filtered Ndc80-WT and Ndc80ΔG480-S493 complex eluted at the same volume, approximately 9mL. 0.5mL fractions were analyzed on 10% acrylamide gels, and peak fractions were flash frozen in aliquots and stored at -80°C. Spc24-his$_6$ levels were analyzed by western blot with a peroxidase-conjugated anti-his antibody (Roche) at a 1:500 dilution.

MT cosedimentation assays

MT cosedimentation (pelleting) assays were performed as described in Cheeseman et al., 2001b. Ndc80 complexes were thawed and dialyzed into 10mM Hepes pH 7, 25mM NaCl, 10% glycerol, 1mM $MgCl_2$, 1mM EGTA, 1mM DTT (working buffer) for 1 hour at 4°C. Bovine tubulin was pre-cleared and polymerized in PEM buffer (80mM PIPES, 1mM EGTA, 1mM $MgCl_2$) plus 1mM GTP 35°C for 30 min, stabilized by the addition10µM taxol, then centrifuged over a warm 40% glycerol (in PEM plus 1mM GTP and 10µM taxol) cushion. The pellet (polymerized MTs) was gently resuspended in warm working buffer plus 1mM GTP and 10µM taxol, and various concentrations were combined with 1µM pre-cleared Ndc80 complexes in 30 microliter reactions (in TLA100 tubes), incubated at room temperature for 15 min, then centrifuged at 85,000rpm for 20 min at 35°C. Supernatants were immediately removed and pellets were resuspended in SDS loading buffer. Equal portions of supernatants and pellets were run on 10% SDS-PAGE gels and either stained with Coomassie or transferred and probed with anti-his antibody as above.

Electron Microscopy

EM samples of Ndc80 complex were prepared essentially as described in Wang et al., 2008. Briefly, 5 microliters of 10-50nM Ndc80 complex in PBS were deposited

onto a glow-discharged copper mesh grid coated with continuous carbon and stained with 2% uranyl acetate. The samples were imaged on an FEI Tecnai 12 electron microscope operated at 120 keV at a magnification of 49 K. The images were collected on a Gatan CCD camera as well as on films that were later digitized on a Nikon Super CoolScan 8000.

Table 3.1 Yeast strains used in this study

Strain name	mating type	genotype	source
DDY 902	*MATa*	*his3Δ200 ade2-1 ura3-52 leu2-3,112* (wild type)	Drubin/Barnes Lab
DDY 904	*MATα*	*his3Δ200 lys2-801 ura3-52 leu2-3,112* (wild type)	Drubin/Barnes Lab
APY 29	*MATα*	*ndc80ΔG480-S493::NatMX*	this study
APY 30	*MATα*	*ndc80ΔG480-G504::NatMX*	this study
APY 45	*MATα*	*ndc80-1*	from the lab of Kim Naysmyth, backcrossed into DDY904 background for this study
DDY 1788	*MATa*	*mad2Δ::URA3*	Drubin/Barnes Lab
APY 47	*MATα*	*ndc80-1 mad2Δ::URA3*	this study
APY 48	*MATα*	*ndc80ΔG480-S493::NatMX mad2Δ::URA3*	this study
APY 49	*MATα*	*ndc80ΔG480-G504::NatMX mad2Δ::URA3*	this study
DDY 1929	*MATa*	*PDS1-18MYC::LEU2*	Iain Cheeseman
APY 32	*MATa*	*ndc80ΔG480-S493::NatMX PDS1-18MYC::LEU2*	this study
APY 35	*MATa*	*ndc80ΔG480-G504::NatMX PDS1-18MYC::LEU2*	this study
DDY 1925	*MATa*	*HIS3::pCu-LacI-GFP, leu2-3,112::lacO::LEU2*	Cheeseman et al., 2001a
APY 38	*MATa*	*ndc80ΔG480-S493::NatMX HIS3::pCu-LacI-GFP, leu2-3,112::lacO::LEU2*	this study

Table 3.2 Plasmids used in this study

plasmid name	resistance	description	source
pAP 18	Chloramphenicol	Ndc80–6xHis/Nuf2 in pACYduet-1	Lampert et al., 2010
pAP 19	Ampicillin	Spc24–6xHis/Spc25 in petDuet	Lampert et al., 2010
pAP 20	Chloramphenicol	Ndc80ΔG480-S493–6xHis/Nuf2 in pACYduet-1	this study
pAP 21	Chloramphenicol	Ndc80 ΔG480-G504–6xHis/Nuf2 in pACYduet-1	this study

Chapter 4: Perspectives and Future Directions

The She1 project I have been involved with for the past year and a half is intriguing, as it has begun to shed light on the idea that homeostasis mechanisms such as the Hog pathway have the ability to influence not only cell cycle changes via transcriptional regulation, but also very dynamic processes during mitosis. The Hog pathway clearly influences spindle disassembly by acting on She1, likely through Boi2. It also influences Cdc14 release from the nucleolus (Reiser et al., 2006). One of the interesting implications of this is that while an intact Hog pathway is required to delay mitotic entry in response to osmotic stress, it is also required to drive mitotic exit in cells that have been stressed. Mitosis is one of the most vulnerable times in the cell cycle – the genome is dividing, and much of the cytoskeleton is dedicated to the machinery of division. Perhaps the cell uses the Hog pathway as a strategy to make sure it can get out of mitosis and better dedicate its resources to cope with environmental stress in the next G1 phase.

In the future, I think it will be important to test Hog pathway activity and function over the course of the cell cycle in unstressed cells. There are Hog1 and phospho-Hog1 antibodies which can be used to detect Hog1 activity over a time-course, and I have made a Hog1-GFP strain to characterize its localization over mitosis. It might be that there is a small window of Hog pathway activity that occurs in anaphase – perhaps induced by Cdc42 signaling or structural changes in proteins at the bud neck, and perhaps this activity is important for mitotic exit and spindle disassembly.

A model for She1 function in spindle disassembly

She1 is a fascinating protein. She1 is a microtubule-associated protein which promotes MT catastrophe *in vitro* in centrosome nucleation experiments (Jeff Woodruff unpublished data), yet it is not conserved at a sequence level, and has no recognizable domain structure. In cells it promotes spindle disassembly, yet it is not enriched at the spindle midzone, where the spindle breaks and Ipl1 localizes during anaphase. It is still possible that *in vivo*, She1 acts directly on MTs, but She1 might also be important for the localization of other proteins which promote spindle disassembly, or it might help to coordinate the timing of spindle disassembly with cytokinesis.

Additionally, She1 function at the bud neck is still unclear, as is how it is removed from the bud neck in anaphase. In the future, it would be beneficial to map the structure of She1 by making different mutants (truncations, deletions of regions) and to see where they localize in the cell – if there is a particular region of She1 necessary for binding MTs or directing it to the bud neck, for example.

One of the things that I have struggled with is finding a way to address whether the phosphorylation state of She1 is different depending on its subcellular localization. For example, does Ipl1 phosphorylation of She1 induce its delocalization from the spindle, similar to many other microtubule-associated proteins? Also, does She1 phosphorylation vary depending on whether it is in the nucleus or bud neck, or does it affect She1's ability to traffic between the two? Further study of the phospho-defective and phospho-mimetic She1 alleles will begin to address this. A biochemical approach would be ideal, although I cannot think of a way to isolate nuclear and cytoplasmic extracts that does not rely on spheroplasting cells with sorbitol, which I have found increases She1 phosphorylation. She1-5A was still slightly phosphorylated in my western blots, indicating that She1 may be phosphorylated by kinases other than Ipl1. In

addition to the five Hog1/MAPK consensus sites, She1 also has a Cdk1 consensus site. Understanding the contribution of other kinases to She1's regulation will be critical.

One of the most important priorities for the future is to evaluate She1 dephosphorylation. I am particularly interested in looking at Cdc14 as a candidate phosphatase for She1. Cdc14 has connections to the Hog pathway, and localizes to the bud neck at the end of anaphase. I would like to look at She1 phosphorylation and localization in a *cdc14* mutant, as well as look at Cdc14 localization in a *she1Δ*. It is possible that some of She1's function derives from it being *dephosphorylated* at the correct time or location in the cell.

Ndc80 and Dam1 projects

Looking back on the work I did with Ndc80, I feel remiss for concentrating so much on purifying the Ndc80 complex that I did not focus more on describing the phenotypes of the loopless mutants I generated. If anyone were to go back to the biochemistry, I would suggest that they use a different strategy to express the complex – for example, using the fused Ndc80-Spc25 and Nuf2-Spc24 from the Tanaka lab, eliminating the need for tetramerization. It also might be that the mutant complex I was trying to purify, Ndc80ΔG480-S493, is misfolded, or that the deletion mutation affects the register of the coiled-coil, or that it is simply not as stable as other deletion mutants of the loop.

We now know that this loop is important for Dam1 complex localization to the kinetochore (Maure et al., 2011). However, it is probably not the region of the complex that directly binds Dam1; in MT cosedimentation assays, Dam1 still increased the affinity of loopless Ndc80 for MTs (Maure et al., 2011). So, there is still a question about whether the loop binds another protein directly in budding yeast, or is simply a structural feature that imparts flexibility to the complex. Replacing the loop with 7 alanines does not rescue the growth phenotype of loopless mutants. When I stopped working on this project, I was in the process of constructing strains in which I had replaced the loop with different sequences – some non-specific, and one where I reversed the sequence of the loop. I also had plans to do pulldowns with the loop, by fusing its sequence to an affinity tag and pulling that down from cell extracts, or fusing the loop sequence to GST or MBP, immobilizing it to a resin, and incubating that with cell extract.

References

Albertini, M., Pemberton, L., Rosenblum, J., and G. Blobel. A novel nuclear import pathway for the transcription factor TFIIS. 1998. *J. Cell Biol.*, **143**, 1447-55.

Alushin, G., Ramey, V., Pasqualato, S., Ball, D., Grigorieff, N., Musacchio, A., and E. Nogales. The Ndc80 kinetochore complex forms oligomeric arrays along microtubules. 2010. *Nature*, **467**, 805-10.

Anastasia, S., Nguyen, D., Thai, V., Meloy, M., MacDonough, T., and D. Kellogg. A link between mitotic entry and membrane growth suggests a novel model for cell size control. 2012. *J. Cell Biol.*, **197**, 89-104.

Bergman, Z., Xia, X., Amaro, I., and T. Huffaker. Constitutive dynein activity in She1 mutants reveals differences in microtubule attachment at the yeast spindle pole body. 2012. *Mol. Biol. Cell*, **23**, 2319-26.

Buvelot, S., Tatsutani, S., Vermaak, D. and S. Biggins. The budding yeast Ipl1/Aurora protein kinase regulates mitotic spindle disassembly. 2003. *J. Cell Biol.,* **160**, 329-39

Brewster, J., de Valoir, T., Dwyer, N., Winter, E., and M. Gustin. An osmosensing signal transduction pathway in yeast. 1993. *Science*, **259**, 1760-63.

Chan, C. and D. Botstein. Isolation and characterization of chromosome-gain and increase-in-ploidy mutants in yeast. 1993. *Genetics*, **135**, 677-691.

Cheeseman, I., Enquist-Newman, M., Müller-Reichert, T., Drubin, D., and G. Barnes. Mitotic spindle integrity and kinetochore function linked by the Duo1p/Dam1p complex. 2001a. *J. Cell Biol.*, **152**, 197-212.

Cheeseman, I., Brew, C., Wolyniak, M., Desai, A., Anderson, S., Muster, N., Yates, J., Huffaker, T., Drubin, D., and G. Barnes. Implication of a novel multiprotein Dam1p complex in outer kinetochore function. 2001b. *J. Cell Biol.*, **155**, 1137-1145.

Cheeseman, I., Anderson, S., Jwa, M., Green, E., Kang, J-S., Yates, J., Chan, C., Drubin, D., and G. Barnes. Phospho-regulation of kinetochore-microtubule attachments by the Aurora kinase Ipl1p. 2002. *Cell*, **111**, 163-172.

Chook, Y., and K. Süel. Nuclear import by Karyopherin-βs: recognition and inhibition. 2011. *Biochim. Biophys. Acta,* **1813**, 1593-1606.

Clotet, J. and F. Posas. Control of cell cycle in response to osmostress: lessons from yeast. 2007. *Methods Enyzomol.*, **428**, 63-76.

Costanzo, M., Baryshnikova, A., Bellay, J., Kim, Y., Spear, E., Sevier, C., Ding, H., Koh, J., Toufighi, K. Mostafavi, S., Prinz, J., St Onge, R., VanderSluis, B, Makhnevych, T., Vizeacoumar, F., Alizadeh, S., Bahr, S., Brost, R., Chen, Y., Cokol, M., Deshpande, R.,

Li, Z., Lin, Z., Liang, W., Marback, M., Paw, J., San Luis, B., Shuteriqi, E., Tong, A., van Dyk, N., Wallace, I., Whitney, J., Weirauch, M., Zhong, G., Zhu, H., Houry, W., Brudno, M., Ragibizadeh, S., Papp, B., Pál, C., Roth, F., Giaever, G., Nislow, C., Troyanskaya, O., Bussey, H., Bader, G., Gingras, A., Morris, Q. Kim, P., Kaiser, C., Meyers, C., Andrews, B., and C. Boone. The genetic landscape of a cell. 2010. *Science*, **327**, 425-31.

Cullen, P., Sabbagh, W. Graham, E., Irick, M., van Olden, E., Neal, C., Delrow, J., Bardwell, L., and G. Sprague. A signaling mucin at the head of the Cdc42- and MAPK-dependent filamentous growth pathway in yeast. 2004. *Genes Dev.*, **18**, 1695-708.

D'Amours, D., and A. Amon. At the interface between signaling and executing anaphase – Cdc14 and the FEAR network. 2004. *Genes & Dev.*, **18**, 2581-2595.

DeLuca, J., Gall, W., Ciferri, C., Cimini, D., Musacchio, A., and E.D. Salmon. Kinetochore microtubule dynamics and attachment stability are regulated by Hec1. 2006. *Cell*, **127**, 969-982.

Dewar, H., Tanaka, K., Nasmyth, K., and T. Tanaka. Tension between two kinetochores suffices for their bi-orientation on the mitotic spindle. 2004. *Nature*, **428**, 93-97.

Drees, B., Sundin, B., Brazeau, E., Caviston, J., Chen, G., Guo, W., Kozminski, K., Lau, M., Moskow, J., Tong, A., Schenkman, L., McKenzie, A., Brennwald, P., Longtine, M., Bie, E., Chan, C., Novick, P., Boone, C., Pringle, J., Davis, T., Fields, S., Drubin, D. 2001. A protein interaction map for cell polarity development. *J. Cell Biol.*, **154**, 549-71.

Fang, G., Yu, H., and M. Kirschner. The checkpoint protein Mad2 and the mitotic regulator Cdc20 form a ternary complex with the anaphase-promoting complex to control anaphase initiation. 1998. *Genes & Dev.*, **12**, 1871-83.

Ferrigno, P., Posas, F., Koepp, D., Saito, H, and P. Silver. Regulated nucleo/ cytoplasmic exchange of HOG1 MAPK requires the importin beta homologs NMD5 and XPO1. 1998. *EMBO J.*, **17**, 5606-14.

Ghaemmaghami, S., Huh, W., Bower, K, Howson, R., Belle, A., Dephoure, N., O'Shea, E. and J. Weissman. Global analysis of protein expression in yeast. 2003. *Nature*, **425**, 737-41.

Hardwick, K. and A. Murray. Mad1p, a phosphoprotein component of the spindle assembly checkpoint in budding yeast. 1995. *J. Cell Biol.*, **131**, 709-720.

He, X., Rines, D., Epstein, C. and P. Sorger. Molecular analysis of kinetochore-microtubule attachment in budding yeast. 2001. *Cell*, **106**, 195-206.

Hofmann, C., Cheeseman, I., Goode, B., McDonald, K., Barnes, G., and D. Drubin. *Saccharomyces cerevisiae* Duo1p and Dam1p, novel protein involved in mitotic spindle function. 1998. *J. Cell Biol.*, **143**, 1029-1040.

Hohmann, S., Krantz, M., and B. Nordlander. Yeast osmoregulation. 2007. *Methods Enzymol.*, **428**, 29-45.

Hsu, K.-S. and T. Toda. Ndc80 internal Loop interacts with Dis1/TOG to ensure proper kinetochore-spindle attachment in fission yeast. 2011. *Curr. Biol.*, **21**, 214-220.

Hwang, W., and H. Madhani. Nonredundant requirement for multiple histone modifications for the early anaphase release of the mitotic exit regulator Cdc14 from nucleolar chromatin. 2009. *PLoS Gen.*, **5**.

Janke., C., Ortiz, J., Lechner, J., Shevchenko, A., Shevchenko, A., Magiera, M., Schramm, C., and E. Schiebel. The budding yeast proteins Spc24p and Spc25p interact with Ndc80p and Nuf2p at the kinetochore and are important for kinetochore clustering and checkpoint control. 2001. *EMBO J.*, **20**, 777-791.
Janke, C., Ortiz, J., Tanaka, T., Lechner, J., and E. Schiebel. Four new subunits of the Dam1-Duo1 complex reveal novel functions in sister kinetochore biorientation. 2002. *EMBO J.*, **21**, 181-193.

Jensen, T., Neville, M., Rain, J. McCarthy, T., Legrain, and M. Robash. Identification of novel Saccharomyces cerevisiae proteins with nuclear export activity: cell cycle-regulated transcription factor Ace2p shows cell cycle-independent nucleocytoplasmic shuttling. 2000. *Mol. Cell Biol.*, **20**, 8047-58.

Kang, J-S., Cheeseman, I., Kallstrom, G., Velmurugan, S., Barnes, G., and C. Chan. Functional cooperation of Dam1, Ipl1, and the inner centromere protein (INCENP)-related Sli15 during chromosome segregation. 2001. *J. Cell Biol.*, **155**, 763-774.

Kemmler, S., Stach, M., Knapp, M., Ortiz, J., Pfannstiel, J., Ruppert, T. and J. Lechner. Mimicking Ndc80 phosphorylation triggers spindle assembly checkpoint signalling. 2009. *EMBO J.*, **28**, 1099-110.

Khmelinskii, A., and E. Schiebel. Assembling the spindle midzone in the right place at the right time. 2008. *Cell Cycle*, **7**, 283-6.

Lange, A., Mills, R., Devine, S., and A. Corbett. A PY-NLS nuclear targeting signal is required for nuclear localization and function of the Saccharomyces cerevisiae mRNA-binding protein Hrp1. 2008. *J. Biol. Chem.*, **283**, 12926-34.

Lampert, F., Hornung, P., and S. Westermann. The Dam1 complex confers microtubule plus-end tracking activity to the Ndc80 kinetochore complex. 2010. *J. Cell Biol.*, **189**, 641-9.

Lee, B., Cansizoglu, A., Süel, K., Louis, T., Zhang, Z., and Y. Chook. 2006. Rules for nuclear localization sequence recognition by karyopherin beta 2. *Cell*, **121**, 543-58.

Longtine, M., McKenzie, A., Derarini, D., Shah, N., Wach, A., Brachat, A., Philippsen, P. and J. Pringle. Additional modules for versatile and economical PCR-based gene deletion and modification in Saccharomyces Cerevisiae. 1998. *Yeast*, **14**, 953-61.

Madden, K. and M. Snyder. Cell polarity and morphogenesis in budding yeast. 1998. *Annu. Rev. Microbiol.*, 687-744.

Maddox, P., Bloom, K., and E. Salmon. The polarity and dynamics of microtubule assembly in the budding yeast Saccharomyces cerevisiae. 2000. *Nat. Cell Biol.*, **2**, 36-41.

Maeda, T., Takekawa, M., and H. Saito. Activation of yeast PBS2 MAPKK by MAPKKKs or by binding of an SH3-containing osmosensor. 1995. *Science*, **269**, 554-558.

Maiolica, A., Cittaro, D., Borsotti, D., Sennels, L., Cifferi, C., Tarricone, C., Musacchio, A., and J. Rappsilber. Structural analysis of multiprotein complexes by cross-linking, mass spectrometry, and database searching. 2007. *Mol. Cell Proteomics*, **6**, 2200-11.

Markus, M, Kalutkiewicz, K., and W.L. Lee, She1-mediated inhibition of dynein motility along astral microtubules promotes polarized spindle movements. 2012. *Curr. Biol.*, **22**, 1-10.

Maure, J-F., Kitamura, E., and Tanaka, T. Mps1 kinase promotes sister-kinetochore bi-orientation by a tension-dependent mechanism. 2007. *Curr. Biol.*, **17**, 2175-2182.

McCusker, D., Denison, C., Anderson, S., Egelhofer, T., Yates, K., Gygi, S., and D. Kellogg. Cdk1 coordinates cell-surface growth with the cell cycle. 2007. *Nat. Cell Biol.*, **9**, 506-15.

Mendoza, M., Norden, C., Durrer, K., Rauter, H., Uhlmann, F., and Y. Barral. A mechanism for chromosome segregation sensing by the NoCut checkpoint. 2009. *Nat. Cell Biol.*, **11**, 477-483.

Miranda, J., DeWulf, P., Sorger, P., and S. Harrison. The yeast DASH complex forms closed rings on microtubules. 2005. *Nat. Struct. Mol. Biol.*, **12**, 138-43.

Nakajima, Y., Cormier, A., Tyers, R., Pigula, A., Peng, Y., Drubin, D. and G. Barnes. Ipl1e/Aurora-dependent phosphorylation of Sli15/INCENP regulates CPC-spindle interaction to ensure proper microtubule dynamics. 2011. *J. Cell Biol.*, **194**, 137-53.

Neuber, A., Franke, J., Wittstruck, A., Schlenstedt, G., Sommer, T., and K. Stade. Nuclear export receptor Xpo1/Crm1 is physically and functionally linked to the spindle pole body in budding yeast. 2008. *Mol. Cell Biol.*, **28**, 5348-58.

Neurohr, G., Naegeli, A., Titos, I., Theler, D., Greber, B., Díez, J., Gabaldón, T., Mendoza, M., and Y. Barral. A midzone-based ruler adjusts chromosome compaction to anaphase spindle length. 2011. *Science*, **332**, 465-8.

Nigg, E. Nucleocytoplasmic transport: signals, mechanisms and regulation. 1997. *Nature*, **386**, 779-87.

Norden, C., Mendoza, M., Dobbelaere, J., Kotwaliwale, C., Biggins, S. and Y. Barral. The NoCut pathway links completion of cytokinesis to spindle midzone function to prevent chromosome breakage. 2006. *Cell*, **125**, 85-98.

Pinsky, B. and S. Biggins. The Spindle Assembly Checkpoint: Tension versus Attachment. 2005. *Trends Cell Biol.*, **15**, 486-493.

Pinsky, B., Kung, C., Shokat, K., and S. Biggins. The Ipl1-Aurora protein kinase activates the spindle checkpoint by creating unattached kinetochores. 2006. *Nat. Cell Biol.*, **8**, 78-83.

Polizotto, R., and M. Cyert. Calcineurin-dependent nuclear import of the transcription factor Crz1 requires Nmd5p. 2001. *J. Cell. Biol.*, **154**, 951-60.

Posas, F. and H. Saito. Osmotic activation of the HOG MAPK pathway via Ste11p MAPKKK: scaffold role of Pbs2p MAPKK. 1997. *Science,* **276**, 1702-5.

Queralt, E., Lehane, C., Novak, B. and F. Uhlmann. Downregulation of $PP2A^{Cdc55}$ phosphatase by separase initiates mitotic exit in budding yeast. 2006. *Cell*, **125**, 719-732.

Raitt, D., Posas, F., and H. Saito. Yeast Cdc42 GTPase and Ste20 PAK-like kinase regulate Sho1-dependent activation of the Hog1 MAPK pathway. 2000. *EMBO J.*, **19**, 4623-31.

Reiser, V., D'Aquino, K., Ee, L.-S., and Amon, A., The stress-activated mitogen-activated protein kinase signaling cascade promotes exit from mitosis. 2006. *Mol. Biol. Cell*, **17**, 3136-3146.

Reiser, V., Salah, S., and G. Ammerer. Polarized localization of yeast depends on osmostress, the membrane protein Sho1, and Cdc42. 2000. *Nat. Cell Biol.*, **2**, 620-627.

Rossio, V., Galati, E., Ferrari, M. Pellicioli, A., Sutani, T., Shirahige, K., Lucchihi, G., and S. Piatti. The RSC chromatin-remodeling complex influences mitotic exit and adaptation to the spindle assembly checkpoint by controlling the Cdc14 phosphatase. 2010. *J. Cell Biol.*, **191**, 981-997.

Schwartz, M., and H. Madhani. Principles of MAP kinase signaling specificity in Saccharomyces cerevisiae. 2004. *Ann. Rev. Genet.*, **38**, 725-48.

Scott, R., Cairo, L., Van de Vosse, D., and R. Wozniak. The nuclear export factor Xpo1p targets Mad1p to kinetochores in yeast. 2009. *J. Cell Biol.*, **184**, 21-9.

Shang, C., Hazbun, T., Cheeseman, I., Aranda, J., Fields, S., Drubin, D., and G. Barnes. Kinetochore protein interactions and their regulation by the Aurora kinase Ipl1. 2003. *Mol. Biol. Cell*, **14**, 3342-3355.

Smolka, M., Albuquerque, C., Chen, S., and H. Zhou. 2007. Proteome-wide identification of in vivo targets of DNA damage checkpoint kinases. *Proc. Natl. Acad. Sci.*, **104**, 10364-9.

Stegmeir, F., and and A. Amon. Closing mitosis: the functions of the Cdc14 phosphatase and its regulation. 2004. *Annu. Rev. Genet.*, **38**, 203-32.

Straight, A., Belmont, A., Robinett, C., and A. Murray. GFP tagging of budding yeast chromosomes reveals that protein-protein interactions can mediate sister chromatin cohesion. 1996. *Curr. Biol.*, **6**, 1599-1608.

Sullivan, M., and D. Morgan. Finishing mitosis, one step at a time. 2007. *Nat. Rev. Mol. Cell Biol.*, **8**, 894-903.

Tanaka, K., Kitamura, E., Kitamura, Y., and T. Tanaka. Molecular mechanisms of microtubule-dependent kinetochore transport toward spindle poles. 2007. *J. Cell Biol.*, **178**, 269-281.

Tanaka, K., Mukae, N., Dewar, H. van Breugel, M., James, E., Prescott, A., Antony, C., and T. Tanaka. Molecular mechanisms of kinetochore capture by spindle microtubules. 2005. *Nature*, **434**, 987-994.

Tatebayashi, K., Takekawa, M., and H. Saito. A docking site determining specificity of Pbs2 MAPKK for Ssk2/Ssk22 MAPKKKs in the yeast HOG pathway. 2003. *EMBO J.*, **22**, 3624-34.

Taylor, G., Liu, Y., Baskerville, C. and H. Charbonneau. The activity of Cdc14p, an oligomeric dual specificity protein phosphatase from *Saccharomyces cerevisiae*, is required for cell cycle progression. 1997. *J Biol. Chem.,* **272**, 24054-63.

Tong, A., Drees, B., Nardelli, G., Bader, G., Brannetti, B., Castagnoli, L., Evangelista, M., Ferracuti, S., Nelson, B., Paoluzi, S., Quondam, M., Zucconi, A., Hogue, C., Fields, S., Boone, C., and G. Cesareni. A combined experimental and computational strategy to define protein interaction networks for peptide recognition modules. 2002. *Science,* **295**, 321-4.

Ubersax, J., Woodbury, E., Quang, P., Paraz, M., Blethrow, J., Shah, K., Shokat, K. and D. Morgan. Targets of the cyclin-dependent kinase Cdk1. 2003. *Nature*, **425**, 859-64.

Uhlmann, F., Wernic, D., Poupart, M-A., Koonin, E., and K. Nasmyth. Cleavage of Cohesin by the CD CLAN protease Separin triggers anaphase in yeast. 2000. *Cell*, **103,** 375-386.

Versele, M., Gullbrand, B., Shulewitz, M., Cid, V., Bahmanyar, S., Chen, R., Barth, P., Alber, T., and J. Thorner. Protein-protein interactions governing septin heteropentamer assembly and septin filament organization in *Saccharomyces cerevisiae*. 2004. *Mol. Biol. Cell*, **15**, 4568-83.

Visintin, R., Craig, K., Hwang, E., Prinz, S., Tyers, M., and A. Amon. The phosphatase Cdc14 triggers mitotic exit by reversal of Cdk-dependent dephosphorylation. 1998. *Mol. Cell*, **2**, 709-18.

Wang, H-W., Ramey, V., Westermann, S., Leschziner, A., Welburn, J., Nakajima, Y., Drubin, D., Barnes, G., and E. Nogales. Architecture of the Dam1 kinetochore ring complex and implications for microtubule-driven assembly and force-coupling mechanisms. 2007. *Nat. Struct. Mol. Biol.*, **14**, 721-726.

Wang, H.-W., Long, S., Ciferri, C., Westermann, S., Drubin, D., Barnes, G., and E. Nogales. Architecture and flexibility of the yeast Ndc80 complex. 2008. *J. Mol. Biol.*, **383**, 894-903.

Wang, Y., and D. Burke. Checkpoint genes required to delay cell division in response to nocodazole respond to impaired kinetochore function in the yeast *Saccharomyces cerevisiae*. 1995. *Mol. Cell Biol.*, **15**, 6838-6844.

Wei, R., Al-Bassam, J., and S. Harrison. The Ndc80/HEC1 complex is a contact point for kinetochore-microtubule attachment. 2007. *Nat. Struct. Mol. Biol.*, **14**, 54-59.

Westermann, S., Avila-Sakar, A., Wang, H-W., Niederstrasser, H., Wong, J., Drubin, D., Nogales, E., and G. Barnes. Formation of a dynamic kinetochore-microtubule interface through assembly of the Dam1 ring complex. 2005. *Mol. Cell*, **17**, 277-290.

Westermann, S., Wang, H-W., Avila-Sakar, A., Drubin, D., Nogales, E., and G. Barnes. The Dam1 kinetochore ring complex moves processively on depolymerizing microtubule ends. 2006. *Nature*, **440**, 565-569.

Westermann, S., Drubin, D., and G. Barnes. Structure and functions of yeast kinetochore complexes. 2007. *Ann. Rev. Biochem.*, **76**, 563-91.

Westfall, P., Patterson, J., Chen, R., and J. Thorner. Stress resistance and signal fidelity independent of nuclear MAPK function. 2008. *Proc. Natl. Acad. Sci.*, **105**, 12212-17.

Wigge, P., Jensen, O., Holmes, S., Souès, S., Mann, M., and J. Kilmartin. Analysis of the *Saccharomyces* spindle pole by Matrix-assisted Laser Desorption/Ionization (MALDI) mass spectrometry. 1998. *J. Cell Biol.*, **141**, 167-177.

Wigge, P. and J. Kilmartin. The Ndc80p complex from *Saccharomyces cerevisiae* contains conserved centromere components and has a function in chromosome segregation. 2001. *J. Cell Biol.*, **152**, 349-360.

Wong, J., Nakajima, Y., Westermann, S., Shang, C., Kang, J., Goodner, C., Houshmand, P., Fields, S., Chan, C., Drubin, D., Barnes, G., and T. Hazbun. 2007. *Mol. Biol. Cell*, **10**, 3800-10.

Woodbury, E., and D. Morgan. Cdk and APC activities limit the spindle-stabilizing function of Fin1 to anaphase. 2007. *Nat. Cell Biol.*, **9**, 106-112.

Woodruff, J., Drubin, D., and G. Barnes. Dynein-driving mitotic spindle positioning restricted to anaphase by She1p inhibition of dynactin recruitment. 2009. *Mol. Biol. Cell.*, **20**, 3003-3011.

Woodruff, J., Drubin, D., and G. Barnes. Mitotic spindle disassembly occurs via distinct subprocesses driven by the anaphase-promoting complex, Aurora B kinase, and kinesin-8. 2010. *J. Cell Biol.*, **191**, 795-808.

Xu, D., Farmer, A., and Y. Chook. Recognition of nuclear targeting signals by Karyoherin-β proteins. 2010. *Curr. Opin. Struct. Biol.*, **20**, 782-790.